PB 177 492

REMOVAL OF SO2 FROM FLUE GAS

Avco Missiles, Space and Electronics Group
Wilmington, Massachusetts

November 1967

PB 177492

7

REMOVAL OF SO_2 FROM FLUE GAS

Final Report
Contract No. PH-86-67-51

November 1, 1967

Prepared for

Engineering and Research Section
National Center for Air Pollution Control
U. S. Public Health Service

Submitted by

ADVANCED CHEMICAL PROCESSES SECTION
AVCO SPACE SYSTEMS DIVISION
Wilmington, Massachusetts 01887

Reproduced by the
CLEARINGHOUSE
for Federal Scientific & Technical
Information Springfield Va. 22151

157

This document consists of 164 pages,
40 copies, Series A

REMOVAL OF SO_2 FROM FLUE GAS

AVSSD-0411-67-RR

Final Report
Contract No. PH-86-67-51

November 1, 1967

Prepared for

Engineering and Research Section
National Center for Air Pollution Control
U. S. Public Health Service

Submitted by

ADVANCED CHEMICAL PROCESSES SECTION
AVCO SPACE SYSTEMS DIVISION
Wilmington, Massachusetts 01887

ABSTRACT

Processes for the removal of SO_2 from power plant flue gases were studied. Process models were developed for fluid bed and transport reactor gas-solid contacting. Using the process models, the economics of the two types of processes were compared, and operating and capital costs estimated.

Also, the kinetics of the sorption process were measured and found to be pore diffusion controlled over most of the possible range of sorbent loadings. A rate model describing the sorption process was developed. The rates of regeneration of spent sorbent were also measured. The kinetic data were used as inputs to the process models described above.

Unclassified report

EDITED BY:
EDITORIAL SERVICES SECTION
J. F. Dempsey

BLANK PAGE

CONTENTS

I. SUMMARY 1

A. Parameter Study of Process Economics 1

1. Dispersed Bed Contactor 2
2. Fluid Bed Sorber 2

B. Summary of Kinetics 5

1. Sorption 5
2. Regeneration 10

II. INTRODUCTION 13

III. CALCULATIONS OF SCHEMES FOR RECOVERY OF SO_2 FROM FLUE GAS 15

A. Summary Kinetics of Sorption and Regeneration 15

B. Contactor Models for SO_2 Sorption 16

1. Dispersed Bed Sorber 16
2. Fluid Bed Sorber 25
3. Fixed Bed Sorber 29

C. Alkalized Alumina Process Parameter Study 33

1. Sorption Process 34
2. Regeneration of Alkalized Alumina 43
3. Sulfur Recovery 48

D. Summary Process Calculations 49

E. References 49

IV. KINETICS OF SORPTION AND REGENERATION 53

A. Introduction 53

B. Apparatus 55

1. Cahn Electrobalance Apparatus 55
2. Torsion Balance Apparatus 55

C. Procedure 60

1. Original Torsion Balance Apparatus, Runs S-1, R-1 Through S-73, R-73 60
2. Modified Torsion Balance Apparatus, Runs S-74, R-74 and Later 60

CONTENTS (Concl'd)

D. Sorption Step 61

1. Mathematical Model of Sorption Step 61
2. Determination of Mechanism 66
3. General Treatment of Data 70
4. Effect of Moisture and Oxygen in the Flue Gas 73
5. Fit of Data to Model 81
6. Effect of Particle Diameter 82
7. Effect of Temperature 84
8. Effect of Gas Velocity 84
9. Summary Sorption Model 86
10. Initial Sorption Rate Measurements 88
11. Comparison of Avco Data with Other Data 95

E. Regeneration 100

1. Effect of Hydrogen Partial Pressure 101
2. Extent of Thermal Regeneration 101
3. Effect of Initial Loading 105
4. Effect of Carbon Monoxide 105
5. Effect of Reaction Products 108
6. Effect of Temperature 108
7. Summary of Regeneration Kinetics 111
8. Continued Work on Regeneration 111

F. Chemical and Physical Properties of Sorbent 112

1. Chemical Analysis 112
2. Physical Properties 112

Appendix I. Sample Calculation Run S-82 127

Appendix II. Tabulation of Rate Data 131

ILLUSTRATIONS

Figure 1 Average Sorption Rate Constant at 300° C for Several Conditions 17

2 Comparison of Fixed Bed Model with Data 17

3 Comparison of Well-Stirred Fluid Bed Model with Data [CERL] . 18

4 Calculated Sorbent Terminal Velocity versus Particle Diameter 21

5 Calculated Dispersed Bed Recycle/Feed Ratio versus Sorbent Loading 23

6 Calculated Dispersed Bed Pressure Drop versus Sorbent Loading 27

7 Fluid Bed Operating Parameter 27

8 Fluid Bed Parameters versus Sorbent Loading 30

9 Schematic Diagram of Sorption Process Equipment 35

10 Calculated Dispersed Bed Sorption Cost versus Sorbent Loading 39

11 Calculated Fluid Bed Sorption Cost versus Sorbent Loading (0.060-inch particle size) 41

12 Calculated Fluid Bed Sorption Cost versus Sorbent Loading (0.104-inch particle size) 42

13 Schematic Diagram of Sorbent Heat Recovery System 45

14 Calculated Regeneration Cost versus Sorbent Loading 47

15 Summary Estimated Cost of Dispersed Bed System versus Sorbent Loading 51

16 Summary Estimated Cost of Fluid Bed System versus Sorbent Loading 52

17 TGA Apparatus With Cahn Electrobalance 56

18 Sorption - Regeneration Rate Apparatus Using Precision Torsion Balance 57

19 Modified Reaction Chamber 59

20 Concentration Profiles for Pore Diffusion Controlling, Spherical Particle 61

ILLUSTRATIONS (Cont'd)

Figure 21 Mixed Diffusivity as a Function of Pore Diameter and Temperature 69

22 Sorption Curve for S-79 and S-82 69

23 Sorption Rate Curve for S-79 and S-82 71

24 Reciprocal Rate Plots S-79 and S-82 72

25 Sorption Data for Sample No. 6 76

26 Sorption Data for Sample No. 6 77

27 Sorption Data for Wet and Dry Flue Gas 78

28 Sorption Rate Data, W.R. Grace Sorbent 79

29 Effect of Particle Diameter on Diffusivity 83

30 Effect of Particle Diameter on K_c 83

31 Effect of Temperature on Diffusivity 85

32 Effect of Temperature on K_c 85

33 Comparison of Rate Models with Data 90

34 Initial Sorption Rate Data 92

35 Comparison of Peter Spence and W.R. Grace Sorbents 96

36 SO_2 Sorption Curves of CERL 97

37 CERL Data Fitted to Avco Model 99

38 Comparison of Avco and Amundson Models for CERL Data 99

39 Regeneration R-13 102

40 Regeneration R-58 102

41 Regeneration R-72 103

42 Effect of Hydrogen Content on Regeneration Time 104

43 Effect of Sorption Time on Thermal Regeneration 104

44 Effect of Initial Loading on Regeneration Time 107

ILLUSTRATIONS (Concl'd)

Figure 45 Effect of CO on Regeneration Time 107

46 Unremoved Weight Regenerating in CO 109

47 Regeneration in the Presence of Reaction Products 109

48 Relative Regeneration Time as a Function of Temperature ... 110

49 Pore Size Distribution For W.R. Grace Sorbent, Kelly Data 114

50 Pore Size Distribution For W.R. Grace Sorbent, Field Data 115

51 Pore Size Distribution, Fresh W.R. Grace Sorbent, Aminco Data 116

52 Pore Size Distribution, Used W.R. Grace Sorbent, Aminco Data 117

53 Pore Size Distribution, W.R. Grace Sorbent, Nitrogen Sorption Method 118

54 Pore Size Distribution By Volume, W.R. Grace Sorbent 120

55 Pore Size Distribution, Combined Mercury Intrusion and Nitrogen Sorption Method 121

56 Pore Size Distribution, W.R. Grace Sorbent, H_2 Treated at Avco, 650° C for Ten Hours 122

57 Pore Size Distribution, Peter Spence Sorbent 124

58 Pore Size Distribution Bu Mines Pilot Plant Sorbent 125

TABLES

Table I. Summary of Dispersed Bed Calculations 3

II. Summary of Fluid Bed Calculations 4

III. Fluidization Velocity as a Function of Particle Diameter 26

IV. Computation of Effective Diffusivity 68

V. Summary of Sorption Data 74

VI. Comparison of Sorption Data with Model 89

VII. Summary Data of Initial Rate Studies 94

VIII. Regeneration Data for SO_2 Sorption 106

A-I. Sample Calculations for Run S-82 129

I. SUMMARY

Alkalized alumina has been shown to effectively remove sulfur oxides from flue gases. In this report, the results of parameter studies on the economics of a dispersed bed and a fluid bed sorption system, based on models of the sorption systems, are presented. In conjunction with the parameter calculations, an investigation was carried out on the rate of SO_2 sorption on alkalized alumina and the rate of regeneration of the sorbent.

A. PARAMETER STUDY OF PROCESS ECONOMICS

A parameter study of the alkalized alumina process was carried out. Important process parameters, such as the rates of SO_2 sorption and sorbent regeneration of alkalized alumina, the sorbent loading, and sorbent particle size, were studied, and their effect on process operation and cost was examined.

Two types of contactors for removing the SO_2 by a solid sorbent were considered; the dispersed bed of the Bureau of Mines,[2,3,4] and the fluid bed of CEGB[10]. Equations describing the material and force-momentum balances were developed for each type of contactor, using certain simplifying assumptions. The material balances employed sorption rate expressions which were derived from laboratory data described in this report. The models developed for both contactors are believed to be reasonable, but have not been correlated with pilot plant data.

With the models, typical parameters, such as contactor size and pressure drop, were related to the sorption kinetics, sorbent particle size, fraction of SO_2 removal from the flue gas, and the flue gas velocity through the sorber unit.

In order to study the important parameters of the alkalized alumina process and to compare the two types of contactors, rough costs were developed for the overall process. The process was divided into three separate sections: the sorbers; the sorbent regenerators; and the sulfur recovery section. The loading of SO_2 on the sorbent was the independent parameter relating sorption and regeneration; the cost of operation of the sulfur recovery (Claus unit and gas producer) was taken from Katell[5].

Preliminary calculations indicate that conditions may be obtained under which the alkalized alumina process can be operated with only a small cost penalty. Potentially, with improvement in regeneration and sulfur recovery, the process may be operated at a profit while removing 90 percent, or more, of the sulfur from the flue gas of a power plant. The dispersed and fluid bed sorption contactors would require different modes of operation. The optimum operating conditions were determined by estimating the process cost as a function of sorbent loading (Percent SO_2). The minimum cost conditions for operating either contactor in the alkalized alumina process, is determined from simple economic models and several simplifying assumptions are presented. The SO_2 recovery process is assumed to be in a power plant of several hundred megawatts. The plant utilizes coal containing 3 percent sulfur, and 90 percent of the sulfur is recovered.

1. Dispersed Bed Contactor

By its nature, the dispersed bed sorber operated with relatively short sorbent residence times; longer sorbent contact with the flue gas is obtained by recycling the sorbent through the contactor. Kinetics measurments have shown that extremely high SO_2 sorption rates are obtainable in this type of contactor, but operation of this device is very sensitive to the sorption kinetics. According to the simple cost model, the minimum cost occurs at sorbent loadings of 15 to 20 percent SO_2. The calculations indicate sorber pressure drops in the vicinity of 10 to 15 inches H_2O and sorbent recycle-to-feed ratios of 45/1 to 73/1 with an average sorbent size of 0.060 inch.

A range of operating conditions was obtained by the use of two sorption rate expressions, one more optimistic than the other. The higher rate expression was determined using a flue gas containing 500 ppm NO, while the lower rate was obtained in the absence of NO. The high rate is believed to be more reasonable. A sorber contact time of one minute was assumed. Pertinent parameters for a minimum cost condition are presented in Table I.

2. Fluid Bed Sorber

Calculations on a fluid bed sorber are conservative with respect to the required sorbent inventory and pressure drop in that they are based on a well-stirred gas phase. The unit in a plant would be operated most economically at SO_2 loadings of 20 to 25 percent (wt SO_2/wt sorbent). Three stages are assumed to be required for 90 percent SO_2 removal, but only one or two may be necessary, resulting in slightly lower sorber cost. As in the dispersed bed sorber, costs are sensitive to the sorption rate and thus summary estimates for both optimistic and pessimistic sorption kinetics are presented in Table II for the minimum cost points. The kinetics affect the sorbent inventory, and hence the pressure drop and losses due to attrition.

The development of costs presented in Tables I and II for the two processes led to some interesting conclusions about the alkalized alumina process.

a. The sorption process cost increases with the sorbent loading, while the regeneration cost decreases with increasing sorbent loading. The minimum costs appear to occur at 15 to 20 percent loadings for the dispersed bed unit and greater than 20 percent for the fluid bed sorber.

b. The sorber pressure drop is determined by the overall process economics, and may be expected to be 10 to 15 inches H_2O for the dispersed bed unit, and 5 to 12 inches H_2O for the fluid bed system, depending on the true kinetics in each type of sorber.

c. Based on what are believed to be reasonable assumptions, the alkalized alumina process, as presently conceived, may optimistically be expected to operate at \$1.20 per ton of coal (3 percent sulfur in the coal), and pessimistically at \$1.53 per ton. Assuming that sulfur can be produced for sale at \$30 per ton, the net penalty will be \$0.30 to \$0.63 per ton of fuel.

d. The model for the dispersed bed sorber developed in this study appears to describe the process well. Calculations made with this model, using laboratory rate data agree quite well with the bench scale of Bureau of Mines.

TABLE I

SUMMARY OF DISPERSED BED CALCULATIONS

A. Operating Conditions Sorption Rate Constant*	Avco Curve I	Avco Curve II
% SO_2 recovered	90	90
Sorbent Loss, % thruput	0.005	0.005
ΔP (Sorber)	10 in H_2O	15 in H_2O
R/S	45/1	73/1
Sorbent Loading, % SO_2	20	15
B. Cost Summary		
Sorber	0.66 $/ton coal	0.69 $/ton coal
Regenerator	0.20	0.46
Sulfur Recovery	0.38	0.38
	1.24 $/ton coal	1.53 $/ton coal

*See Figure 1.

TABLE II

SUMMARY OF FLUID BED CALCULATIONS

A. Operating Conditions		
Sorption Rate Constant*	Avco Curve I	Avco Curve III
% SO_2 recovered	90	90
Sorbent Loss, % inventory/day	1	1
ΔP (Sorber), in H_2O	3.13	11.5
Sorbent loading	20%	20%
Sorbent Particle Size	0.060	0.060
B. Cost Summary		
Sorber	$ 0.59	$ 0.76
Regenerator	0.26	0.26
Sulfur Recovery	0.38	0.38
	$ 1.23	$ 1.40

*See Figure 1.

B. SUMMARY OF KINETICS

1. Sorption

a. Scope of study

The purpose of this study was to gather data on the rate of sorption and to use this data to develop a kinetic model for the sorption process. Such a model could then be used in process design and optimization calculations. It could also point out areas for sorbent modification such as pore size-particle size balance and sorbent capacity.

The rate of sorption of sulfur dioxide from a simulated flue gas onto alkalized alumina was measured by observing the rate of weight gain in a TGA type apparatus. The variables considered were sulfur dioxide content of the gas, temperature, particle diameter, gas velocity, moisture content of the gas, and sulfur dioxide loading on the sorbent. Sulfur dioxide content in the gas was varied from 0.06 to 1.0 percent, temperature from 150° C to 350° C, particle diameter from 0.066 inch to 0.102 inch, moisture content from 0 to 10.3 percent, and sulfur dioxide loading of the sorbent from 0 to saturation (approximately 35 percent of fresh sorbent weight). Superficial gas velocity was varied from 0.5 to 7.5 ft/sec.

The majority of the experiments were performed using a procedure in which the first measurements of weight gain were taken at a sorbent loading of 1 to 2 percent SO_2. These data were used to determine the validity of the rate model developed in this work and also the values of the constants in the model. Subsequently, it was found that initial sorption rates i.e., rates at 0 to 2 percent loading, were several times higher than predicted by the model although the model remains accurate above a sorbent loading of 2 percent SO_2. For the lower loadings, values of the sorption rate must be obtained from data presented graphically in the body of the report (Sect. IV.D.10).

b. Experimental

A sample of sorbent was supported in a ½-inch-diameter basket of stainless steel screen. The basket was in turn supported by a platinum wire on the arm of a torque balance and allowed to hang in a vertical quartz tube. A vertical tube furnace was arranged around the quartz tube so that the basket containing sorbent was in the hot zone. With this arrangement it was possible to vary the temperature of the sample and the gas surrounding it at will, all the while having an indication of the sample weight on the torque balance.

In operation, the sample was heated to the desired sorption temperature in nitrogen of the same humidity as the flue gas to be used. When the sample attained constant weight this value was recorded. Simulated flue gas containing nitrogen, oxygen, sulfur dioxide, and water was then substituted for the moist nitrogen for a prescribed period of time. At the end of this time the quartz tube was flushed with moist nitrogen. Then all flow was stopped, and the sample weight recorded. Repetition of the procedure generated a weight gain versus time curve which was the basic datum for this study.

The initial rate studies were made using the same procedure but better resolution was obtained by using a much reduced SO_2 concentration to slow the initial rate. Very small time increments were also used. Switching of flows was accomplished with solenoid valves in all studies.

c. Process chemistry

The following conclusions can be drawn with respect to the sorption chemistry.

1) Sorption occurs as SO_3; or, sorbed SO_2 quickly oxidizes to SO_3. This conclusion is substantiated by thermochemical calculations and by the fact that SO_2 sorbed in the absence of oxygen may be thermally removed whereas a reducing agent (H_2 or producer gas) is required to remove sulfur sorbed from oxygen containing flue gas.

2) The rate of sorption at sorbent loadings greater than 2 percent SO_2 is greatly enhanced by the presence of moisture in the flue gas. At ten percent sorbent loading the rate is over 100 times as fast in the presence of 5-7 percent moisture as in dry flue gas. On the basis of some rough experiments and computations neither capillary condensation nor surface diffusion appear to be responsible for this difference. Thus, some form of catalysis of the surface sorption reaction must take place in the presence of water. Sufficient water is sorbed to form a monolayer on the pore walls of the sorbent.

d. Sorption model

A mathematical model was developed assuming the sorption process to be initially controlled by mass transfer from the gas to the outer surface of the sorbent and in the later stages by the diffusion of SO_2 in the pores of the sorbent. During the pore diffusion controlling stage a sorption front is assumed to proceed through the particle from the outside to the center. Outside the front the sorbent particle is completely saturated, whereas, inside the front no sorption has occured. Sorption occurs very rapidly at the front. The assumptions of the model provide the boundary conditions to solve the differential equation for diffusion in a spherical particle. The equation and its method of solution are given in section IV.D.1. The rate equation obtained from solving the differential equation is

$$\frac{dS}{dt} = \left\{ \frac{6\, k_c\, M\, C_o}{d\, \rho\, W_o} \right\} \left[\frac{1}{1 + \left\{ \frac{k_c\, d}{2D} \right\} \left\{ \frac{1 - (1 - S)^{1/3}}{(1 - S)^{1/3}} \right\}} \right]$$

where

S = sorbent loading fraction of saturation

t = time

At $S \leq 0.25$ a simplified expansion of the model is sufficiently accurate for some purposes:

$$\frac{dS}{dt} = \left\{ \frac{6\, k_c\, M\, C_o}{d \rho\, W_o} \right\} \left[\frac{1}{1 + \frac{k_c\, d}{6 D}\, S} \right]$$

Fitting the model to the data for a given sorbent material is then a matter of determining the diffusivity D, and the mass transfer coefficient k_c, as functions of the experimentally variable parameters, d, T and C.

e. Validity of sorption model

The validity of the sorption model may be checked in several ways.

1) The sorption data from individual sorption runs should fit the form of the rate model.

2) The values of effective diffusivity, D, and mass transfer coefficient, k_c, should be close to values predicted from theory.

3) Runs made under varying temperatures and particle diameters should yield values of D and k_c that vary with d and T in the manner predicted by theory.

To fit the data to the model the integral data were first converted to rate data. This was accomplished by numerical differentiation using a three point Lagrangian rule. The rate data so obtained were plotted as reciprocal rate versus $\left[\frac{1-(1-S)^{1/3}}{(1-S)^{1/3}} \right]$ as suggested by Equation 30. As shown in Figure 24 the data for two example runs fit a straight line over a wide range of loading, S. From the constants of the straight lines the coefficients in Equation (40) were computed and predicted integral sorption curves for each run computed. The computed curves and the data are given in Figure 22. The fit of the curves to the data is excellent from the first data point at $S = 0.06$ up to $S = 0.8$.

Values of effective diffusivity from 0.007 to 0.02 cm^2/sec were obtained from the data. These are 5 to 10 times lower than the values computed from theory, for mixed Knudsen and bulk diffusion (See Figure 21). This difference is in good agreement with the commonly accepted lowering of diffusivity due to the porosity of the particle and tortuosity of the diffusion path.

The diffusivity was found to increase with the 1.8 power of T. This is higher than the value of 1.0 estimated from theory. The scatter of the data is considerable as shown in Figure 31 and this may account for the discrepancy.

The diffusivity was found to increase with the square of the diameter rather than to be independent of diameter (See Figure 29). According to the rate model the rate should be proportional to $\frac{D}{d^2}$ in the pore diffusion controlling regime. If, in fact, the rate were independent of diameter then the computed D would increase as d^2. This could occur if the particle pore structure consisted of large pores of negligible diffusional resistance feeding cells of less than particle diameter containing pores in which the rate limiting diffusion took place. In such a case the diffusion rate would be independent of particle diameter.

According to Section IV.D. there is a mode in the pore size distribution in W. R. Grace sorbent at 20-30 micron pore size. Such pores would provide the postulated channels of negligible resistance.

The model is not correct in its assumption that the initial sorption rate in the experiments described up to this point is mass transfer controlled. Initial sorption rates obtained in experiments to be described later were much higher than the rates described up to this point. However, since the form of the rate equation satisfactorily fits the rate data it has been retained for a semi-empirical description of the rate.

In summary, it is felt that in the pore diffusion region the model gives a good account of itself both in theory and in its ability to correlate data. The rates obtained at the lowest loadings (2 to 5 percent SO_2) were not mass transfer rates, but the form of the rate equation does fit the data well in this region. The model gives a satisfactory description of the sorption rate at loadings exceeding 2 percent SO_2.

f. Summary sorption model

The following rate model is the summary sorption model to be applied for SO_2 loadings greater than 2 percent. In this region the rate has been found independent of oxygen and water partial pressure. The constants were obtained from the average behavior of a large number of runs under varying conditions.

$$\frac{dS}{dT} = \left\{ \frac{0.00231\ T^{0.76}\ \pi}{\pi_o\ d} \right\} \left\{ \frac{y_o}{1 + \frac{1.37}{d} \left\{ \frac{1 - (1 - S)^{1/3}}{(1 - S)^{1/3}} \right\}} \right\} min^{-1}$$

For values of $S \leq 0.25$ the following approximation is satisfactory

$$\frac{dS}{dT} = \left\{ \frac{(0.00231)\ T^{0.76}\ \pi}{\pi_o\ d} \right\} \left\{ \frac{y_o}{1 + \frac{0.46}{d}\ S} \right\} min^{-1}$$

As $S = 0.20$ the model fits the integral data with an average error of 4 percent and an rms error of 29 percent. At $S = 0.5$ the average error is 2 percent and the rms error is 21 percent. Thus, the variations from run to run as indicated by the rms error are much greater than the error in the fit of the model to any one run indicated in Figure 22.

g. Comparison with CERL data

CERL has obtained sorption rate data in a differential fixed bed of Peter Spence sorbent. The exposure time to flue gas was varied and the amount of sorption during the exposure determined by sulfur analysis of the sorbent. The integral data so obtained were differentiated and the rate data plotted in Figure 38. Also plotted is the Avco pore diffusion model fitted to the CERL data.

The integral data were fitted to an integrated form of the Amundson rate equation

$$\frac{dT}{dt} = Ky\,(1 - S).$$

The resulting Amundson rate model was also plotted in Figure 38. It is clear that the data are much more accurately represented by the pore diffusion model. Inasmuch as the Peter Spence sorbent used by CERL was of the same order of magnitude with regard to particle size, pore size, and sorption rate as the W. R. Grace sorbent studied at Avco this is not surprising.

h. Initial rate data

By using a low concentration of SO_2 in the true gas and short intervals of exposure of the sorbent to SO_2 between weighings a much improved resolution of the initial rate was obtained. The data are shown in Figure 34 along with the Avco rate model for greater than 2 percent loading. The initial rates are seen to be many times higher than predicted by the model. At loadings of 2 percent SO_2 or greater the model and the new data agree.

Runs $ISR-2^1$, $ISR-4^1$, and $ISR-5^1$ show an increasing rate at loadings less than 2 percent as the water content of the true gas increases from 4.3 to 10.4 percent.

It is felt that the initial rates are probably mass transfer controlled in these experiments. As the rate begins to fall off chemisorption on the external surface of the particle may become the rate limiting step. This could then be followed by an increasing degree of pore diffusion control as the loading increased above 5 percent and penetration of the particle occurred.

2. Regeneration

a. Scope of work

The rate of regeneration of alkalized alumina sorbent has been measured at various levels of initial loading from less than ten percent of saturation to almost complete saturation. Temperature has been varied from 550° C to 700° C. The effect of hydrogen partial pressure has been measured from 0.12 atm to 1 atm. The effects of carbon monoxide, carbon dioxide, and the reaction products water and hydrogen sulfide have also been measured. The extent of thermal regeneration upon heating from sorption to regeneration temperature in nitrogen was also measured.

The data is not sufficiently complete to allow the development of a kinetic model for the regeneration process. The data have been presented as plots of the effect of each of the several variables on the time required for the regeneration to be 75 percent complete. From the data presented it is possible to estimate the required residence time of the sorbent in the regenerator under conditions of interest.

b. Experimental

The measurements were performed in the same apparatus described for the sorption rate measurements. At the end of the sorption cycle the sample was heated to the regeneration temperature in flowing nitrogen. The weight loss in nitrogen was recorded. Then the gas was switched from nitrogen to the desired reducing gas, usually hydrogen. A sufficiently low flow was used that it did not affect the balance reading. Because of this, flow was not interrupted at intervals to weigh the sample as in sorption. Rather, the times required for the sample to attain preselected weights were recorded. The resulting weight vs. time data were the basic data for the study. Plots of such data are shown in Figures 37 thru 41.

c. Effect of hydrogen partial pressure

The effect of hydrogen partial pressure on regeneration time was measured in a series of nine runs. The hydrogen was diluted with nitrogen to give partial pressures from 0.12 to 1.0 atm. Initial loadings of SO_2 on the sorbent varied from 3.6 w/o to 5.5 w/o. The results are given in Figure 42. The regeneration time is seen to increase with decreasing hydrogen pressure, varying from 8 minutes in pure hydrogen to over 20 minutes at 12 percent hydrogen.

d. Thermal regeneration

Sulfur oxides were driven from the sorbent upon heating from the sorption temperature to the regeneration temperature. The heating was done in nitrogen. The thermal weight loss varied from about 5 to 35 w/o of the SO_2 gained during sorption.

The percent thermal regeneration was found to decrease as the length of the sorption cycle increased. This effect is shown in Figure 43 for several regeneration temperatures and concentrations of SO_2 in the sorption gas. The effect is felt to result from an increased degree of diffusion of the sorbate into the crystals of the solid sorbent or from an increased degree of oxidation from sulfite to sulfate, both stabilizing the sorbate.

The designer of a regenerator must account for the thermal weight loss during sorbent heatup. For sorbent cycles of less than ten minutes approximately thirty percent thermal regeneration can be expected.

e. Initial sorbent loading

The regeneration time was found to increase rapidly with initial SO_2 loading of the sorbent, varying from 3 to 90 minutes at 650° C. The results of several experiments are shown in Figure 44. This figure also indicates the rapid decrease in regeneration time as the temperature is increased.

f. Effect of carbon monoxide and carbon dioxide

In order to simulate the use of reformed natural gas or producer gas as a regenerating gas, mixtures of hydrogen and carbon monoxide were used. There was no measurable reduction in the time required for the sorbent to regenerate to constant weight as the gas composition was varied from pure hydrogen to pure carbon monoxide. It is concluded that such gas mixtures should be satisfactory from the point of view of rate.

However, in the presence of hydrogen and carbon monoxide the regeneration does not go to completion. The residual weight increased with increasing CO content of the gas as shown in Figure 46. As much as 25 percent of the initial loading is unremoved when pure CO is the regeneration gas.

This result is contrary to that obtained by the Bureau of Mines using reformed natural gas as the regenerating gas. It was felt that the presence of CO_2 in the reformer gas might be somehow beneficial. This was checked by regenerating in a gas containing 21.4 percent CO_2, 31.4 percent CO, 47.2 percent H_2. Two runs were made at 650° F with initial loadings of 15.8 percent. In both runs regeneration was complete and rates consistent with the rest of the data obtained. Thus, reformed gases appear satisfactory as regenerating gases.

g. Effect of reaction products

Regenerations were performed in which the regeneration reaction products, H_2S and H_2O were included in the gas. In one case a stoichiometric mixture ($3/1 = H_2O/H_2S$) comprised 30 percent of the gas with the balance being hydrogen. In a second case an estimated five percent H_2S was added to pure hydrogen. In both cases there was no diminution in the rate of approach to equilibrium but as in the case of CO containing mixtures the regeneration was only about 75 percent complete. Pure hydrogen was required to complete the regeneration.

The effect of reaction products is not felt to be a serious problem as in a counter-current device sorbent leaving the regenerator would be in contact with fresh regeneration gas containing no reaction products.

h. Effect of temperature

Runs were made at 550° C and 650° C at initial loadings of about 4.3 w/o. The regeneration time decreased by a factor of 4.8 as the temperature was increased. Also, runs were made at 650° C and 700° C at loadings of about 37 percent w/o. Here the regeneration time decreased by a factor of 3.6. Relative regeneration time is plotted versus temperature in Figure 48. The time at 650° C is arbitrarily selected to be unity.

These results compare well with those obtained by Bu Mines and reported in RI 7021. The ratio of regeneration times for regeneration in pure hydrogen at 650° C and 700° C was 3.76, a value in good agreement with the value of 3.6 obtained in this study.

i. Summary of regeneration kinetics

The regeneration data, although not exhaustive, are sufficient to roughly size a regenerator. The procedure is as follows

1) From Figure 43 determine the extent of thermal regeneration. This will establish the quantities of SO_2 removed in heat up and in the regenerator.

2) From Figure 44 estimate the regeneration time in pure hydrogen at 650° C.

3) From Figure 48 find the regeneration time at the actual regeneration temperature.

4) From Figures 39, 40 and 41 it is seen that at a time of twice $t_{0.75}$ the regeneration is more than 90 percent complete and at four $(t_{0.75})$ the regeneration is essentially complete. A factor of two, four or some other is selected depending upon the requirements of the regeneration and the time from step (3) multiplied by this factor. The resulting number is the regeneration residence time.

For example, consider a sorbent with an initial loading of 5 w/o to be regenerated at 670° C. From Figure 43 the thermal regeneration would be 30 percent of the initial loading. From Figure 44 the regeneration time in pure H_2 at 650° C is 8.8 minutes. At 670° C this time would be reduced to 5.6 minutes. To effect complete regeneration a residence time of 4 times this value or 22.4 minutes should be allowed.

II. INTRODUCTION

For several decades there has been concern about the pollution of air by sulfur oxides resulting from the combustion of oil and coal. In recent years, several techniques for controlling sulfur oxide emissions from electric power plants have evolved. One of the more promising processes is based on contact of a flue gas with a dry, alkalized alumina sorbent which was developed by the Bureau of Mines, Pittsburgh, Pa. The effectiveness of this sorbent in removing sulfur oxides from flue gas under conditions normally encountered in a power plant led to the development of a dispersed bed or transport reactor contactor system in which the flue gas contacted the sorbent as it moved through a tall tower. The chemistry of alkalized alumina showed that in order to recover the sulfur from the expensive sorbent, a reducing gas such as hydrogen or carbon monoxide must be employed.

This investigation was carried out to obtain basic sorption and regeneration data for alkalized alumina using a TGA technique. Mathematical models were developed for the sorption of SO_2 in fixed,fluidized, and dispersed bed contactors, and using these models, a process parameter study was made.

BLANK PAGE

III. CALCULATIONS ON SCHEMES FOR RECOVERY OF SO_2 FROM FLUE GAS

A. SUMMARY KINETICS OF SORPTION AND REGENERATION

A simple expression for the sorption rate of sulfur dioxide on alkalized alumina is desirable for modeling flue gas-sorbent contactors. A detailed development on the kinetics of SO_2 sorption is given in Section IV. The results of these studies have undergone several modifications in recent months, which affect the use of the data in calculations.

The rate equation can be expressed as a product of two terms: one dependent only on sorbent loading, and a second dependent only on the partial pressure of SO_2. Thus,

$$\frac{dw}{dt} = r(w)\,y$$

where w is the sorbent loading, wt. SO_2/wt sorbent, y is the mole fraction of SO_2 in the flue gas, and t is time. From the data described in Section IV, the sorption rate constant, $r(w)$, is high at zero loading of SO_2 where rate values approach those due to interphase mass transfer. As sorbent loading increases from zero the rate decreases significantly as shown in Figure 1. The high initial rate is very important in the operation of the dispersed bed sorber. From loadings of a few percent up to saturation, the rate of sorption can be described by an intraparticle diffusion mechanism. Just recently, it has been learned that the presence of about 500 PPM NO_x in the gas increases the sorption rates, except at zero loading, by a factor of two or three throughout the range of SO_2 loadings.

In the dispersed and fluid bed contactors, it is necessary to consider that at any point in the contactor, the sorbent particles may have a distribution of sorbent loadings. For simplicity in calculations, an averaged sorption rate constant, $\bar{r}(w)$ has been defined. In using this constant, it is assumed that the flue gas contacts particles with a uniform distribution of SO_2 loadings from the feed concentration to that of the sorbent leaving the contactor. By definition

$$\bar{r}(w) = \frac{\int_{w_1}^{w_2} r(w)\,dw}{(w_2 - w_1)}$$

While this kinetic expression is crude, it does allow for a decrease in rate as moderate-to-high loadings are achieved in a contactor. The calculated average sorption rates are shown in Figure 1. Four curves are shown. The highest measured rate (Curve I) was obtained with 500 PPM NO_x in a simulated flue gas. A lower rate was obtained without NO_x in a simulated flue gas (Curve II). The lowest rate (Curve III) was measured with less sensitive laboratory conditions in which the high initial rate did not appear, although the sorption rate constant, $r(w)$, at high loadings was the same as Curve II. Thus, the effect of the initially very high rates on the average rate is apparent from a comparison of Curves II and III.

The rate constant used in design calculations can be very important. The rates of Curve I with NO_x agree reasonably well with rates computed from the data of the Bureau of Mines Pilot Plant, and are believed to be the best description of the sorption kinetics.

At larger particle sizes, the rate of sorption is decreased as described in Section IV. For comparison, an average rate constant is presented as Curve I-A in Figure 2 for 0.104 inch particles.

Comparison of calculations of contactor performance made using these kinetic data with experimental data on contactor demonstrates the utility of the data for contactor modeling. At CERL[2], simulated flue gas was passed through a small diameter, batch fluidized bed sorber. To model this experiment, in which the height to diameter ratio was about 1, it was assumed that the gas passed through the reactor in plug flow, and that the solid phase was well-mixed. The CERL sorption rate data was used in the calculations. The comparison presented in Figure 2 shows reasonably good agreement between the calculations and data, for times greater than five minutes. However, the model suggests less sorption at the beginning of the experiment than was actually observed. Recent sorption kinetics have shown that the initial sorption rates are probably higher than those shown on the CERL curve, and with higher initial rates the model agrees more closely with the data. Calculations with the sorption rate model are also compared with experimental data obtained in fixed bed experiments[3] in Figure 3 and the agreement is also good, except at the initial points. While the sorption model is not exact, it nevertheless does allow for a decrease in sorption rate as the sorbent loading increases. Uncertainties in the contactor models are probably greater than the inaccuracy of the sorption rate expression.

An analytical rate expression has not been obtained for the regeneration kinetics. In the TGA studies described in Section IV, it was determined that a regeneration time of about 1 hour would be reasonable to recover the sulfur from nearly saturated alkalized alumina in a device in which the sorbent passed counter-current to regeneration gas. This regeneration time applied even to a producer gas.

B. CONTACTOR MODELS FOR SO_2 SORPTION

1. Dispersed Bed Sorber

The concept of the dispersed bed contactor was developed at the U.S. Bureau of Mines[3,5]. In principle, flue gas passes upward through a tower. The gas is contacted with particles of sorbent which, as a dilute phase, may move either with or against the gas current. The direction of sorbent flow and its contact time is governed by the particle settling velocity and its relationship to the upward gas velocity.

An ideal model for the dispersed bed contactor assumes that flue gas and sorbent move through the contactor at constant velocity and temperature. There are no velocity gradients, no channeling or bypassing of the flue gas, but there may be considerable backmixing of the sorbent phase.

a. Material balance

The change in SO_2 concentration in the gas is related to the sorption rate constant and sorbent concentration as shown in Equation 1.

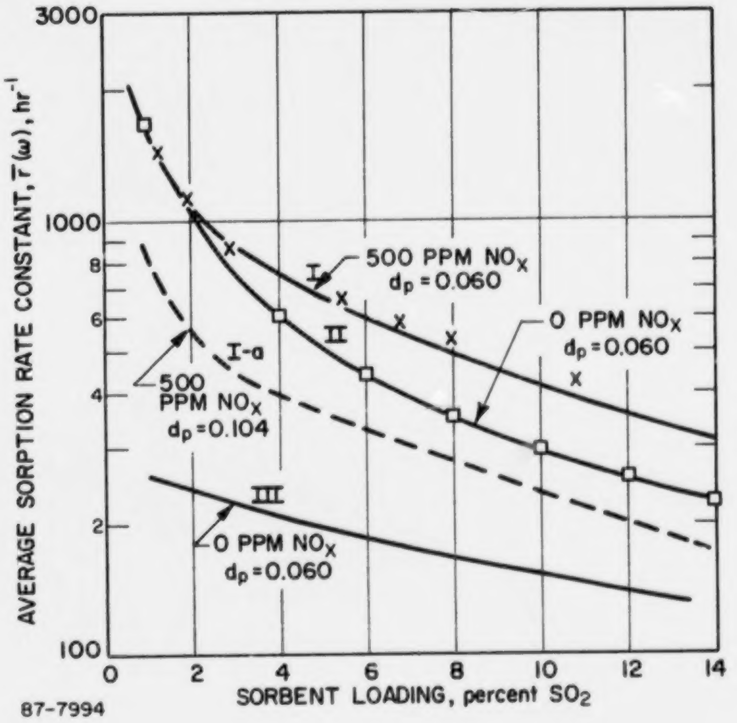

87-7994

Figure 1 AVERAGE SORPTION RATE CONSTANT AT 300° C FOR SEVERAL CONDITIONS

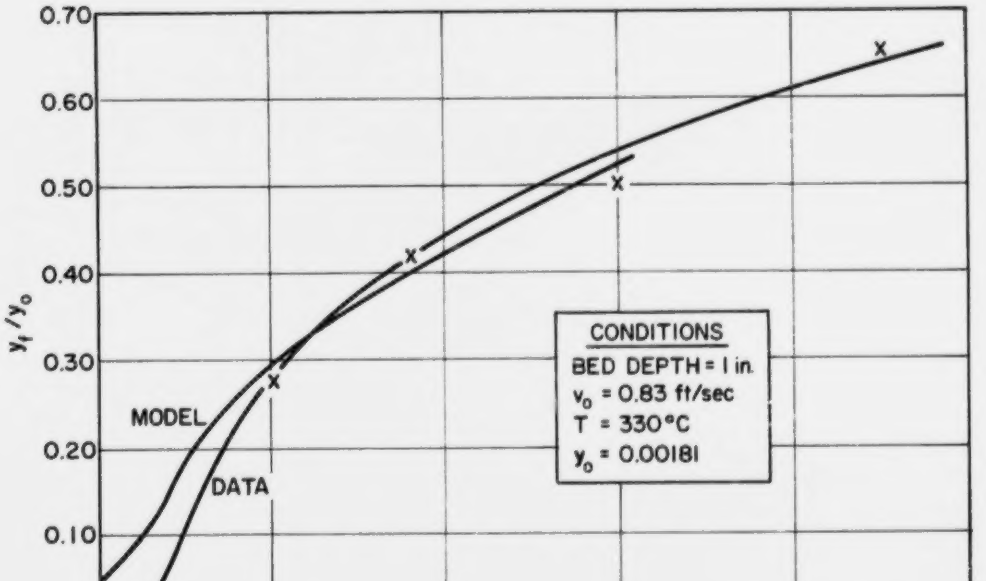

87-7995

Figure 2 COMPARISON OF FIXED BED MODEL WITH DATA

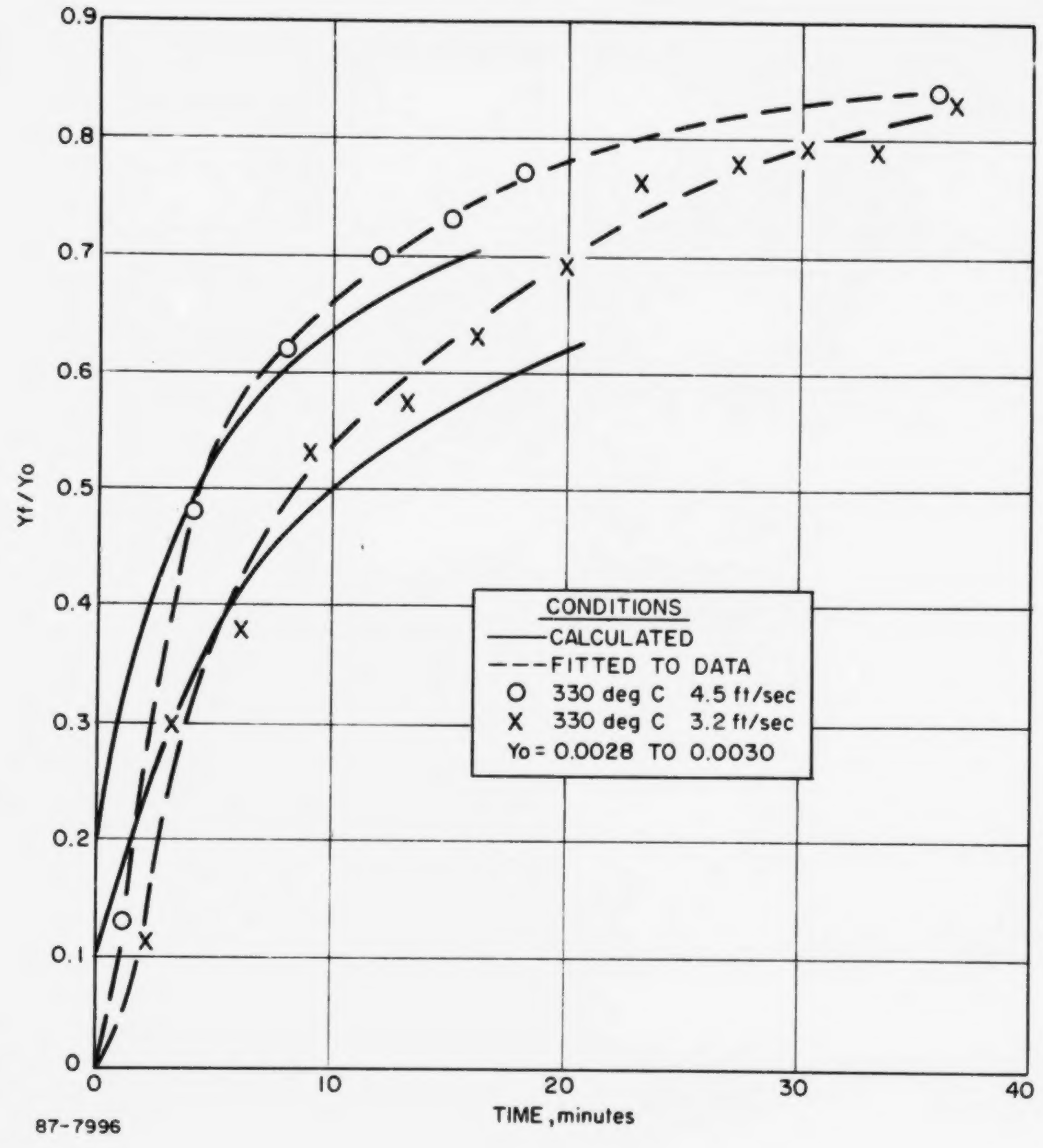

Figure 3 COMPARISON OF WELL-STIRRED FLUID BED MODEL WITH DATA [CERL]

$$-VG \frac{dy}{dz} = r(w)\, \rho_s (1-\epsilon) \cdot y$$

$$= S \frac{dw}{dz} \qquad (1)$$

where G is the mass flux of flue gas, $\rho_s (1-\epsilon)$ is the sorbent density in the contactor, S is the sorbent mass flux, V is a conversion factor, and y is the mole fraction of SO_2 in the flue gas. The overall material balance for the contactor is:

$$VG\,(y_o - y_f) = S_F\,(w_f - w_o) \qquad (2)$$

If an average value for the rate constant, $\bar{r}(w)$, can be assumed, then (1) integrates to:

$$\frac{y_o}{y_f} = exp \left\{ \frac{\bar{r}(w) \cdot \rho_s (1-\epsilon) H}{VG} \right\} \qquad (3)$$

b. Equations of motion

In the theoretical dispersed bed contactor, the sorbent is injected either at the top or bottom of the contactor, depending upon the mode of operation. The particles accelerate to a terminal velocity, and it has been calculated that this process occurs within a few seconds and in a few feet of the contactor. For the contactor, it is assumed that there is a negligible velocity of the sorbent at the point of entry. By summing the forces and momentum fluxes of the gas and sorbent streams, neglecting friction losses with the contactor walls the equation of motion for the overall contactor is:

$$\frac{-S^2}{\rho_s (1-\epsilon) g_c} + (P_1 - P_2) - H\,[\rho_g \epsilon + \rho_s (1-\epsilon)]\, \frac{g}{g_c} = 0 \qquad (4)$$

where H is the total contactor height, and ρ_g the gas density. Thus, the pressure drop through the contactor, assuming an adiabatic system, is related to the sorbent throughput. For the most generally conceived operation of the dispersed bed system, the momentum term for the sorbent is negligibly small compared to the other terms. Thus,

$$[\rho_g \epsilon + \rho_s (1-\epsilon)]\, H = P_1 - P_2 \qquad (5)$$

c. Particle terminal velocity

For the operation of the dispersed bed contactor, the terminal velocity for the sorbent particles is an important factor since the sorbent residence time is determined by the net velocity difference between the flue gas and the sorbent. The terminal velocity for spheres is a function of the particle diameter, the particle density of the sorbent, and the properties of the flue gas. The velocity for a particle Reynolds Number of 2 to 500 is given by:

$$v_{\rho_1 t} = \frac{(0.152)\, D_p^{1.14}\; g^{0.714}\; (\rho_s - \rho_g)^{0.714}}{\mu_g\; \rho_g^{0.285}} \tag{6}$$

where D_p is the particle diameter and μ_g the flue gas viscosity.

The terminal velocity increases only slightly with gas temperature due to the compensating effects of temperature on both the viscosity and density of the gas. Assuming that the viscosity is proportional to $T^{1/2}$; then the terminal velocity is proportional to $T^{0.071}$. For a gas temperature of 300° C, the terminal velocity is plotted in Figure 4.

d. Operating parameters

Operating conditions for the dispersed bed contactor are determined from (3), (5) and (6). The sorbent density in the contactor, $\rho_s\,(1-\epsilon)$, may relate to the total sorbent feed rate, S_T, and a "superficial" or "effective" sorbent velocity, v_s , through the contactor. This velocity may be used to describe either or both a rising or falling sorbent phase. Thus,

$$S_T = v_s\, \rho_s\, (1-\epsilon) \tag{7}$$

Substituting this expression into (5), then the pressure drop is related to the operating variables:

$$\Delta P = \frac{g}{g_c} \left[\rho_g\, \epsilon\, H + S_T\, \frac{H}{v_s} \right] \tag{8}$$

The effective sorbent velocity, v_s, may be obtained from experimental data where the pressure drop is measured as a function of sorbent feed rate. The total sorbent feed rate required to accomplish a given removal of SO_2 is obtained from the material balance:

$$\frac{S_T}{G} = \frac{V\, \ln\left(\frac{y_o}{y}\right)}{\bar{r}(w)} \left(\frac{v_s}{H}\right) \tag{9}$$

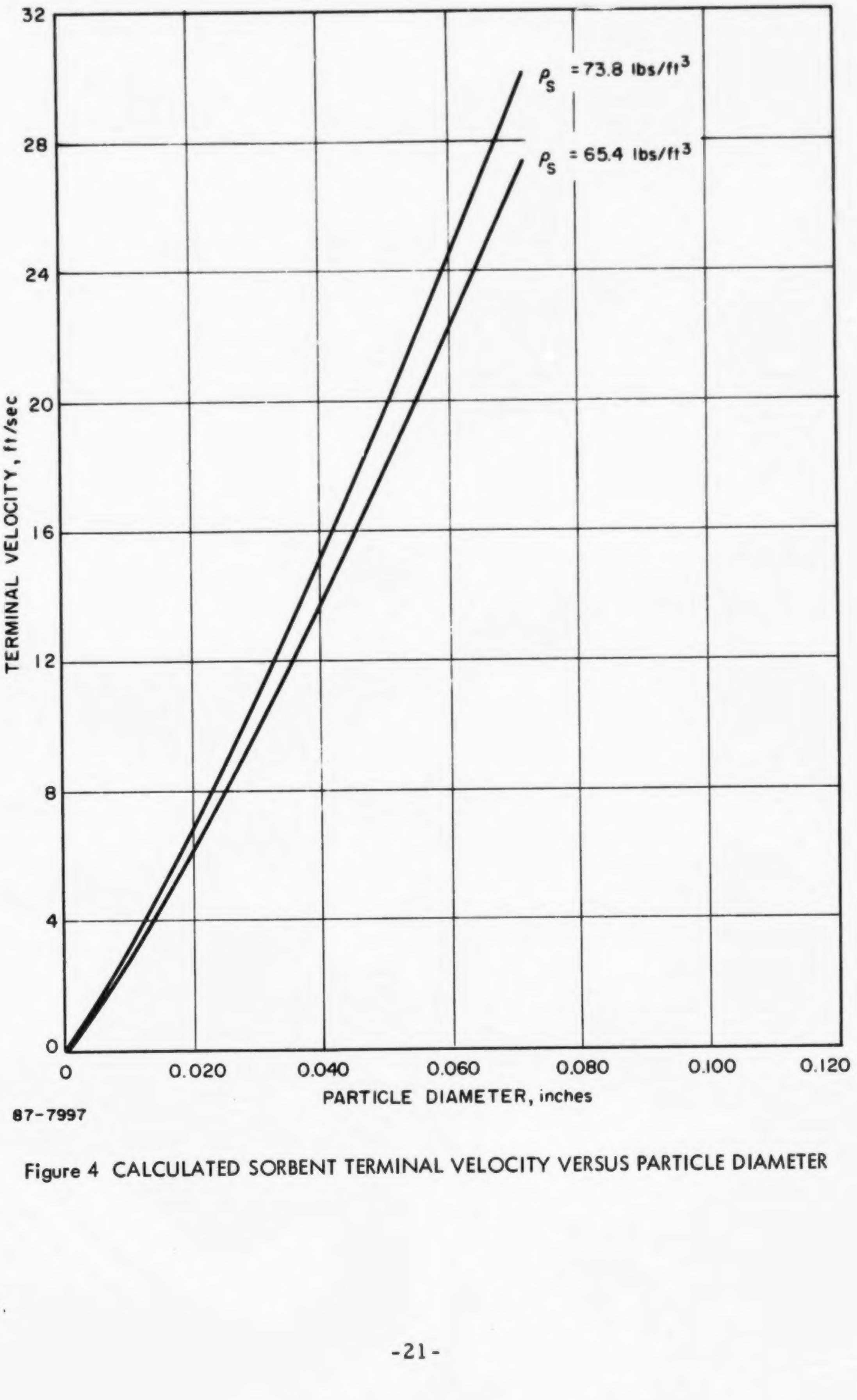

Figure 4 CALCULATED SORBENT TERMINAL VELOCITY VERSUS PARTICLE DIAMETER

and is a function of the average sorbent residence time, (v_s/H), and the sorption rate constant. The recycle to sorbent feed ratio is obtained from (2) and (9)

$$\frac{R}{S_F} = \left(\frac{S_T}{G}\right)\left(\frac{G}{S_F}\right) - \left(\frac{S_F}{S_F}\right)$$

$$= \left[\frac{w_f \ln\left(\frac{y_o}{y_f}\right)}{y_o \left(1 - \frac{y_f}{y_o}\right) \bar{r}(w_f)} \left(\frac{v_s}{H}\right) - 1\right] \qquad (10)$$

where S_F is the sorbent feed rate, S_T is the total sorbent throughput, R is the recycle flow rate, and w_f is the total sorbent loading.

Equation 10 is instructive in that it shows how the required sorbent recycle is related to the characteristics of the contactor. As the effective sorbent velocity through the bed is decreased, the recycle is diminished and in the limit approaches zero as the residence time of the sorbent gets very large. Conversely, as the sorbent velocity becomes very large, the sorbent recycle rate becomes very large. The recycle rate is also governed by the degree of SO_2 recovery that is desired, and by the sorbent loading. The recycle rate is also inversely proportional to both the sorption rate constant and the contactor height. The recycle feed ratio is represented as a function of sorbent loading in Figure 5.

The pressure drop is related to the degree of SO_2 removal, the sorption rate constant, and the flue gas velocity by combining (8) and (9).

$$\Delta P = \frac{g}{g_c}\left[\rho_g \epsilon H + \frac{V G \ln\left(\frac{y_o}{y_f}\right)}{\bar{r}(w_f)}\right] \qquad (11)$$

As an example, the pressure drop is plotted in Figure 5 to show the effect of sorbent loading and particle size (Sorption Rate Curve II of Figure 1 was used in the calculations). To obtain a maximum sorbent residence time, the flue gas velocity is approximately equal to the settling velocity of the average particle size.

The model was compared to the Bureau of Mines 1.6 inch diameter unit 4. Average sorption rate constants were calculated by employing the data in (11). These rates agree reasonably well with the Avco TGA data, as shown below.

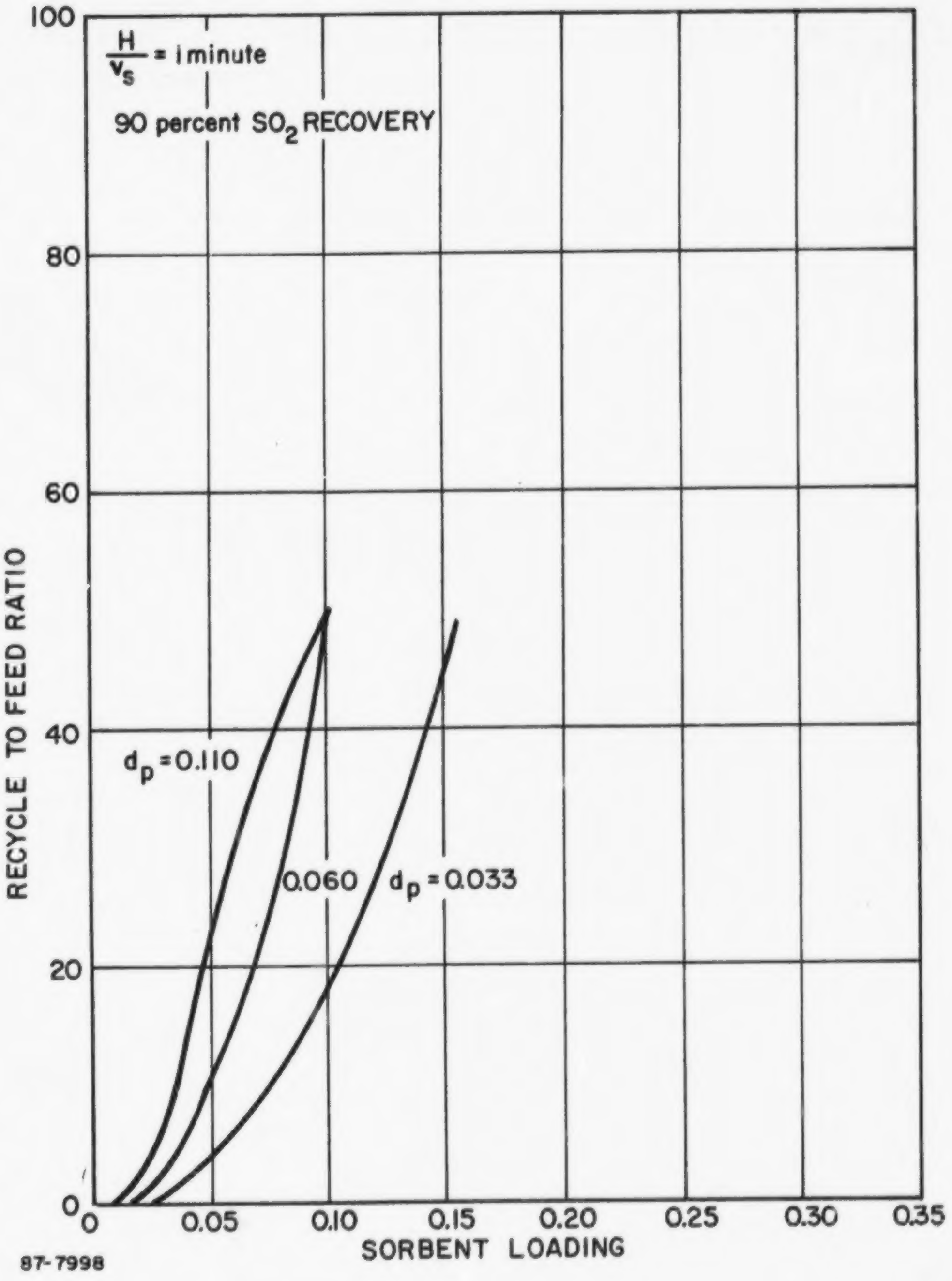

Figure 5 CALCULATED DISPERSED BED RECYCLE/FEED RATIO VERSUS SORBENT LOADING

SO_2 Loading	Average Sorption Rate Constant, hr^{-1}			
	Avco Data*		Bu Mines[4]	
	Curve I	Curve II	Run 4A	Run 6A
0.046	700	560	515	---
0.038	790	630	---	776

*See Figure 1.

The preliminary pilot plant data show less agreement with laboratory rate data. Average sorption rate constants were calculated from the data of three runs, and are shown below.

Comparison of Bu Mines Pilot Plant Data[11] with Avco Sorption Rate Data

Run No.	C-1	C-4	C-5
ΔP (in H_2O)	0.05	1.00	1.10
Average Sorbent velocity, ft/sec	3	3	3
Recycle ratio, R/S_F	0	5/1	5.5/1
Flue gas mass rate, lbs/ft^2-sec	0.920	0.920	
Average Sorbent loading, wt SO_2/wt sorbent	0.029	0.04	0.036
$\bar{r}(w)$ from P. P. Data, hr^{-1}	2900	2420	2520
$\bar{r}(w)$, from Avco Data, Curve I, Figure 1, and adjusted to avg. diameter	1110	1100	1100
Average bottoms sorbent particle size, inches	0.060	0.072	0.062
Average overhead sorbent particle size, inches	0.031	0.035	0.020

In general, the sorption rates obtained by using the pilot plant data in the Avco model, 2400 to 2900 hr^{-1}, compared to the values of about 1100 hr^{-1} determined from the kinetics work of this study. The agreement is not considered to be very bad considering two important facts. First, the pilot plant data was obtained in an actual flue gas, while the kinetics measurements were made with a synthetic gas mixture. Secondly, in the pilot plant operation, there was an extremely large particle size distribution, with much of the material less than 0.060 inches. Thus, the laboratory data would have to be extended to the lower sizes; and this was done using a 1/d relationship for the mean particle size. This comparison suggests that either (1) the pilot plant still does not confirm the model; or (2) that higher sorption rates are achieved in the actual contactor than are measured in the laboratory.

2. Fluid Bed Sorber

CEGB [10] has suggested that flue gas be contacted with alkalized alumina sorbent in a fluid bed contactor. An advantage of this system over the dispersed bed is that the sorbent residence time can be controlled independently of the flue gas flow. In principle, a bed of sorbent particles is maintained above a perforated plate or tray. New sorbent is added to the bed continuously, and spent sorbent is removed through a standpipe. The particle size and density of the sorbent affects the operation of the bed and is an important consideration.

a. Minimum fluidization velocity

As a gas is passed through a bed of solid particles, the pressure drop increases with velocity until incipient fluidization occurs. At this point of operation, the minimum fluidization velocity is reached. The pressure drop is approximately equal to the weight of the bed. Narsimhan[8] derived an expression for the minimum fluidization velocity by equating the Ergun pressure drop equation to the weight of the bed. With correc- [illegible]

$$v_{mf} = \frac{(42.9)\,(1-\epsilon_{mf})\,\mu_g}{\rho_g\ \phi\ D_p} \left\{ \left[1 + \frac{(0.000310)\,\phi^2\ D_p^{\ 2}\ \rho_g\ \ (\rho_f - \rho_g)\,g_c\ G}{(1-\epsilon)^2\ \mu_g\ g} \right]^{1/2} - 1 \right\} \tag{12}$$

Given the properties of the flue gas, the velocity is a function of the particle size and a shape factor, ϕ. Assuming spherical sorbent particles ($\phi = 0$) the effect of diameter on the minimum velocity is presented in Table III.

Over a wide range of gas velocity, in excess of the minimum fluidization velocity, the pressure drop is related to the depth and void fraction of the bed.

$$\Delta P = \frac{\rho_s\ (1-\epsilon)\ H g}{g_c} \tag{13}$$

TABLE III

FLUIDIZATION VELOCITY AS A FUNCTION OF PARTICLE DIAMETER

Particle Diameter, in.	Minimum Fluidization Velocity (330° C) ft/sec
1/8	4.9
1/16	2.4
1/32	0.81
1/64	0.21

b. Material balance

The performance of a fluidized bed for solid-gas reactions is difficult to describe because the contactor geometry is very important. Optimistically, the bed would operate as 1) plug flow for the gas phase, and 2) well-stirred for the solid phase. At the other extreme, the contactor would behave with 1) a well-stirred gas phase, and 2) a well-stirred solid phase. A further consideration is that in actual practice, the sorbent will probably translate across a tray, complicating a description of the behavior of the sorbent in the contactor. While it is more efficient for a contactor to operate with the gas phase in plug flow, the second extreme is more conservative for design considerations.

1) Model for plug flow of gas phase -- A simple model for this case is described by (15). It is obtained by using an average sorption rate constant, $\bar{r}(w)$, and is the same general equation as obtained for the dispersed bed model.

$$\frac{y_o}{y_f} = exp \left\{ \frac{\bar{r}(w)\ \rho_s (1-\epsilon) H}{V G} \right\} \qquad (14)$$

By substituting (13) into (14) and rearranging, the pressure drop due to the sorbent inventory mass flow rate gas in the contactor, and the degree of SO_2 recovery.

$$\Delta P = \frac{V G\ ln \left(\frac{y_o}{y_f} \right)}{g_c\ \bar{r}(w_f)} \qquad (15)$$

The sorption rate constant, $\bar{r}(w)$, is a function of the distribution of SO_2 loading on the particles in the bed.

2) Model for well-stirred gas phase -- In the well-stirred approximation, the average SO_2 concentration of the gas in the single stage is equal to the concentration in the gas leaving the bed. The material balance is described by

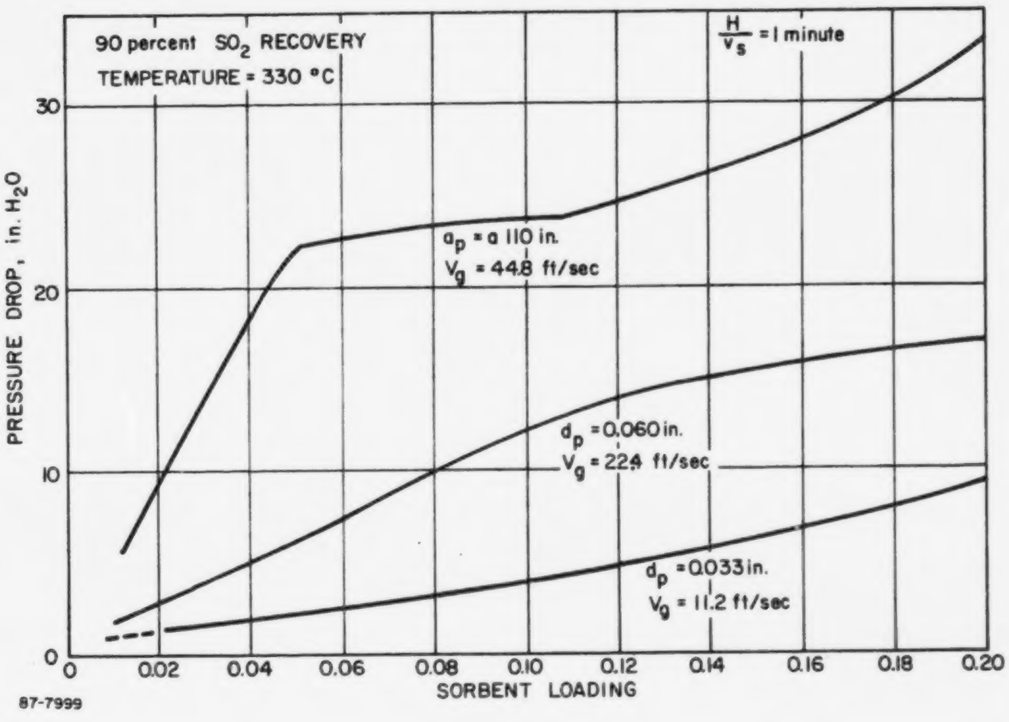

Figure 6 CALCULATED DISPERSED BED PRESSURE DROP VERSUS SORBENT LOADING

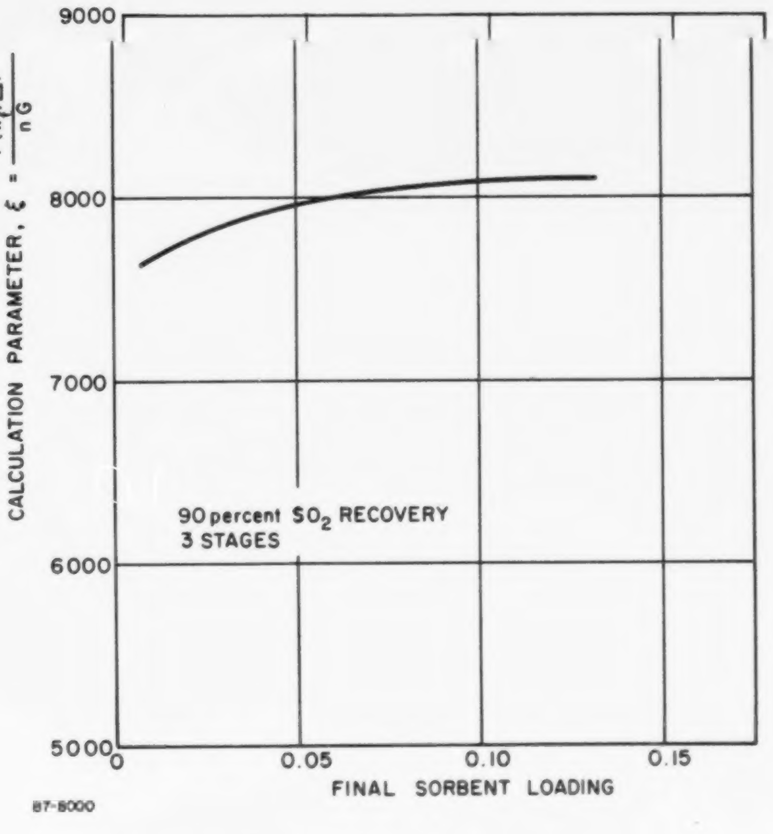

Figure 7 FLUID BED OPERATING PARAMETER

$$\frac{y_f}{y_o} = \frac{1}{\left[1 + \frac{\bar{r}(w)\rho_s(1-\epsilon)H}{VG}\right]} \qquad (17)$$

since the flue gas velocity or mass flux is determined by stability of of bed and the allowable entrainment of sorbent through the contactor, the depth of sorbent or pressure drop is a function of the sorption rate constant and the degree of sulfur removal.

$$\Delta P = \frac{VG\left[\frac{y_o}{y_f} - 1\right]}{\bar{r}(w)\ g_c}$$

If more than one stage is required, then (18) applies.

$$\frac{y_n}{y_o} = \frac{1}{\left[1 + \frac{\bar{r}_n(w)\Delta P}{VGn}\right]} \cdot \frac{1}{\left[1 + \frac{\bar{r}_{n-1}(w)\Delta P}{VGn}\right]} \cdots \qquad (18)$$

where n = number of stages.

In this equation, the independent parameter is $\frac{\Delta P}{Gn}$. The sorbent loading, and hence, the average sorption rate constant is computed for each stage by a material balance.

$$w_n = w_o - \frac{VG\,y_o}{S}\left[1 - \frac{y_{n-1}}{y_o}\right] \qquad (19)$$

Calculations of the operating conditions for a contactor consisting of more than one stage must be performed by trial and error using (16) and (19). At the chosen values of y_n, y_o, n and ΔP, a trial value of $\frac{\Delta P}{Gn}$ is selected. Values of w at each stage are then computed from (19). From values of $\bar{r}(w)$ at each stage y_n/y_o is computed from (16). Trial values of $\Delta P/Gn$ are selected and the process repeated until the computed value of y_n/y_o agrees with the initially chosen value. The parameter, $\frac{\Delta P}{Gn}$, has been calculated for a 90 percent recovery of SO_2 for a 3 stage unit. A new parameter, $\bar{r}(w)\Delta P/Gn$ is defined as $\psi(w_n)$ and is presented in Figure 7. It is easier to use in calculations and applies to a wide range of sorption rate constants. From this figure, it is apparent that as the sorbent loading is increased, the maximum mass flux of flue gas through the contactor decreases. Furthermore, much higher gas throughputs are attainable with 3 stages than with only one. The effect of sorbent loading on the estimated bed depth and pressure drop are shown in Figure 8.

3. Fixed Bed Sorber

Conceivably, the recovery of SO_2 can be carried out in a fixed bed contactor, although there are many operating problems. A number of experiments on the sorption of SO_2 on alkalized alumina have been carried out on a laboratory scale in a fixed-bed device. An analytical model has been developed for the fixed bed and correlations with the experimental data are good.

a. Material balance

The material balances for the gas and sorbent phases, respectively, are:

$$\frac{\partial y}{\partial z} = - \frac{\rho_g}{G} \; r(w) \cdot y \qquad (18)$$

$$\frac{\partial w}{\partial z} = r(w) \cdot y \qquad (19)$$

[illegible]

$$r(w) = \frac{KP}{L + w} \qquad (20)$$

then an analytical solution of (18) and (19) can be found. Thus,

$$w_L = \frac{y_L}{1 - y_L} \left\{ \alpha \, \eta_L - \beta \ln \left(\frac{1}{y_L} \right) \right\} \qquad (21)$$

$$r = \frac{1}{\alpha} \left\{ \frac{w_L^2}{2 y_L} + \beta \frac{w_L}{y_L} \right\} \qquad (22)$$

where

$$\alpha = \frac{KPH \rho_s (1 - \epsilon)}{VG \, w_o}$$

$$\beta = 4 \frac{L}{w_o}$$

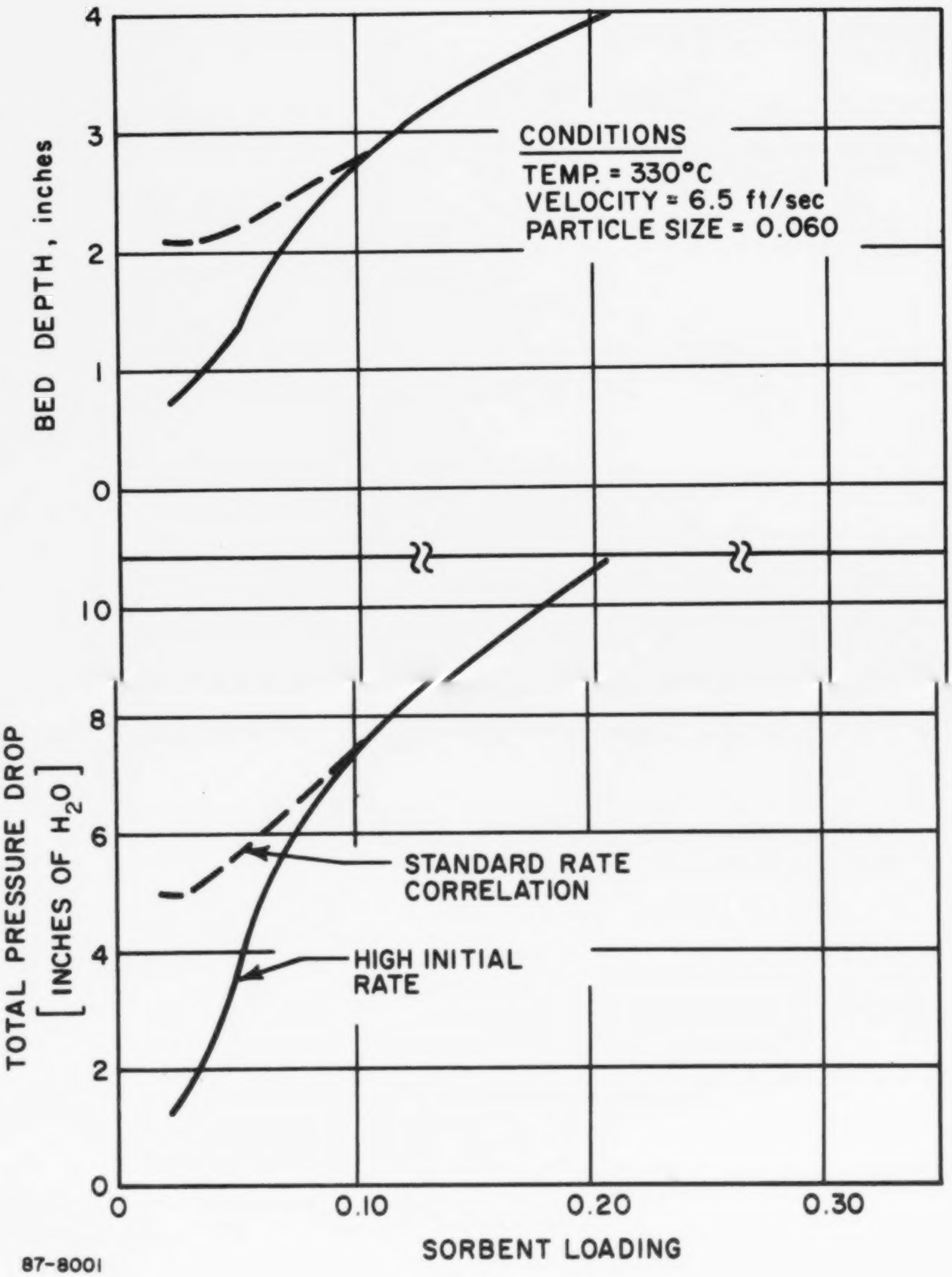

Figure 8 FLUID BED PARAMETERS VERSUS SORBENT LOADING

$$\theta_\beta = H \rho w_o / V G y_o$$

$$t = \tau \theta_\beta$$

There is a limitation in this solution: since the sorption rate expression is valid only for moderate sorbent loadings, calculations either for very long beds, or for very long sorption times can be erroneous. The limitation is obtained from (23).

$$\tau_o = \frac{2\beta + 1}{2a} \tag{23}$$

When τ in (22) exceeds τ_o, the solution does not hold, as the computed sorbent loading at the bed inlet would be greater than saturation.

From these equations, the time of operation t, at which the SO_2 concentration reaches a value of y_L can be computed.

b. Pressure drop

The pressure drop for a fixed bed is given by the Ergun Equation (9)

$$\frac{\Delta P}{H} = \frac{(150)\mu\, G\,(1-\epsilon)^2}{D_p^{\,2}\, \rho_g\, \epsilon^3\, g_c} + \frac{(1.75)\, G^2 (1-\epsilon)}{D_p\, \rho_g\, \epsilon^3\, g_c} \tag{24}$$

This equation applies to gases only where the total pressure drop is small and an average density of the gas may be used.

c. Sample calculation

Problem: Determine the time of bed operation t, for the following conditions:

1) Allowed pressure drop: 12 in. H_2O

2) Height of bed: 1 foot

3) Initial SO_2 concentration in flue gas: 0.2 percent (mole basis)

4) Maximum SO_2 concentration in exit gas: 0.02 percent

Solution:

1) Data:

$$\rho_g = \frac{(1\ atm)\left(29\ \frac{lbs}{mole}\right)}{\left(0.730\ \frac{ft^3\ atm}{mole\ {}^\circ R}\right)(1085^\circ R)} = 0.0366\ lb/ft^3$$

$\mu_g \cong 0.0730\ lb/hr\text{-}ft$ (Ref. 8)

$V = 2.21$

$W_o = 0.25\ lb\text{-}SO_2/lb\ sorbent$

$\epsilon = 0.35$

$D_p = 0.125\ in. = 0.01042\ ft^2$

$$y_L = \frac{0.02}{0.20} = 0.10$$

$K = 3.37\ hr^{-1}$

$L = 0.0144$

$P = 1\ atm$

$\rho_s = 65\ lb\ sorbent/ft^3$

$(1-\epsilon) = 0.65$

2) Calculations:

a) Determine flue gas mass flux from Equation (24)

$$\frac{\left(12\ in\ H_2O \times 5.19\ \frac{lb^m}{ft^2\text{-}in}\right)}{(1\ ft)} = \left\{\frac{(150)\left(0.073\ \frac{lb^m}{ft\text{-}hr}\right) G\ (1-0.35)^2 \left(32.2\ \frac{ft}{sec^2}\right)}{(0.01042\ ft)^2 \left(0.0366\ \frac{lb^m}{ft^3}\right)(0.35)^3 \left(32.2\ \frac{lb^m}{lb^f}\ \frac{ft}{sec^2}\right)} + \frac{(1.75)\,G^2\ (1-0.35)\ (32.2\ ft/sec^2)}{(0.1042\ ft)\left(0.0366\ \frac{lb^m}{ft^3}\right)(0.35)^3 \left(32.2\ \frac{lb^m}{lb^f}\ \frac{ft}{sec^2}\right)}\right\}$$

By trial and error,

$$G = 575\ \frac{lb^m}{ft^2\text{-}hr}$$

The superficial velocity is:

$$v = \frac{G}{\rho_g} = 4.36\ ft/sec$$

For the material balance:

$$a = \frac{(3.37\ hr^{-1})\ (1\ atm)\ (1\ ft)\left(65\ \frac{lb}{ft^3}\right)(0.65)}{(2.21)\left(575\ \frac{lb^m}{ft^2-hr}\right)(0.25)} = 0.28$$

$$\beta = \frac{(0.0144)}{(0.25)} = 0.0576$$

$$w_L = \frac{(0.1)}{(1-0.1)} \left\{ (0.28)(1) - (0.0576) \ln \left(\frac{1}{0.1} \right) \right\} = 0.01745$$

$$\tau = \frac{1}{(0.78)} \left\{ \frac{(0.01745)^2}{(2)(0.1)} + (0.0576) \frac{(0.01745)}{(0.1)} \right\} = 0.0414$$

$$t = (0.0414) \left[\frac{(1\ ft) \left(65 \frac{lb}{ft^3} \right) (0.65)(0.25)}{(2.21) \left(575 \frac{lb^m}{ft^2\text{-}hr} \right) (0.002)} \right] = 0.172\ hrs$$

$$\equiv 10.3\ min.$$

By these calculations, relationships were determined between the sorption time of the bed and the pressure drop and recovery of SO_2. The fixed bed will be considered in more detail in a later report.

C. ALKALIZED ALUMINA PROCESS PARAMETER STUDY

The alkalized alumina process is comprised of three basic operations: 1) sorption, 2) sorbent regeneration, and 3) sulfur recovery. The sorption process cost is a function of the degree of sorbent loading, and increases as the loading of SO_2 is increased. Basically, the sorption cost is increased because there is a longer sorption residence time in the contactor, and under these conditions the overall SO_2 sorption rate is diminished from the rate obtainable at low loadings. In contrast, the cost of regeneration diminishes as the loading is increased. The reason for this is that a major expense in regeneration is the preheating of the sorbent prior to chemical regeneration, and recovery of this energy afterward. Clearly, as the loading is increased, lower heating costs are required per unit of sulfur recovered. The cost of sulfur recovery is essentially independent of the sorbent loading and other process conditions, and is determined by the quantity of sulfur recovered from the flue gas. An optimum operating point is computed by estimating the costs of (1) sorption, (2) regeneration, and (3) sulfur recovery as a function of sorbent loading, and the lowest overall cost determines the operating point.

Process costs have been estimated in this study in order to ascertain process parameters, and also the sorbent properties. Costs are presented on the basis of dollars per ton of coal, for four major cost elements. In this way, it is hoped that the model can be readily modified as improvements in the process, and estimates of plant costs, etc. become available.

1. Sorption Process

Using the sorption models described previously, costs for sorber operation may be estimated. Katell[9] has presented a cost estimate for an 800 Mw Power Plant, and this paper serves as a basis for these estimations made in this study. As Katell pointed out, the process cost is based upon four major items: (1) capital charges, (2) labor, maintenance, and overhead, (3) utilities, and (4) raw materials.

a. Equipment

The sorption process is assumed to comprise the following equipment (1) the sorbers, (2) dust collectors (cyclones), (3) fans or blowers (to supply power to move the flue gas through the pressure drop of the sorption equipment), (4) dampers to seal off the sorber, and (5) a sorbent transport system. The flow sheet is shown schematically in Figure 9.

The size and cost of fans and dust or sorbent collectors are assumed to be dependent only on the power plant size, or flue gas flow rate. Costs used for calculations are: $0.10/CFM flue gas for both the I.D. Fan and sorbent collection system.

The dampers, three per sorber unit, are roughly estimated at $10,000 each. The sorbent transport system is calculated to be a small cost item. The sorber is the remaining equipment item, and the cost is a function of the type of sorber, and the operating conditions. For a preliminary estimate, the sorbers are assumed to be 20 feet in diameter. The height and number of contactors is determined by the allowable velocity through the unit. Thus, the mass velocity is a parameter of operation.

1) Dispersed bed sorber -- The estimated cost of the dispersed bed sorber, 120 feet high, as a function of mass velocity of flue gas is $\left[\frac{510}{G}\right]$ \$/ton coal/yr. Combining the associated dampers, sorbent transport, and peripheral equipment, the equipment cost, exclusive of the fans and dust collectors is $\left[\frac{832}{G}\right]$ \$/ton coal/yr.

Assuming that the sorbent collection system operates at 330° C [1.35 CFM/ton coal/yr] and the fan at 130° C [0.0905 CFM/ton coal/yr], these equipment costs are 0.135 and 0.0905 \$/ton coal/yr, respectively.

On a basis of the plant cost being 3.5 times the major equipment cost, the sorption plant cost is estimated as

$$\left[\frac{832}{G} + 0.226\right] \ \$/ton\ coal/yr$$

2) Fluid bed sorber -- Compared to the dispersed bed sorber, the fluid bed is a shallow device. Preliminary calculations indicate that

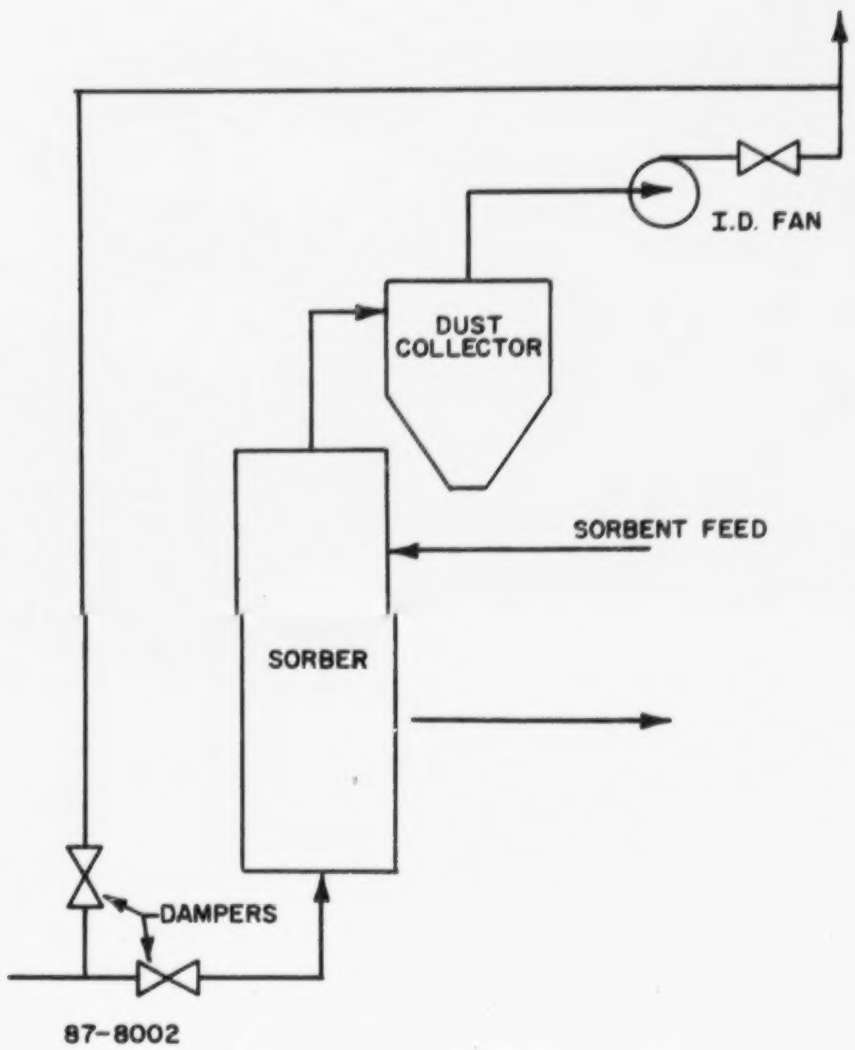
I.D. FAN
DUST COLLECTOR
SORBENT FEED
SORBER
DAMPERS
87-8002

Figure 9 SCHEMATIC DIAGRAM OF SORPTION PROCESS EQUIPMENT

for 90 percent SO_2 recovery the contactor should have 3 stages (conservative). The overall height is about 15 feet, and to facilitate comparison with the dispersed bed contactor, it is assumed that each unit is 20 feet in diameter. The number of units is a function of the allowable mass flow rate through the contactor. It was further assumed that there are 6 towers, each containing several fluid bed units stacked one above the other.

Since the number of units is determined by the mass flue gas flow rate, the total estimated sorber cost is $\left[\frac{110}{G}\right]$ \$/ton coal/yr. Including the cost of dampers for six towers, fans, and sorbent dust collectors, the total equipment cost is estimated at

$$\left[\frac{110}{G} + 0.151\right] \text{\$/ton coal/yr.}$$

b. Labor and maintenance

From the work of Katell[5], the cost of labor and maintenance, including appropriate overheads, is assumed to be roughly independent of the number or type of sorber. Accordingly, these costs are assumed to be 0.074 \$/ton coal.

c. Utilities

The major utilities cost is the power required for the fans to move the flue gas through the sorber. The pressure drop is composed of (1) 3 inches H_2O for a sorbent collector and peripheral equipment and (2) the pressure drop due to the sorbent hold up and static head of flue gas in the sorber.

1) Dispersed bed -- The contactor pressure drop is estimated from Equations 9 and 11 as a function of the mass flow rate of flue gas, the sorption rate constant, and the degree of SO_2 removal. Using a removal of 90 percent of SO_2, the power cost for the sorber is computed as

$$\left[(0.4 \times 10^{-5})\, H + (0.0144) + \frac{(0.0052)\, G}{\bar{r}(w)}\right] \text{\$/ton coal} .$$

where H is the contactor height (feet), G is the flue gas mass flow rate (lbs/ft^2-hr), and $\bar{r}(w)$ is the sorption rate constant (hr^{-1}).

2) Fluid bed -- The pressure drop through the fluid bed sorber due to the sorbent is obtained from (13) and is directly proportional to the mass flow rate of flue gas and the fluid bed sorption parameter, and inversely proportional to the sorption rate constant. Allowing that the contactor has three stages and that the pressure drop through the distributors is equivalent to the drop through the sorbent, the cost of power to move the flue gas through the contactor and 3 inches of water for the cyclones is

$$\left[(0.0187) + (1.654 \times 10^{-6}) \quad \frac{\psi(w)}{\bar{r}(w)}\right] \qquad \$/\text{ton coal}$$

where

$\psi(w)$ is a design parameter for a three stage fluid bed.

d. Raw materials - sorbent makeup

The major raw material for the sorption process is makeup of sorbent. The required rate of sorbent makeup may be determined either by (1) loss in SO_2 sorption activity, or (2) losses due to attrition of the material. Due to a lack of further information, it has been assumed that sorbent makeup is determined solely by losses due to attrition which are related to the sorbent throughput in the case of the dispersed bed sorber, and the sorbent inventory in the case of the fluid bed.

1) Dispersed bed -- Since sorbent attrition is probably directly related to the flow rate in a short residence time contactor, the losses are computed as a fraction of the total sorbent flow rate (fresh sorbent feed plus recycle). On the basis of the Bureau of Mines work[4], and other sparsely published data on large catalytic reactors and hypersorption units, it was assumed, as a best estimate, that the attrition was 0.005 percent of the throughput. This number is a function of the sorbent properties and method of transport.

The total sorbent throughput in the dispersed bed contactor (feed plus recycle) is obtained from (9) and is related to the sorbent residence time, fraction of SO_2 removed, mass flow rate of flue gas, and the sorption rate constant. From this equation, the cost per ton of coal is given by

$$\left[\frac{68{,}500\ B.C}{\bar{r}(w)}\right] \qquad \$/\text{ton coal}$$

where B is the sorbent loss as a fraction of the sorbent throughput, and C is the cost of the new sorbent (\$/lb), and 90% of SO_2 is removed.

2) Fluid bed -- For the fluid bed contactor, the sorbent losses are assumed to be a fraction of the inventory. Since this type of contactor requires an inherently long residence time, the attrition due to sorbent transport is considered as included in the fractional loss based on inventory. The total sorbent inventory for a 3 stage contactor is computed from (19). Converting this information to a cost per ton of fuel, the cost as a function of operating parameters is

$$\left[(0.825)\ a \cdot C \quad \frac{\psi(w)}{\bar{r}(w)}\right] \qquad \$/\text{ton coal}$$

where α is the sorbent makeup as a fraction of sorber inventory per day, C is the cost of the sorbent and $\psi(u)$ is the fluid bed parameter.

e. Summary of sorption process

Using the assumptions described previously, the sorption process cost can be computed as a function of several process variables, such as sorbent size, flue gas flow rate, sorbent loading, and the sorption rate constant.

1) Dispersed bed -- In computing the sorption process cost per ton of coal, it is assumed that capital charges are 14 percent of the plant cost per annum. Combining the four major cost elements, the unit sorption cost is

$$C\ (\$/\text{ton-coal}) = \underbrace{\left[\frac{408}{G} + 0.111\right]}_{\text{Capital Charges}} + \underbrace{\left[(0.0187) + \frac{(0.0052)\,G}{\bar{r}(w)}\right]}_{\text{Power}}$$

$$+ \underbrace{[0.074]}_{\substack{\text{Labor and}\\ \text{Maintenance}}} + \underbrace{\left[\frac{(68{,}500)\,B\cdot C}{\bar{r}(w)}\right]}_{\text{Sorbent Makeup}}$$

where G is the mass flow rate of flue gas (lbs/ft^2-hr), $\bar{r}(w)$ is the average sorption rate constant (hr^{-1}), B is the sorbent makeup rate (percent of sorbent), and C is the unit cost of sorbents.

From this equation, it is apparent that the basic process parameters are the mass flow rate of flue gas, G, and the sorption rate constant. Both of these parameters are a function of the average sorbent particle size. Other important factors which affect the process cost and parameter selection are the sorbent makeup rate, the value of the electric power, and the rate of capital charges.

a) Effect of sorbent loading -- As the average loading of the sorbent is increased, the sorption process cost is increased with respect to the power requirement and the sorbent makeup. The cost accorded to sorbent loading is presented in Figure 10 for an average sorbent particle size of 0.060 inch. From a basic cost of about 35 cents per ton at negligible sorbent loadings, the cost increases markedly as loading is increased. This effect is caused by the marked increase in recycle ratio as the sorption rate decreases, and the attendant larger sorber hold up of alkalized alumina. The higher sorber throughput produces greater sorbent makeup requirements, according to the assumptions in the model, and the larger sorbent inventories cause greater pressure drop and higher electric power costs.

b) Effect of sorbent particle size -- The dispersed bed contactor design requires that the flue gas velocity be approximately equal to the terminal velocity of the particle. On this basis, the mass velocities of flue gas are 11.2, 22.4, and 44.8 ft/sec for particle sizes of 0.033,

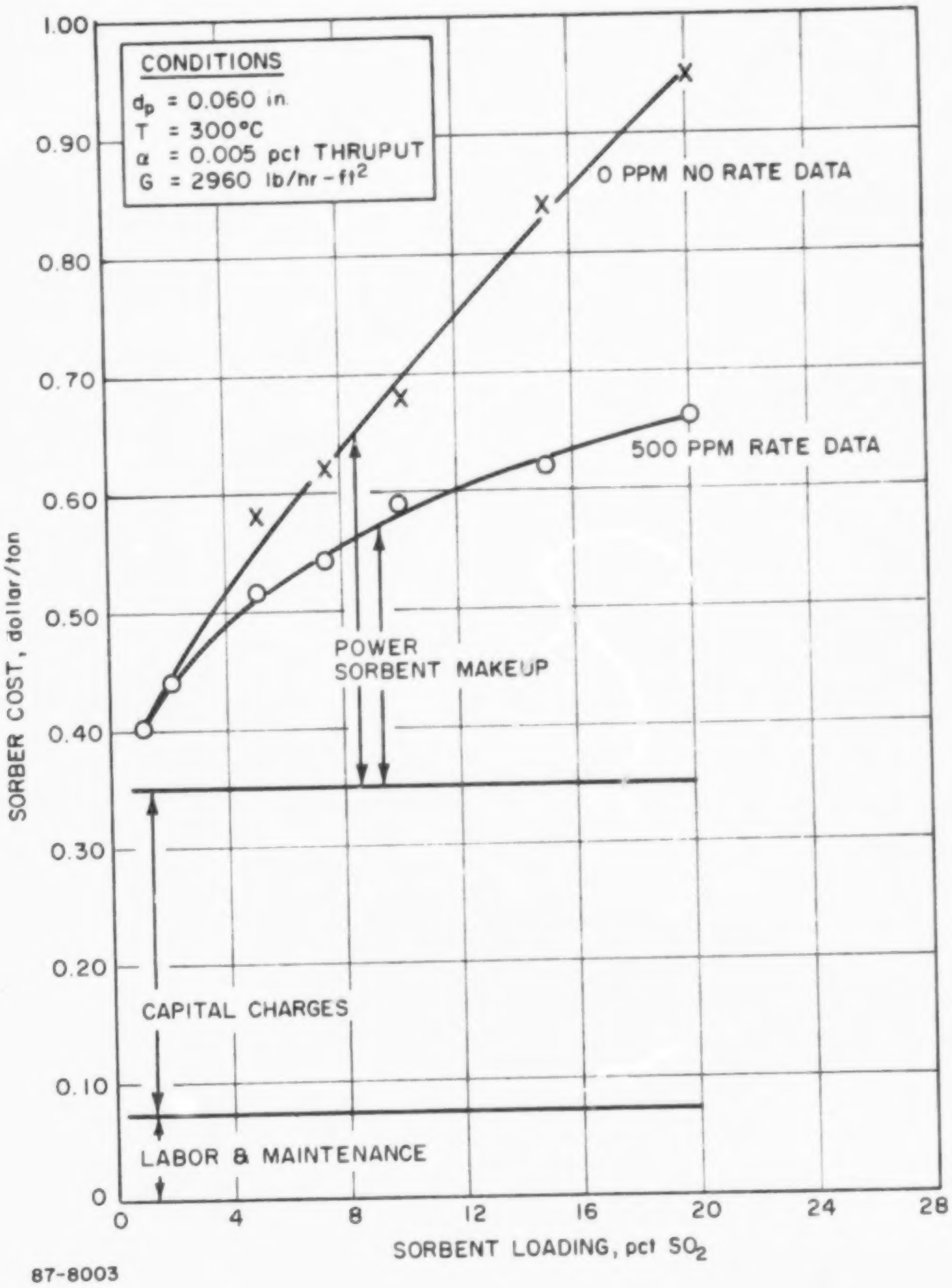

Figure 10 CALCULATED DISPERSED BED SORPTION COST VERSUS SORBENT LOADING

0.060, and 0.110 inch, respectively. The effect of particle diameter in this size range on the overall sorption cost is small. However, the distribution of costs is different. At the large sorbent size, the capital charges are reduced, because fewer sorbers are required, but the power and sorbent makeup are increased due to the lower effective sorption rate constants. The inverse situation pertains at the smaller particle size.

c) Effect of sorption rate constant -- Since high sorbent loadings are desirable, the effective sorption rate is important, as apparent from Figure 10. According to the design models used, the power and sorbent makeup costs will increase with loading, and improvements in the sorption rate at high loadings would have a significant effect on the cost of operation.

2) Fluid bed -- The overall estimated cost for the fluid bed sorber is

$$C = \underset{\text{Capital Charges}}{\left[\frac{110}{G} + 0.151\right]} + \underset{\substack{\text{Labor and}\\ \text{Maintenance}}}{[0.074]} + \underset{\text{Power}}{\left[(0.0187) + (1.624 \times 10^{-6})\,\frac{\psi(w)}{\bar{r}(w)}\right]}$$

$$+ \underset{\text{Sorbent makeup}}{\left[(0.825)\; a \cdot C\;\frac{\psi(w)}{\bar{r}(w)}\right]}$$

In the fluid bed sorber, the design flow rate of flue gas is slightly higher than the neighborhood of the minimum fluidization velocity. In order that the capital charges be reasonable, it is important that the flue gas velocity be greater than 1-2 feet per second (330° C). Greater velocities are theoretically achievable with larger sorbent particle sizes.

a) Effect of sorbent loading and sorption rate expression -- The sorption process cost is relatively insensitive to the sorbent loadings as shown in Figure 11. The data are based on an average sorbent size of 0.060 inch, and an average gas velocity of 3 feet per second (330° C) which is about 50 percent greater than the minimum velocity. Under these conditions, there is an estimated basic cost of 51 cents per ton of coal. The power requirement and sorbent makeup are a function of the applicable sorption rate curve. Three sorption rate curves have been considered. The data in Figure 11 show how the costs increase as the effective sorption rate changes. The capital charges are the dominant factor, and the total cost increases by only about 10 to 20 percent with loadings up to 20 percent.

b) Effect of particle size -- Because the capital charges were large for the case of 0.060 inch sorbent, the effect of increasing the sorbent to 0.104 inches, assuming a fluid bed would operate properly, was investigated. In the calculations, which are shown in Figure 12, the

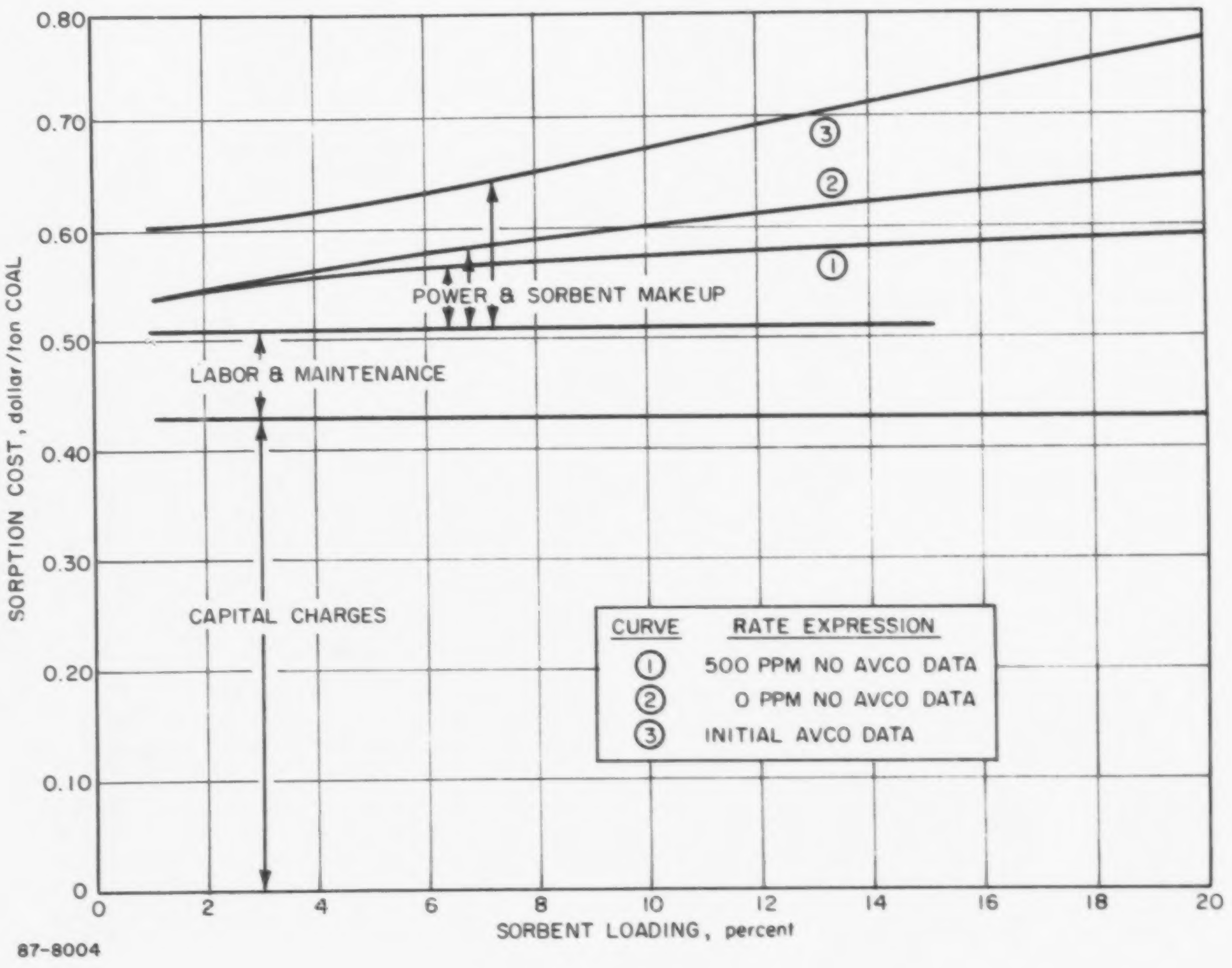

Figure 11 CALCULATED FLUID BED SORPTION COST VERSUS SORBENT LOADING
(0.060-INCH PARTICLE SIZE)

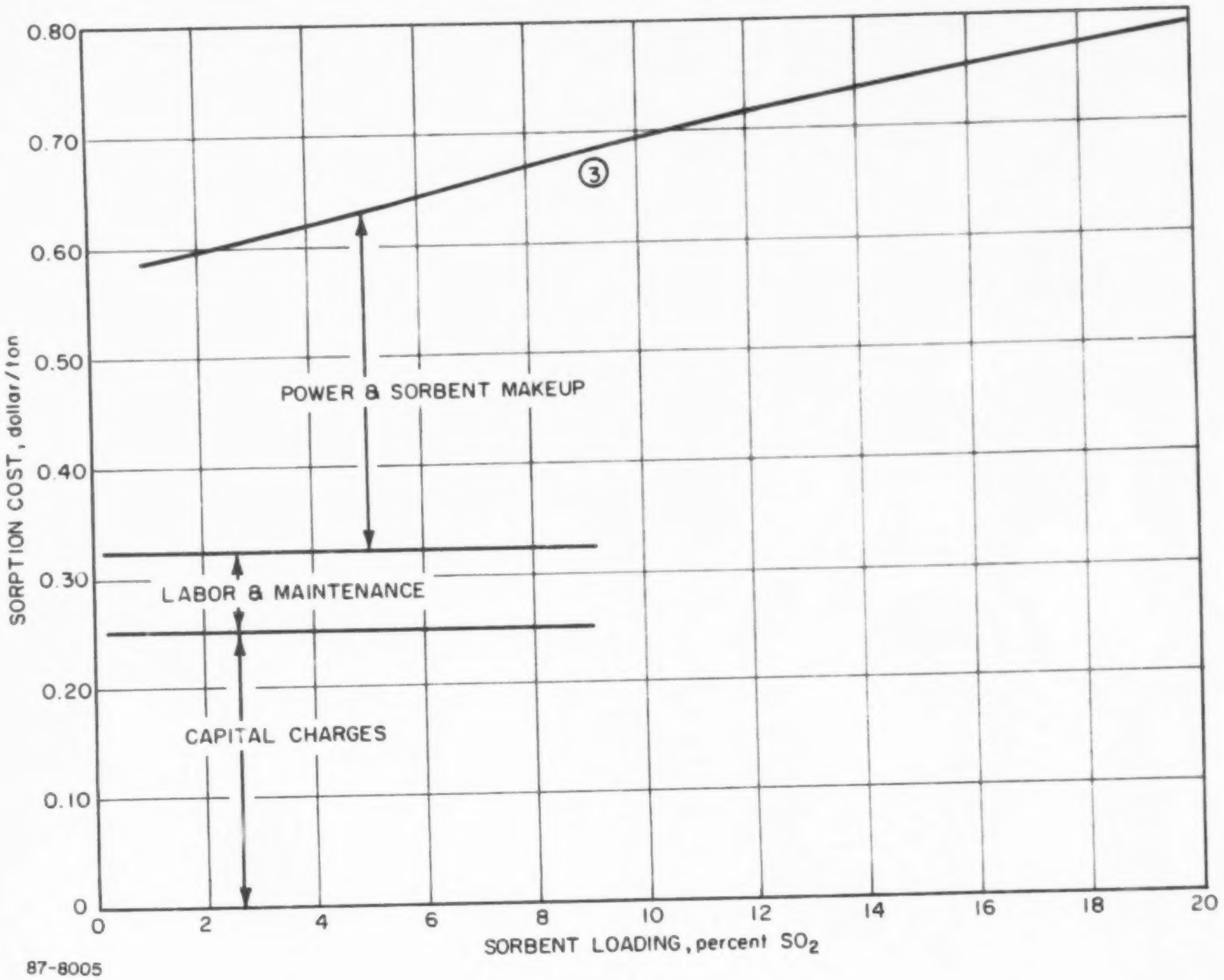

87-8005

Figure 12 CALCULATED FLUID BED SORPTION COST VERSUS SORBENT LOADING
(0.104-INCH PARTICLE SIZE)

flue gas velocity was 5 ft/sec (330° C), and the pessimistic rate constant was used. Although the capital charges, by virtue of a smaller plant, are decreased substantially, the overall cost is not changed markedly from the case with 0.060 inch particles, because larger sorbent inventories, and hence greater power requirements and sorbent makeup, are required.

2. Regeneration of Alkalized Alumina

Sulfur is recovered from alkalized alumina sorbent by chemical reduction at elevated temperature. Regeneration of the sorbent requires three basic steps: (1) heating the sorbent to 650-700° C, (2) chemically recovering the sulfur from the alkalized alumina with a reducing gas, and (3) recovering the sensible heat of the sorbent above sorption temperatures. The first and third steps are accomplished in economizers, and the second step is carried out in a regenerator.

a. Chemical regeneration

Regeneration is assumed to be carried out by moving the sorbent countercurrent to a producer gas in a moving bed type of device. Bienstock and Katell have given details on the producer gas composition from which a material balance is determined.

As was explained in Section III.A, the kinetics of alkalized alumina regeneration have not been reduced to a rate equation. Consequently, a regenerator design is based upon a sorbent residence time of one hour, estimated from the regeneration data.

1) Equipment -- The regenerator is assumed to be a tower 20 feet in diameter, the height being determined by the kinetics of regeneration. The unit is constructed of a stainless or clad material, costing one dollar per pound fabricated. Two dampers are required for each unit, and because of the high temperature, corrosive service, they are estimated to cost $20,000 each. The sorbent enters and leaves the regenerator through a sorbent feeder device. The pressure drop for the regenerator is generated at the gas producer and the cost of the fan is assumed included in the cost of the gas producer. The summary cost, including the 3.5 plant factor is

$$[(0.0204)\,N + (0.122)]\ \$/\text{ton coal/yr.}$$

where N is the number of units.

2) Labor and Maintenance -- The cost of labor and maintenance is estimated to be $(0.0186)N$ \$/ton coal.

3) Utilities - Electric Power -- As for the sorption process, the major utility cost for regeneration is the electric power for the fans. The power requirement is calculated by trading the cost of equipment against the cost of power. Using a power cost of 6 mils per kilowatt-hour the annual cost of power for pushing the producer gas through the regenerator is

$$\frac{1}{w_f}\left[\frac{(0.02195)}{N^2} + \frac{(0.00694)}{N^3}\right] \quad \$/\text{ton coal}$$

4) Materials - sorbent makeup -- The attrition, and subsequent losses of sorbent account for the major materials costs in the chemical regenerator. In the moving bed system, attrition is measured as a percent of the sorbent flow rate. In this analysis, the sorbent loss is assumed to be 0.05 percent of the throughput. At 25 cents per pound, the cost of sorbent makeup is

$$\left[\frac{0.0126}{w_f}\right] \quad \$/\text{ton coal}$$

5) Annual operating cost -- The annual operating cost comprises 1) operating labor and maintenance including overhead, 2) utilities and raw materials, and 3) amortization of the plant investment including the working capital. The annual cost of regeneration is modeled as

$$C_{RGN} = \left\{ \underbrace{(0.0174) + (0.0221)\,N}_{\substack{\text{Capital Charges,}\\ \text{Labor and Maintenance}}} + \underbrace{\frac{(0.0146)}{w_f}}_{\substack{\text{Sorbent}\\ \text{Makeup}}} + \underbrace{\frac{1}{w_f}\left[\frac{(0.0220)}{N^2} \quad \frac{(0.00694)}{N^3}\right]}_{\text{Power}} \right\} \$/\text{ton coal}$$

According to the model, there is an optimum number of regenerator units for each sorbent loading. This optimum is obtained by balancing capital and operating charges against power requirements for moving the gas through the regenerator. The minimum estimated cost is presented as a function of sorbent loading in Figure 14. The unit regeneration cost decreases continuously as the sorbent loading increases.

b. Sorbent heat economizers

In heating the sorbent from the 330° C sorber temperature to 650-700° C for chemical regeneration, the sensible heat increase of the sorbent exceeds the energy of chemical reaction, except for near saturation loadings. It is essential that this energy be recovered.

One scheme for energy conservation involves a gas stream which recovers heat from the regenerated sorbent and then preheats the incoming sorbent as shown in Figure 13. The requirements for the step are (1) moving bed contactors for the gas-sorbent heaters, (2) a source of high temperature heat, and (3) fans for moving the gas stream through the equipment. The flow rate of gas in the system, and heat loads are proportional to the sorbent throughput, and consequently inversely proportional to the sorbent loading.

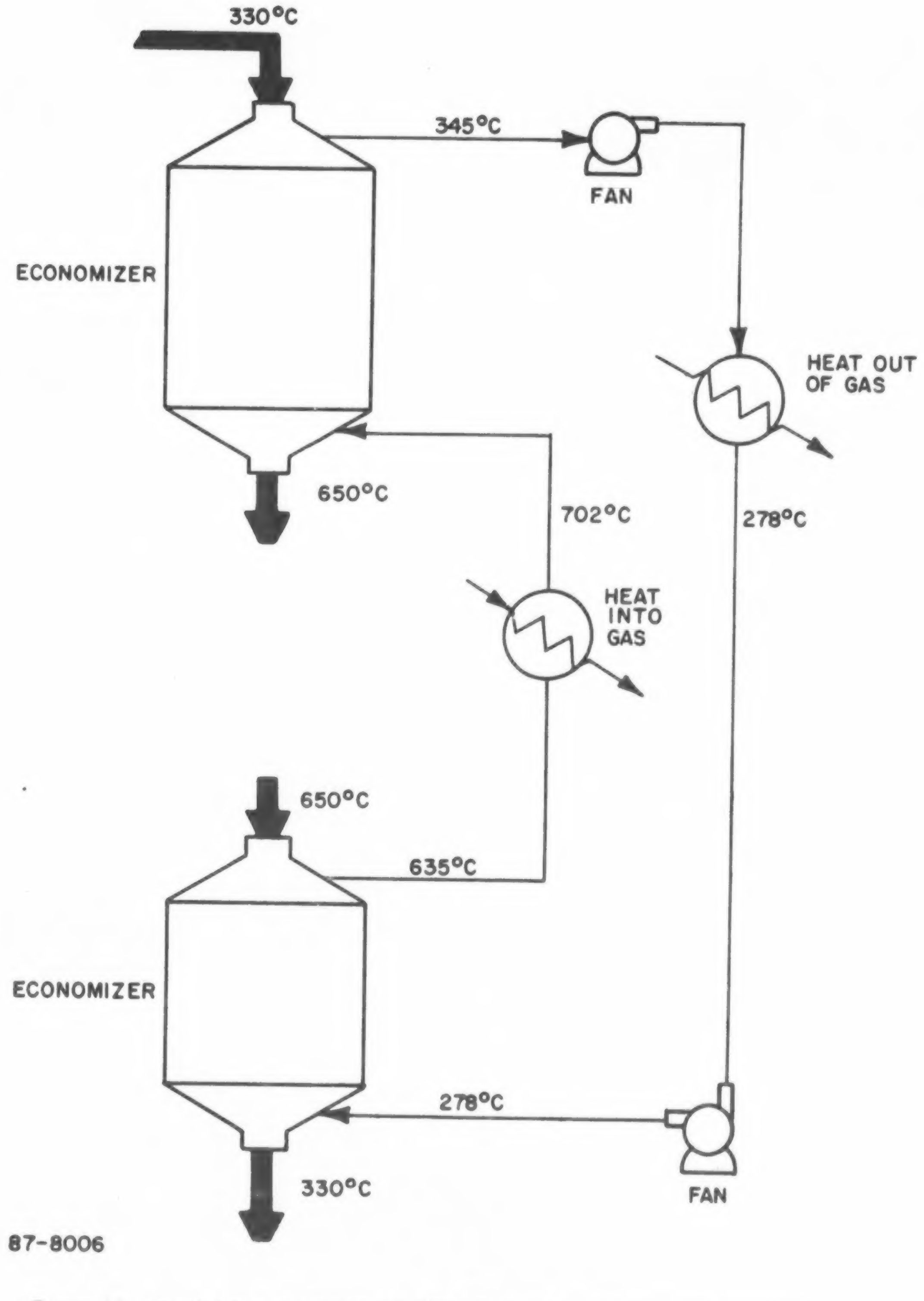
330°C
345°C
FAN
ECONOMIZER
HEAT OUT OF GAS
650°C
702°C
278°C
HEAT INTO GAS
650°C
635°C
ECONOMIZER
278°C
FAN
330°C
87-8006

Figure 13 SCHEMATIC DIAGRAM OF SORBENT HEAT RECOVERY SYSTEM

The theoretical height of each economizer is determined by heat transfer between the gas and sorbent. A 15° C temperature difference is used throughout the exchanger.

The number of economizers was set equal to the number of regenerators, and the diameter was determined by the pressure drop considerations. The following bases were used for preparing a cost estimate: (1) power at 6 mils/kw-hr, (2) stainless steel vessels at $1.00 per pound, fabricated, (3) labor and maintenance at $20,000 per unit per year, (4) capital charges at 14 percent per year. On these bases, the cost was obtained as a function of (1) the number of regenerator units, (2) the size of the sorber, and (3) sorbent loading. The estimated costs are presented in Figure 14 and show a decrease with increasing sorbent loading.

Costs were made for three particle sizes and indicated only a small effect on particle size.

Heat must be added to the economizer gas prior to the unit where the sorbent is heated to 650° C. Because the gas leaving this unit has a higher temperature than the 330° C desired for the sorbent returning to the sorber, the gas temperature must be reduced before being returned to the economizer. Neglecting the heat losses in the cycle, but including losses for the economizers, the heat load in the exchangers is related to the sorbent throughput.

$$Q = \frac{0.298}{w_f} \quad Btu/ton\ coal \tag{28}$$

At a cost of 70 cents per million BTU for the high temperature heat, the cost is

$$C_H = \frac{0.00165}{w_f} \quad \$/ton\ coal \tag{29}$$

A credit for the low temperature heat at 50 cents per million BTU is

$$C_C = \frac{0.001185}{w_f} \quad \$/ton\ coal \tag{30}$$

c. Summary

The cost for the regeneration process including the energy economizers has been estimated as a function of sorbent loading. The data are presented in Figure 14 and illustrate how these costs decrease with increase in sorbent loading. The calculations assume 1 hour of sorbent residence time in the chemical regenerator, and the residence time of the sorbent is also about 1 hour in each of the economizers. The equipment was sized based on the assumptions given, and no effort was made to effect an optimum utilization of the heat involved.

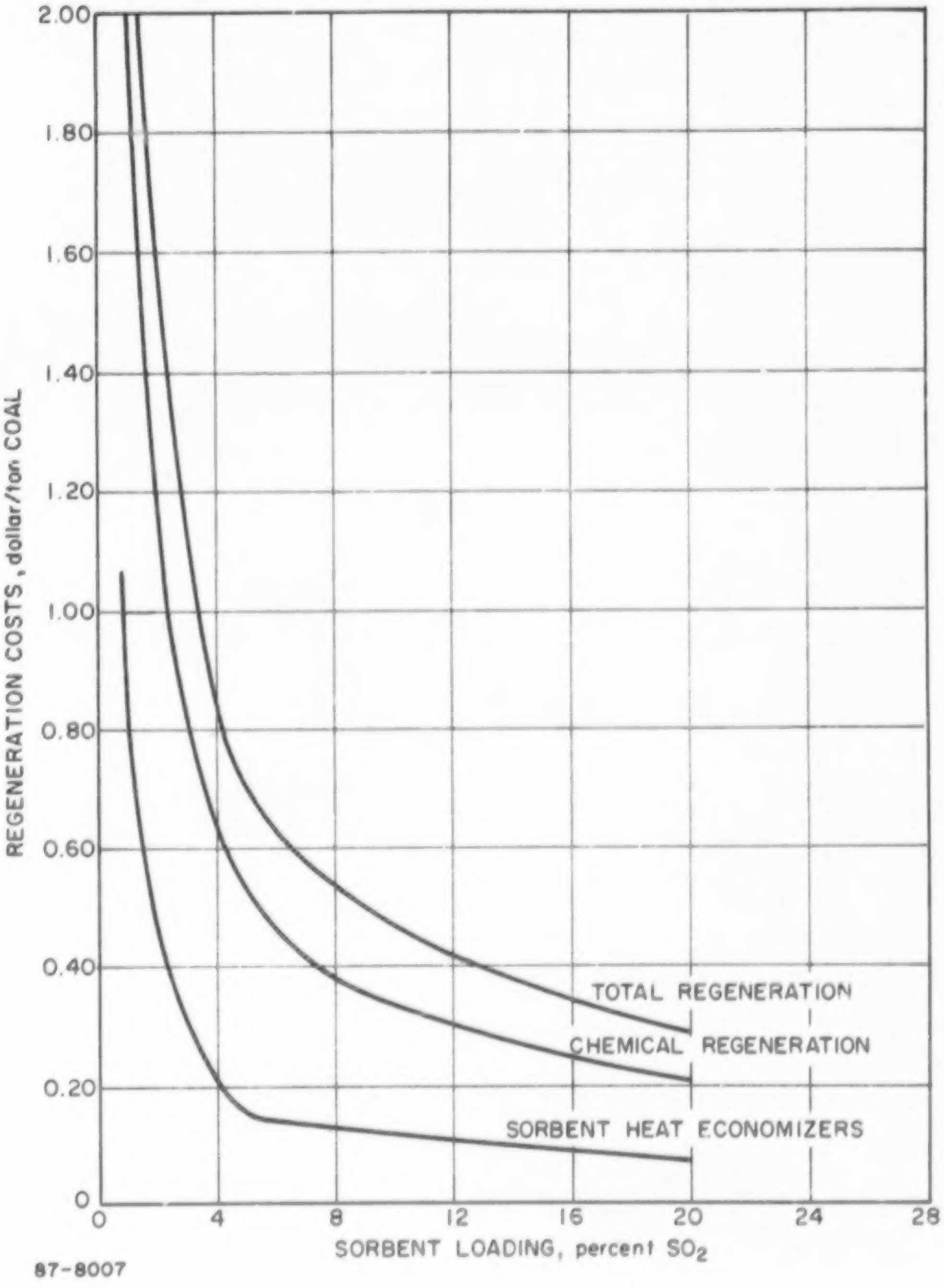

Figure 14 CALCULATED REGENERATION COST VERSUS SORBENT LOADING

Calculations with sorbent particle sizes of 0.033 to 0.104 inch showed that there was only a small effect of size on the overall cost.

3. Sulfur Recovery

Recovery of the sulfur from the sulfate form of the alkalized alumina may be accomplished by reacting the sorbent with producer gas. The hydrogen sulfide formed is then reduced to elemental sulfur. Thus, two units are required for the alkalized alumina process; a gas producer and a Claus Unit. The costs associated with these items are fixed by the size of the power plant and are independent of the type of sorber.

a. Gas producer

The cost of a gas producer (installed) for an 800 Mw plant has been estimated, by Katell[9], at $650,000. Operation includes raw materials, labor and maintenance, and amortization of the investment.

1) Labor and maintenance -- A crude estimate of operating labor is $23,120 per year, including overheads, and of maintenance is $36,800 per year.

The most important raw materials are coal and water. At $5 per ton, the coal for the producer costs 0.245 $/ton coal a year and the water cost is negligibly small. The fuel cost which represents a major operating cost for this unit may be considerably higher depending on the location of the power plant.

The total investment is 0.364 $/ton/yr, and with an amortization of 14 percent per year, the capital charges contribute 0.051 $/ton/coal to the annual cost.

Capital charges	0.051 $/ton
Materials	0.246
Labor and Maintenance	0.027
Total cost	0.324 $/ton coal

b. Sulfur recovery - Claus unit

The gas stream from the regenerator contains nitrogen, hydrogen, carbon monoxide, hydrogen sulfide, and other trace gases. The hydrogen sulfide is converted to sulfur by combustion in a controlled amount of air, according to

$$H_2S + \frac{1}{2} O_2 = S + H_2O \qquad \Delta H_{298} = -53\ kcal$$

Effective operation of the hydrogen sulfide converter requires that a low temperature be maintained, even in the presence of combustion. The regenerator gas, at about 650° C, must be cooled to 300° C before the Claus Unit. Because of the composition of the regenerator gas (presence of CO, H_2 and illuminants), approximately 10.1 kcal of heat will be produced per mole of gas fed to the unit, and this heat may be used in the plant with a credit toward the SO_2 process.

The cost of a Claus unit with a capacity of 8.4 tons of sulfur per hour has been costed by Katell[5]. The investment for such a unit is $1,780,000.

Operation of the Claus Unit, assumed to require 3 men each for operation and maintenance, and with capital charges of 14 percent per year, adds 0.288 $/ton coal. There is a net heat production which credited at 50¢/10^6BTU offsets the cost by about 24¢/ton coal.

D. SUMMARY PROCESS CALCULATIONS

Costs were estimated for the sorption, regeneration, and sulfur recovery steps in the process as a function of sorbent loading. Because the regeneration cost decreases so markedly with increased sorbent loading, the process should be operated at high sorbent loadings. The estimated costs for the process using a dispersed bed sorber are shown in Figure 15. Two sorption rate curves (obtained from Figure 1) were used. At the highest rates the minimum cost occurs at 20 percent loadings, or greater. Very high recycle ratios e.g. 45, are calculated for this case; pressure drops are about 10-15 inches of water. As the effective sorption rate decreases, the optimum loading decreases. For sorption rate curve II, for example, the lowest cost occurs at loading of about 15 percent.

The calculated costs for the process with a fluid bed sorber are presented in Figure 16. The costs were minimized at 20 to 25 percent SO_2 loadings. The process cost is sensitive to the effective sorption rate, particularly at high loadings, but it is less sensitive than the dispersed bed sorber. Cost should be in the vicinity of $1.20 to $1.40 per ton of coal.

E. REFERENCES

1. Bienstock, D. et al., Bureau of Mines, IC 7836, U. S. Department of Interior, 1958.

2. Bienstock, D., J. H. Field and J. G. Myers, Bureau of Mines RI 5735, U. S. Department of Interior. 1961.

3. Bienstock, D., J. H. Field and J. G. Myers, Bureau of Mines RI 5735, U. S. Department of Interior, 1961.

4. Bienstock, D., J. H. Field and J. G. Myers, Bureau of Mines RI 7021, U. S. Department of Interior, July, 1967.

5. Katell, S., Removing SO_2 from Flue Gases, Chem. Eng. Prog., 62, 10, October, 1966.

6. Bienstock, D., J. H. Field and J. G. Myers, Removal of Sulfur Oxides from Flue Gas with Alkalized Alumina at Elevated Temperatures, J. Eng. Power, pp. 353-360, July, 1964.

E. REFERENCES (Concl'd)

7. Narsimham, G., On Generalized Expression for Prediction of Minimum Fluidization Velocity, A.I.Ch.E. Journal, 11, 3, 550-554 (1965)

8. Bird, R. B., W. E. Stewart and E. N. Lightfoot, Transport Phenomena, John Wiley and Sons, New York, pg 200, (1960).

9. Newell, J., Conference on Alkalized Alumina Process, Slade, Kentucky, September, 1967.

10. Air Pollution Research Progress Report. U. S. Bureau of Mines, June 30, 1967.

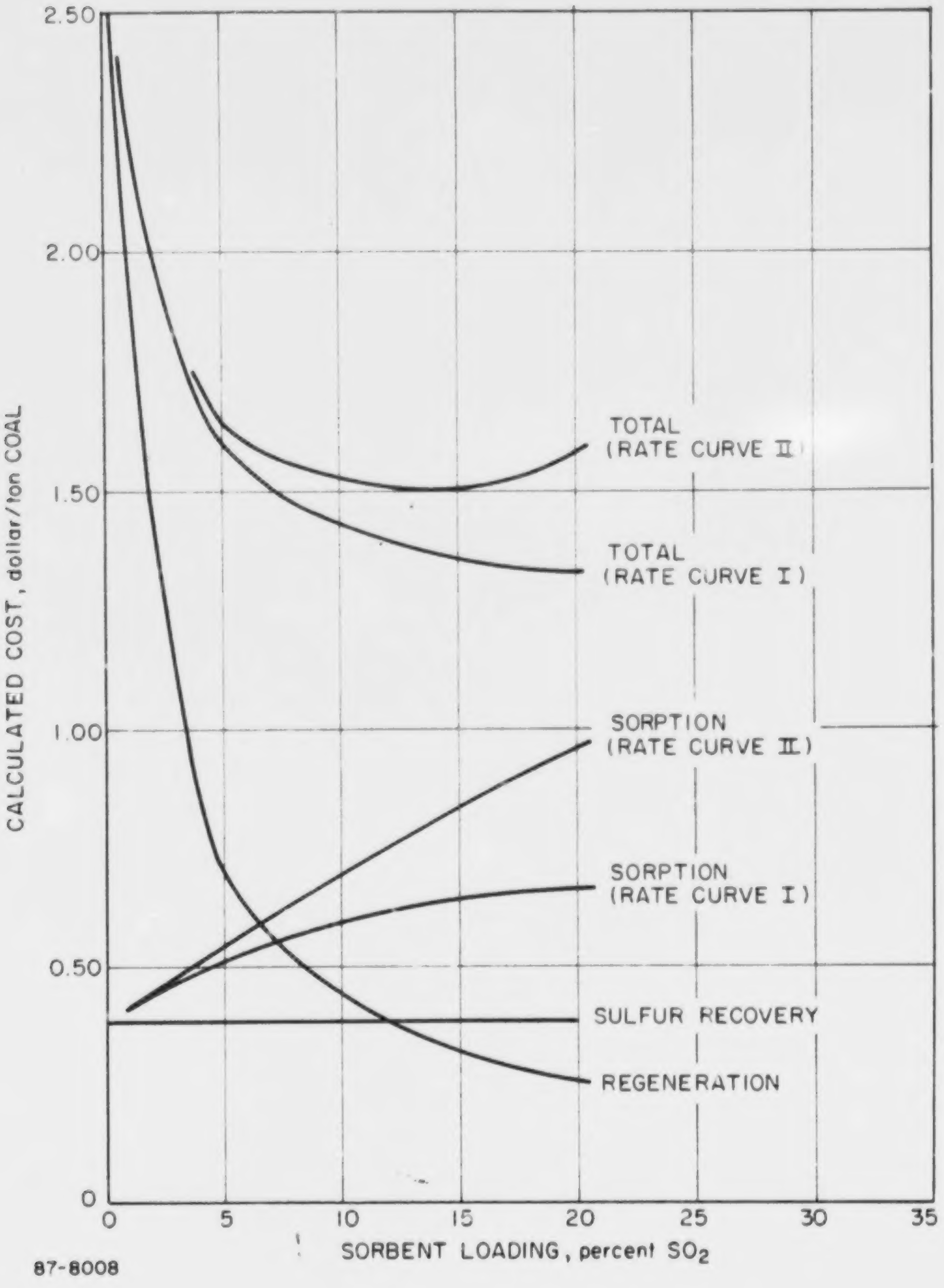

Figure 15 SUMMARY ESTIMATED COST OF DISPERSED BED SYSTEM VERSUS SORBENT LOADING

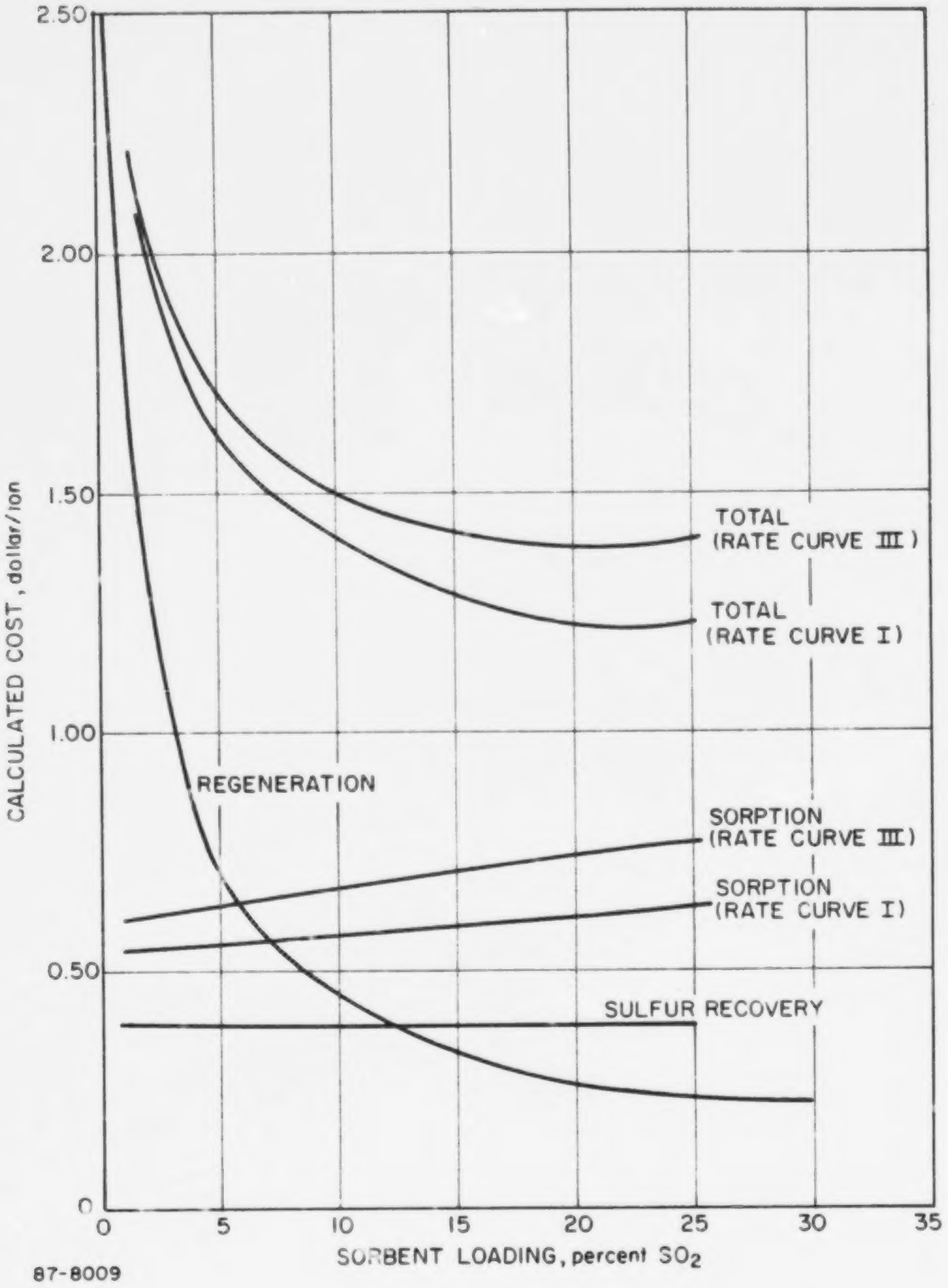

Figure 16 SUMMARY ESTIMATED COST OF FLUID BED SYSTEM VERSUS SORBENT LOADING

IV. KINETICS OF SORPTION AND REGENERATION

A. INTRODUCTION

The rate of sorption of sulfur dioxide from a simulated flue gas onto alkalized alumina has been investigated. The effect of several important variables on the sorption rate has been measured experimentally. The rate was determined as a function of sulfur dioxide loading on the sorbent, the gas velocity past the sorbent particles, sorbent temperature, particle diameter, SO_2 partial pressure, and moisture content of the flue gas. Particle diameter was varied from 0.066 inch to 0.10 inch, and sorption temperature from 150° C to 350° C. The concentration of SO_2 was varied between 0.07 and 1.0 percent while the moisture content was 0 to 10 percent. Sorbent loading was varied from zero to essentially complete saturation.

The sulfur dioxide levels chosen for most of the runs are somewhat higher than those found in actual flue gas. The higher values were used in order that the SO_2 analyses could be reasonably accurate. The analyses were carried out with a Perkin-Elmer chromatograph.

The sorption is believed to take place as SO_3 rather than SO_2. The envisioned reaction is $SO_2 + \frac{1}{2}O_2 + Na_2O \rightarrow Na_2SO_4$. Sorption in the absence of oxygen in the simulated flue gas (SFG) produced a sorbate which was completely removed while heating to 650° C in vacuum. On the other hand a reducing atmosphere was required to regenerate sorbent which was saturated with SO_2 in the presence of oxygen, indicating the formation of the more stable sulfate.

The conclusion that the sorbate is a sulfate is further substantiated by equilibrium computations for the following reaction which indicate that the oxidation step from sulfite to sulfate is favored at stack conditions.

$$Na_2SO_3 + \frac{1}{2} O_2 \rightarrow Na_2SO_4$$

T, ° C	ΔF, kcal	$P_{O_2} = 1/K_p^2$, atm
25	-63.28	$10^{-93.0}$
700	-46.7	10^{-21}

In addition, the following computations indicate the feasibility of regeneration of sulfite in high vacuum and of sulfate in hydrogen.

$$Na_2SO_3 \rightarrow Na_2O + SO_2$$

T, ° C	ΔF, kcal	P_{SO_2}, atm = K_p
25	68.71	$10^{-50.5}$
200	55.03	$10^{-25.5}$
400	39.03	$10^{-12.73}$
700	21.08	$10^{-4.75}$

$$Na_2SO_4 + 4H_2 \rightarrow Na_2O + H_2S + 3H_2O$$

T, ° C	ΔF, kcal	K_p	$(P_{H_2S}/P_{H_2}) = \frac{1}{228} K_p^{1/4}$*
25	31.97	$10^{-23.5}$	$10^{-6.21}$
150	23.27	$10^{-12.02}$	$10^{-3.37}$
300	13.25	$10^{-5.06}$	$10^{-1.627}$
500	0.75	$10^{-0.212}$	$10^{-0.41}$
700	-11.4	$10^{+2.34}$	$10^{0.225}$

* assuming $P_{H_2O} = 3P_{H_2S}$

X-ray analysis of the sorbent indicates that it is sodium aluminate ($NaAlO_2$) rather than sodium oxide (Na_2O) on alumina. Thus, the equilibrium computations are not strictly applicable. Nonetheless these computations should still suffice to indicate the differences between sulfite and sulfate sorption and regeneration. Finally, chemical analysis of saturated sorbent for sulfur indicated that the weight gained corresponded to SO_2 in the absence of oxygen and SO_3 in the presence of oxygen.

The rate of regeneration was also measured over a range of variables. Temperature was varied from 550° C to 700° C. The regeneration gas was usually pure hydrogen although for various runs it was diluted with nitrogen, carbon monoxide, or the reaction products water and hydrogen sulfide. Sorbent loading was varied from less than ten percent of saturation to essentially complete saturation.

B. APPARATUS

A differential or shallow bed reactor was used to bring the sorbent in contact with the flue gas. This allowed the gas composition to be taken as the value at the inlet of the reactor. The bed temperature and sorbent loading could be considered spatially uniform.

1. Cahn Electrobalance Apparatus

Initial experiments were performed in the TGA type device indicated schematically in Figure 17. A sample of sorbent placed in the sample pan was exposed to various gases passed through the hangdown tube. The sample temperature was maintained with a furnace surrounding the tube. The weight of the sample was continuously recorded on a strip chart using a Cahn Electrobalance. Thus it was possible to continuously follow the sorption and regeneration steps with various gas compositions and at various temperatures.

The system suffered from the disadvantage that the output of the Cahn balance was noisy at the flow rates required and the accuracy and precision of the equipment was compromised. Also, the working parts of the balance were exposed to the same atmosphere as the sorbent and corrosion soon rendered the balance inoperative.

2. Torsion Balance Apparatus

As a result of the difficulties experienced in using the Cahn balance and as a result of its mechanical failure, a second facility was set up using a precision torsion balance to determine the sample weight. The new system had the advantage that the balance was not exposed to the corrosive atmosphere at the sample.

The torsion balance readout is not automatic, however, requiring closer operator attention than the Cahn. The balance can be read to 0.1 mg but a standard error of about 0.3 mg seems likely. The sample weights were about 250 mg.

A diagram of the new system is given in Figure 18. The figure is divided into sections A, B, and C for ease of description.

Section A consists of the quartz tube reaction chamber mounted in a vertical muffle furnace. Furnace temperature is controlled to ±10° C during sorption and ±3° C during regeneration by a West saturable reactor type controller. The torsion balance is mounted directly above the furnace. A stainless steel screen basket to carry the sorbent is supported from the balance on fine platinum wire. Reactant gases enter the reaction chamber at the bottom. A nitrogen purge at the top of the chamber prevents reactants from escaping to the room, but does not mix with the reactants at the sample.

Section B contains the equipment to make up sorption gas mixtures. The make-up procedure is as follows. The cylinder marked SFG + SO_2 is pumped down. Then SO_2 and SFG (standard flue gas N_2 - 81.3 percent, CO_2 - 15.1 percent, O_2 - 3.6 percent) are charged to this cylinder to the desired partial pressures. Alternately, SO_2, O_2, N_2 and CO_2 may be charged individually.

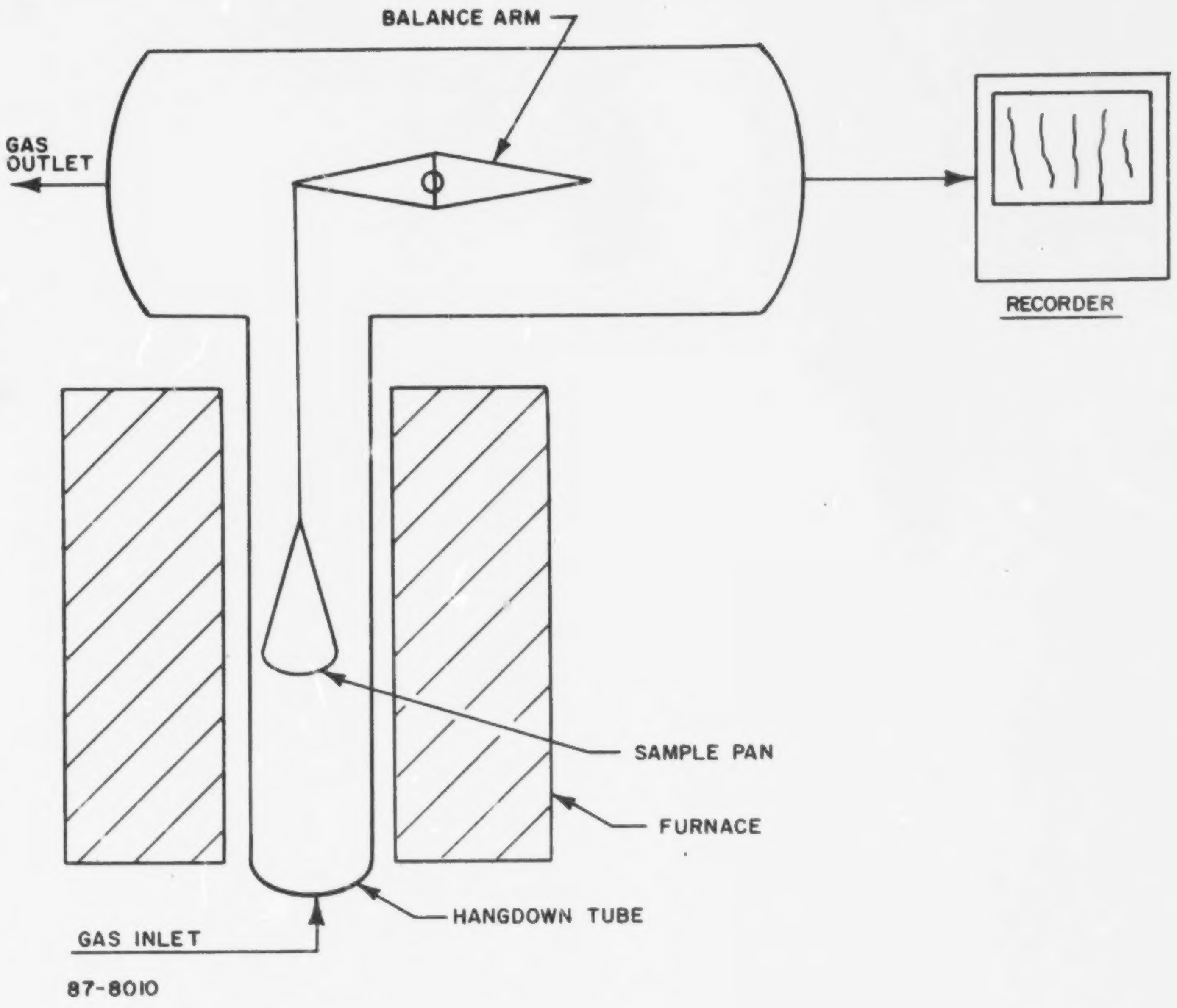
BALANCE ARM
GAS OUTLET
RECORDER
SAMPLE PAN
FURNACE
HANGDOWN TUBE
GAS INLET
87-8010

Figure 17 TGA APPARATUS WITH CAHN ELECTROBALANCE

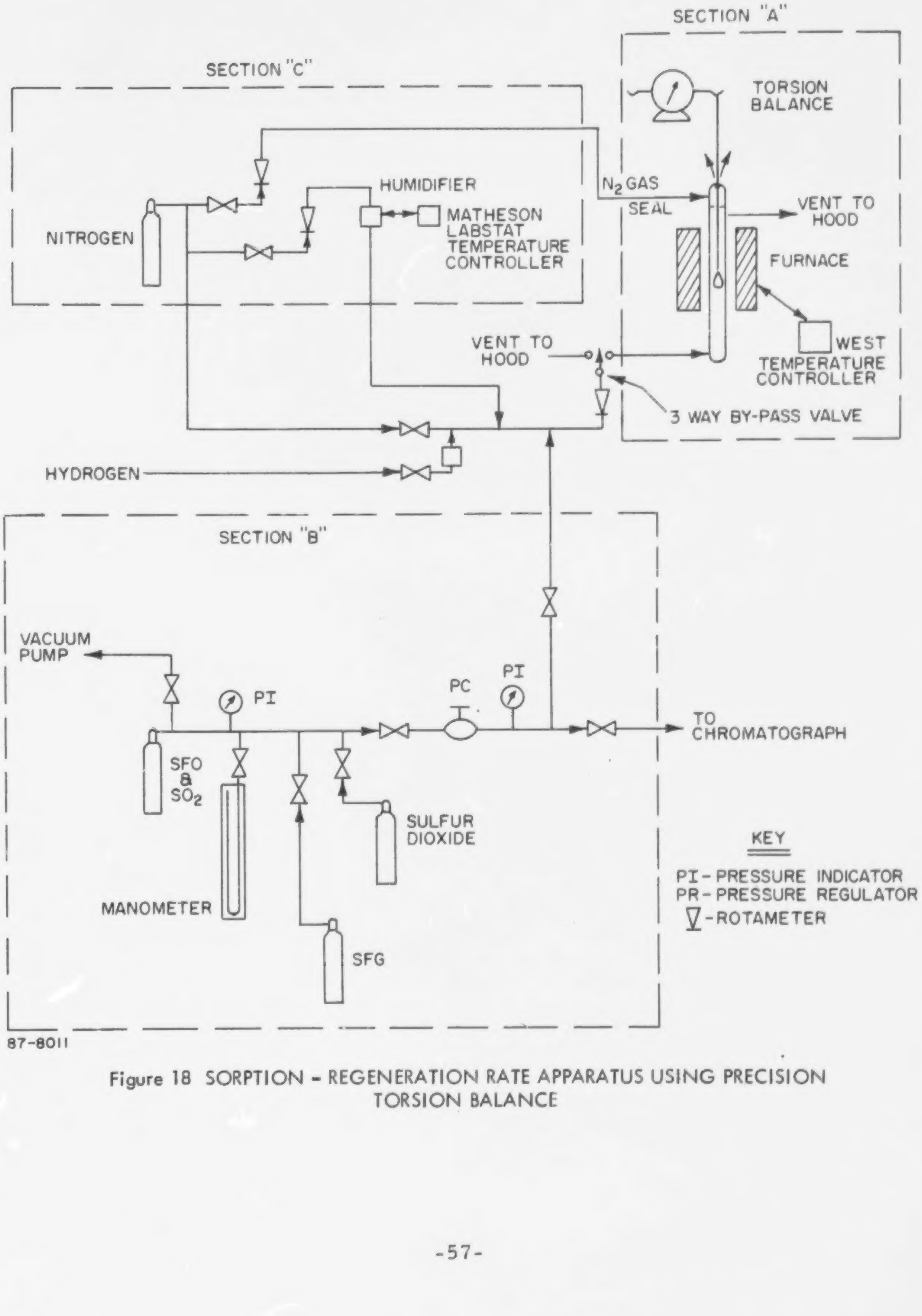
SECTION "A"
TORSION BALANCE
SECTION "C"
HUMIDIFIER
N_2 GAS SEAL
VENT TO HOOD
NITROGEN
MATHESON LABSTAT TEMPERATURE CONTROLLER
FURNACE
VENT TO HOOD
WEST TEMPERATURE CONTROLLER
3 WAY BY-PASS VALVE
HYDROGEN
SECTION "B"
VACUUM PUMP
PI
PC
PI
TO CHROMATOGRAPH
SFO & SO_2
SULFUR DIOXIDE
MANOMETER
SFG
KEY
PI - PRESSURE INDICATOR
PR - PRESSURE REGULATOR
▽ - ROTAMETER
87-8011

Figure 18 SORPTION - REGENERATION RATE APPARATUS USING PRECISION TORSION BALANCE

Section C provides purge N_2 to both the top and bottom of the reaction chamber. Nitrogen is also provided to a humidifier from which N_2 with a controlled moisture content may be added to the reactant gases. The humidifier water temperature is controlled to ± 0.2° C with a Matheson Lab-Stat controller.

A chart recorder or stop watch provides a time base for the experiments depending on the mode of operation.

A chromatograph is used to analyze the reactant gases for SO_2. This provides a more accurate check of SO_2 concentration than the estimation of the concentration from the measured partial pressure of SO_2 introduced into the sample gas cylinder.

A Perkin-Elmer Model 154 chromatograph with a printing integrator attachment is being used. The column is either Triton X-305 on Chromosorb P on Teflon and is operated at 50° C. The peak area has been shown to be linear in SO_2 concentration of the sample. Accuracy is estimated to be within 5 percent of the reading at the low concentrations being used.

Two configurations in the sorption chamber have been employed. For runs S-1, R-1, through S-73, R-73, the basket containing the sample was allowed to hang freely in the reactor and the weight of the sorbent during sorption and regeneration was continuously observed on the torsion balance. The same procedure was followed for both sorption and regeneration.

With this apparatus, there was a possibility that the gas by-passed the sample basket and under these conditions the actual gas velocity past the sorbent particles was not known. Consequently, it could not be determined whether the initial rate was controlled by bulk convective transfer or by a kinetic process. In order to check this point the reaction tube was modified to the configuration shown in Figure 19.

During sorption, the sample basket was allowed to rest on the screen covering the end of the inner quartz tube. As the basket was approximately the same diameter as the inner tube by-passing was eliminated. Sorption was run for periods timed with a stop watch. At the end of the desired period solenoid valves were actuated to sweep out the reaction tube with nitrogen. The sweep out time was about one second. The sample was then raised to the point that it could hang freely on the torsion balance, and weighed. The sample was then lowered and the flue gas mixture introduced, again with solenoid valves, thus beginning the next sorption period. No regeneration data have been taken in this modified device. Due to the high concentration of reactants in the regeneration gases interphase reactant mass transfer is not a problem in regeneration.

Until this modification, the temperature had been measured with a thermocouple on the outer surface of the reaction tube. Because of the high gas velocities in the latest configuration it has been discovered that a temperature difference of as much as 50° C existed between the outside and the center of the tube, during the sorption cycle only. Beginning with run S-78 the temperature has been monitored with a thermocouple located within the reaction tube, just below the end of the inner tube. The temperature within the chamber was maintained ±10° C during sorption.

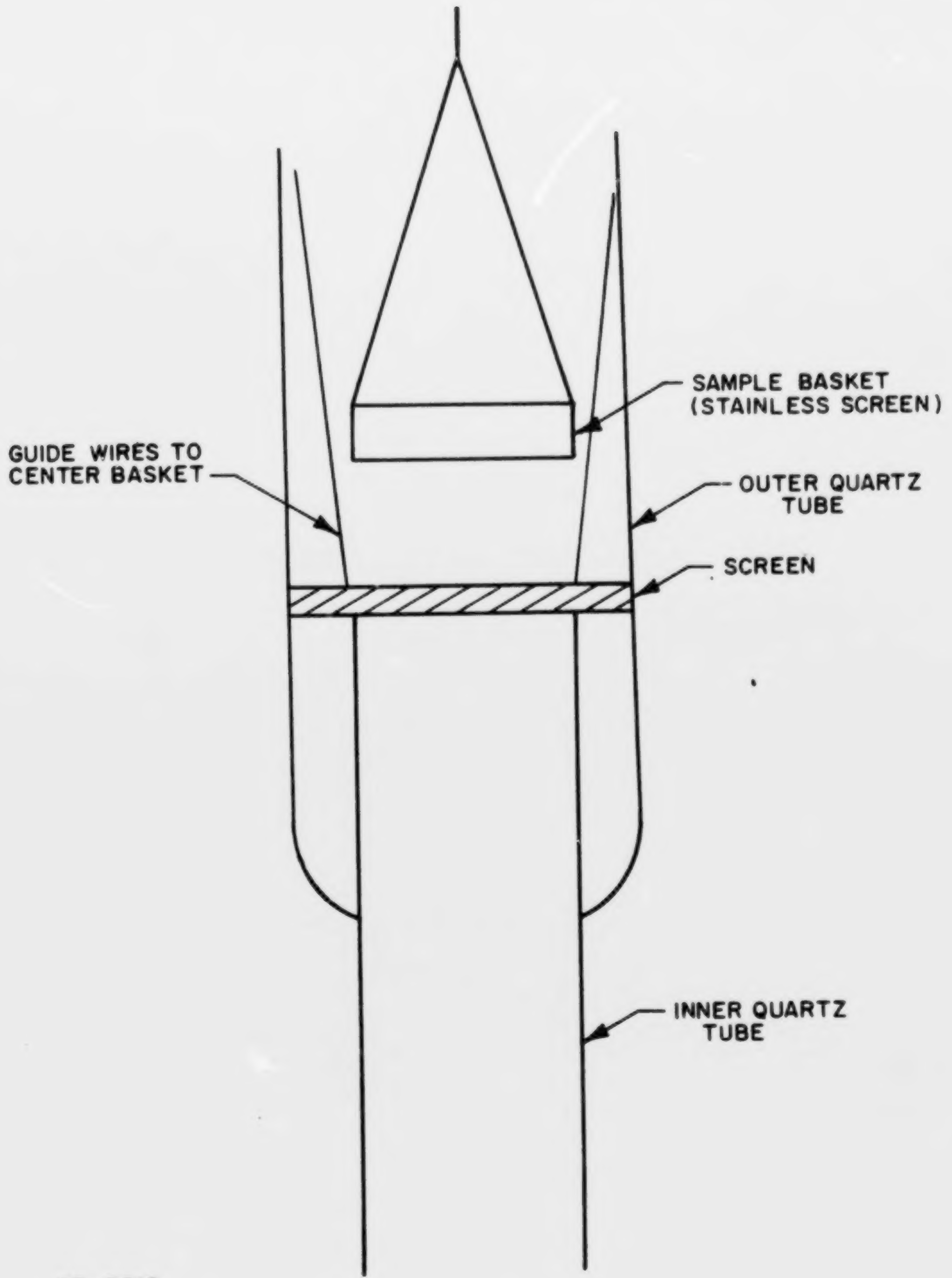

SAMPLE BASKET (STAINLESS SCREEN)
GUIDE WIRES TO CENTER BASKET
OUTER QUARTZ TUBE
SCREEN
INNER QUARTZ TUBE

87-8012

Figure 19 MODIFIED REACTION CHAMBER

C. PROCEDURE

1. Original Torsion Balance Apparatus, Runs S-1, R-1 Through S-73, R-73

a) Sorption

A sample of sorbent was weighed out on a laboratory balance and charged to the reaction tube. The indication of the torsion balance was recorded. Then the sample was heated to 300° C in nitrogen and the weight loss (assumed to be water) was noted.

Nitrogen was then introduced to the reaction chamber at the same flow rate to be used for flue gas. The sample weight in flowing nitrogen was noted and recorded as the initial weight. (The initial weight so obtained can be several milligrams less than the weight with no flow due to aerodynamic drag on the sample.) The nitrogen was then by-passed from the reaction chamber, simulated flue gas was substituted for nitrogen and humidified nitrogen mixed with the flue gas. A few minutes were allowed for the humidifier to come to equilibrium and then the moist flue gas was diverted to the reaction chamber.

The starting time was recorded by pulsing the input to a strip chart recorder with a known chart speed. The torsion balance was then set to a higher weight and when balance was indicated by the balance pointer the timer was again pulsed and the weight was recorded. This procedure was carried out without interruption of the flow until sorption was complete.

b) Regeneration

At the completion of the sorption step the reactor was completely purged with nitrogen and the temperature raised to the regeneration temperature. When the temperature was steady at the desired value the regeneration gas (usually hydrogen) was substituted for nitrogen and the weight and time recorded as during the sorption. The flow rate of hydrogen was sufficiently small that there was not a significant difference between static and flowing weights. The weight loss in nitrogen upon heating from the sorption temperature to the regeneration temperature was taken as the difference between the weight gain during sorption and the weight loss during regeneration. Runs S-1, R-1 through S-73, R-73 were made with this procedure.

2. Modified Torsion Balance Apparatus, Runs S-74, R-74 and Later

The sample was introduced into the apparatus just as previously described. After heating to constant weight in nitrogen the gas flow was by-passed from the reactor. Then the SO_2 containing flue gas and humidified nitrogen were started flowing through the by-pass. The initial weight of the sample was determined and the sample was then lowered so that it rested on the screen in the reactor. The moist flue gas was then diverted to the reactor and a stop watch started. At the end of the desired sorption cycle the flue gas was diverted from the reactor and the reactor swept out with nitrogen. The change of the environment was accomplished quickly and timed accurately by the use of solenoid valves. Sweep out time was about one second.

All gases to the reactor were then by-passed, the sample basket raised from the screen and the sample weighed.

The sample was then lowered and another cycle begun. The process of sorbing and weighing was repeated until the sorbent was essentially saturated. Note that during weighing the sample was elevated only high enough to allow the sample basket to swing freely and that the sample remained in the hot zone of the reactor during weighing.

D. SORPTION STEP

1. Mathematical Model of Sorption Step

The kinetics of absorption on a porous material can be treated analytically for the pore diffusion controlling case. In this situation, the sorbate is sorbed instantly upon contact with fresh sorbent as a wave with a steep front. For a spherical particle, Figure 20 depicts the concentration profiles in the gas and solid phases.

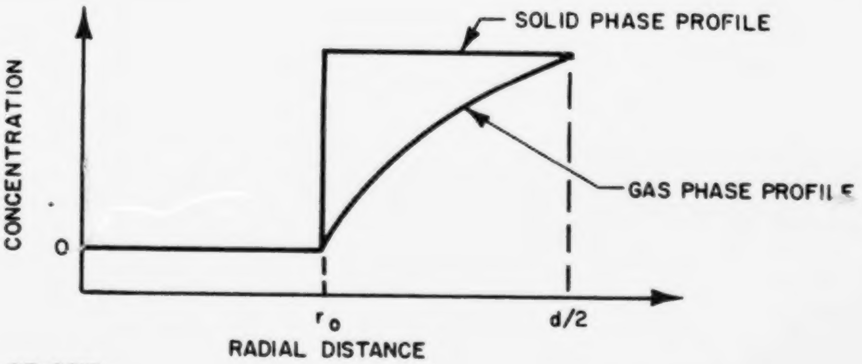

87-8013

Figure 20 CONCENTRATION PROFILES FOR PORE DIFFUSION CONTROLLING, SPHERICAL PARTICLE

The SO_2 diffuses through the outer shell of saturated sorbent (d/2 to r_o) and upon reaching the unsaturated sorbent at r_o the SO_2 is immediately sorbed causing the shell of saturated sorbent to further penetrate the solid.

It should be noted that the rate of the initial sorption on the outer surface of the particle cannot be pore diffusion controlled. Rather, a more rapid process such as bulk gas mass transfer, or chemical reaction will be rate controlling initially. The extent of loading at which pore diffusion becomes the rate limiting step will depend upon the sorbent properties (pore diameter and chemical sorption rate) and the conditions of the experiment.

For a spherical particle, the problem can be treated mathematically as follows:

1) Solve Laplace's equation, $\nabla^2 C=0$ between r_o and d/2 with C=0 at r_o and $C = C_o$ at d/2 where C_o is the bulk gas SO_2 concentration.

2) Compute the rate of diffusion of SO_2 as

$$\text{rate} = \pi d^2 D \left.\frac{\partial C}{\partial r}\right|_{r=\frac{d}{2}} \quad \frac{\text{moles } SO_2}{\text{particle, unit time}} \tag{31}$$

where D is the effective pore diffusivity of SO_2 and d is the particle diameter.

3) Compute $\partial C/\partial r$ as a function of the fractional saturation of the solid, S giving the rate as a function of S.

These computations will be carried out. A simplified approximation to the solution will be obtained.

The approximate solution will then be combined with a rate expression for bulk diffusion to find rate equations of the form

$$dW/dt = \frac{K\pi y}{1 + BW} \quad or$$

$$dW/dt = K\pi y(1 - BW) \text{ for } BW << 1$$

which have been proposed to describe the sorption kinetics.

Here

π = total pressure

t = time

W = gms SO_2/gm sorbent

y = mole fraction SO_2 in bulk gas

K, B = constants

It should be noted that $\nabla^2 C = 0$ was derived from a material balance on a spherical shell assuming a diffusion equation of the form

$$N_A = -D_{AB} \nabla C_A$$

where

N_A = total molar flux of A, moles/area, time

D_{AB} = diffusivity of A in B

∇C_A = spatial gradient of concentration of A

Spatial coordinates are fixed with respect to the particle.

This equation applies rigorously only to the Knudsen diffusion regime where diffusing molecules collide mainly with pore walls rather than other gas molecules. For diffusion in the bulk regime (larger pores) an equation of the same form will apply but with coordinates moving in the particle with the molar average velocity.* Thus, in coordinates fixed in the particle

$$N_A = -D_{AB} \nabla C_A + y_A (N_A + N_B)$$

where y_A is the mole fraction of A and where the second term on the right gives the contribution to the total flux of A due to net molar flow. In the case of SO_2 diffusing through a nearly stagnant mixture of the remaining components of flue gas in the sorbent pores, $N_B = 0$ and

$$N_A = \frac{-D_{AB} \nabla C_A}{1 - y_A}$$

But $y_A \ll 1$ for all cases considered here and to an excellent approximation

$$N_A = -D_{AB} \nabla C_A$$

for both bulk and Knudsen diffusion. Thus, the equation $\nabla^2 C = 0$ should be sufficiently accurate.

Solution of $\nabla^2 C = 0$

Assuming spherical symmetry, the solution of $\nabla^2 C = 0$ for a spherical particle is

$$C = a + \frac{b}{r}$$

Applying the boundary conditions gives

$$a + 2b/d = C_o$$

$$a + b/r_o = 0$$

---

*Bird, Stewart and Lightfoot, Transport Phenomena, Wiley, N.Y.

Solving for a and b gives

$$\frac{C}{C_o} = \frac{1}{1 - \frac{2r_o}{d}} - \frac{1}{r\left(\frac{1}{r_o} - \frac{2}{d}\right)} \tag{32}$$

Differentiating (32) with respect to r and substituting for $\partial C/\partial r$ in (31) gives

$$rate = \frac{4\pi D r_o C_o}{1 - \frac{2r_o}{d}} \qquad moles\ SO_2/particle,\ unit\ time \tag{33}$$

Now $(2r_o/d)^3 = 1-S$ where S is the fraction of the pellet saturated with SO_2. Hence,

$$rate = 2\pi d D C_o \left[\frac{(1-S)^{1/3}}{1-(1-S)^{1/3}}\right] \tag{34}$$

The rate may also be expressed as

$$rate = \frac{\pi d^3 W_o \rho}{6M} \left[\frac{dS}{dt}\right] \tag{35}$$

where

ρ = density of sorbent pellet

t = time

W_o = lbs SO_2/lb sorbent at saturation

M = molecular weight of SO_2

Equating (34) and (35) gives

$$\frac{dS}{dt} = \left[\frac{12 M D C_o}{d^2 \rho W_o}\right] \frac{(1-S)^{1/3}}{1-(1-S)^{1/3}} \tag{36}$$

This is the basic rate equation for the pore diffusion controlled model. Upon integration assuming S is zero initially we obtain

$$\frac{1}{2}\left[1-(1-S)^{2/3}\right] - \frac{S}{3} = \left[\frac{4 M D C_o}{d^2 \rho W_o}\right] t \tag{37}$$

a. Effect of bulk gas diffusional resistance

The effect of bulk gas mass transfer resistance on the overall rate can be developed from theory and is given here. The effect of the rate of chemisorption cannot be included as the rate of this process is unknown.

The rate of mass transfer of SO_2 to a spherical sorbent particle from the surrounding gas is given by

$$k_c \, (C_o - C_s) \, \pi \, d^2 \qquad \text{moles } SO_2/\text{particle, unit time} \tag{38}$$

where

C_o = bulk gas molar concentration of SO_2

C_s = molar concentration of SO_2 at particle surface

k_c = mass transfer coefficient, ft/hr.

Equating this rate to the rate of pore diffusion given by (34) gives

$$k_c \, (C_o - C_s) \, \pi \, d^2 = 2\pi \, d D C_s \left\{ \frac{(1-S)^{1/3}}{1-(1-S)^{1/3}} \right\}$$

Solving for C_s and replacing C_o in (36) gives the basic rate equation for combined bulk gas and pore diffusion controlling.

$$\frac{dS}{dt} = \left\{ \frac{6 \, k_c \, M \, C_o}{d \, \rho \, W_o} \right\} \frac{1}{1 + \dfrac{k_c \, d}{2D} \left\{ \dfrac{1-(1-S)^{1/3}}{(1-S)^{1/3}} \right\}} \tag{39}$$

b. Expansion for small loading

The function $(1-S)^{1/3}$ may be expanded as

$$(1-S)^{1/3} = 1 - \frac{1}{3} S + \frac{1}{9} S^2 + \ldots$$

To a first approximation let

$$(1-S)^{1/3} \cong 1 - \frac{1}{3} S$$

At $S = 0.5$ the approximation is still good to better than 5 percent, at $S = 0.75$ the approximation is in error by 15 percent. Substituting this approximation in (40) gives

$$\frac{dS}{dt} \simeq \left\{ \frac{6\, k_c\, M\, C_o}{d \rho\, W_o} \right\} \left[\frac{1}{1 + \frac{k_c}{6D} \left\{ \frac{S}{1 - S/3} \right\}} \right] \tag{40}$$

We may neglect $S/3$ compared to unity to an accuracy of 10 percent for $S = 0.25$.

Making this approximation and writing $W = S W_o$

$$\frac{dW}{dt} \simeq \left\{ \frac{6\, k_c\, M\, C_o}{d \rho} \right\} \frac{1}{1 + \left\{ \frac{k_c\, d}{6 D\, W_o} \right\} W} \tag{41}$$

Thus, a rate expression of the form

$$\frac{dW}{dt} = \frac{K \pi y_o}{1 + BW} \tag{42}$$

has been obtained.

We may also write

$$\frac{1}{1 + BW} \simeq 1 - BW\,, \quad \textit{at least for } BW << 1$$

and

$$\frac{dW}{dt} \simeq K \pi y_o (1 - BW) \tag{43}$$

Note that this last rate equation may also be obtained by assuming that the kinetics are chemically controlled and proportional to the partial pressure πy_o and the unreacted solid $(1 - BW)$, if $B = \frac{1}{W_o}$.

2. Determination of Mechanism

The proposed sorption mechanism (bulk plus pore diffusion) may be tested in several ways. The fit of sorption data to the modelling equations may be checked. The values of effective diffusivity computed from the data may be compared with those calculated, based on the sorbent pore structure. Finally, the correctness of the model in accounting for the effects of variations in temperature, diameter of particles, and other terms appearing in the constants of the modelling equation can be tested.

To examine the fit of the sorption data to the modelling equations, the data have been numerically differentiated to give the sorption rate, dS/dt, as a function of loading, S. Rewriting (40) gives

$$\frac{1}{dS/dt} = \frac{d \rho W_o}{6 M k_c C_o} + \frac{d^2 \rho W_o}{12 M D C_o} \left\{ \frac{1-(1-S)^{1/3}}{(1-S)^{1/3}} \right\} \tag{44}$$

Thus, a plot of reciprocal rate versus the complicated function of S should give a straight line if the model is correct. From the intercept the mass transfer coefficient, k_c, may be computed and from the slope and this value of k_c the effective diffusivity, D, may be computed.

Due to the scatter inherent in differentiation of data, fairer comparison of the accuracy of fit of the model would be obtained from the original integral data. Integration of (40) gives

$$t = \frac{d^2 \rho W_o}{8 M D C_o} \left[1-(1-S)^{2/3} \right] + \frac{d \rho W_o}{6 M k_c C_o} \left[1 - \frac{k_c d}{2D} \right] S \tag{45}$$

or

$$t = \frac{3}{2} (slope) \left[1-(1-S)^{2/3} \right] - (slope - intercept)\, S \tag{46}$$

where the slope and intercept of the reciprocal rate plots are referred to. Thus, from the slope and intercept of these plots parameters can be obtained for computing an integral curve (S versus t) to be compared with the original data.

To estimate the effective diffusivity for comparison with the values obtained above the following processes must be considered:

1) Knudsen diffusion

2) bulk diffusion

3) surface diffusion

Surface diffusion is discussed in Section IV.D.5. and appears to be negligible.

The combined gas phase diffusion coefficient due to bulk and Knudsen diffusion may be estimated as

$$\frac{1}{D_{mix}} = \frac{1}{D_K} + \frac{1}{D_B} \quad * \tag{47}$$

The Knudsen diffusivity is computed as

$$D_K = (9.7)\,(10^3)\,r\left(\frac{T}{M}\right)^{1/2} \tag{48}$$

where

T = temperature, $^{\circ}$K

M = molecular weight

r = pore radius, cm

The bulk gas diffusivity may be computed from molecular force parameters. The results of these computations for several pore diameters are given in Table IV.

TABLE IV

COMPUTATION OF EFFECTIVE DIFFUSIVITY

T, °C	D_B (cm^2/sec)	(d = 0.05μ)		(d = 0.09μ)		(d = 0.15μ)	
		D_K	D_{mix}	D_K	D_{mix}	D_K	D_{mix}
25	.126	.0522	.0369	.094	.0538	.157	.0675
120	.208	.060	.0470	.108	.0712	.180	.0964
300	.405	.072	.0612	.130	.0984	.216	.141

A log-log plot of D_{mix} versus T for each pore diameter is given in Figure 21. It has been found by many experimenters that measured effective diffusivities are about an order of magnitude less than the computed values. This reduction is due partly to the tortuosity of the diffusion path and partly to the reduction in the area available for flow due to the very presence of the sorbent particle.

Finally, the temperature dependence of the effective diffusivity computed from the sorption data should be compared with theory which predicts a temperature dependence of $T^{1/2}$ for Knudsen diffusion and approximately $T^{3/2}$ for bulk diffusion. The measured effect should then lie between $T^{1/2}$ and $T^{3/2}$ depending upon which diffusion mechanism predominates in the pores of the

---

* Rothfield, AIChE Journal, 9, 19-24 (1963).

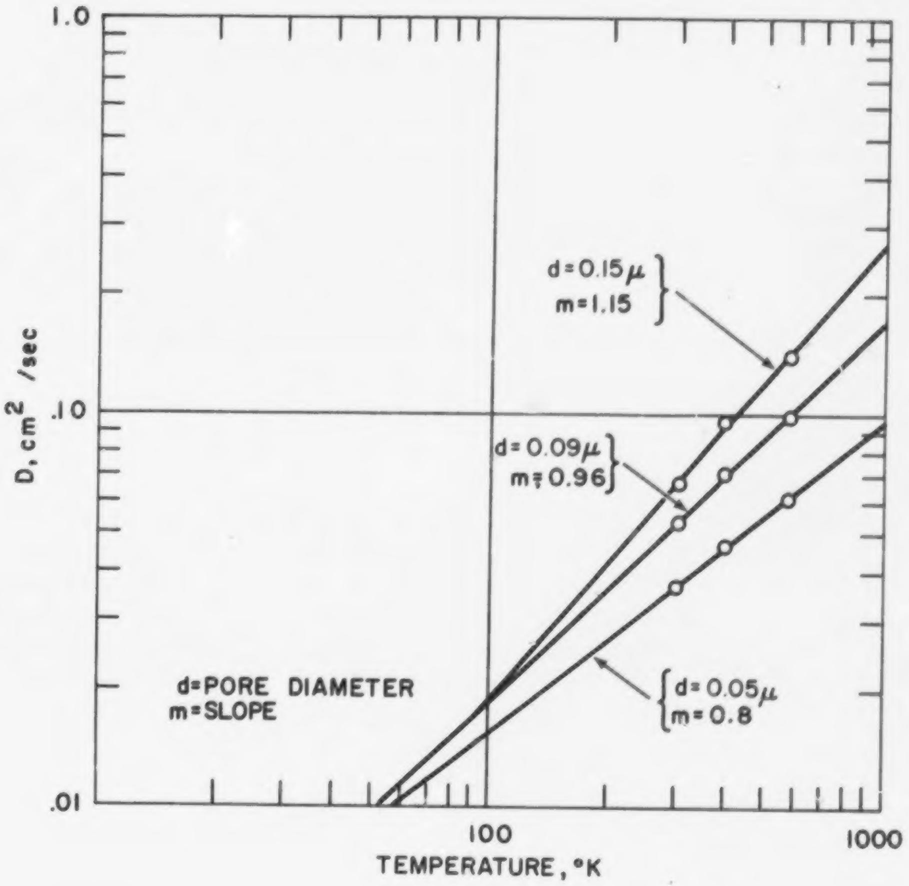

27-3823

Figure 21 MIXED DIFFUSIVITY AS A FUNCTION OF PORE DIAMETER AND TEMPERATURE

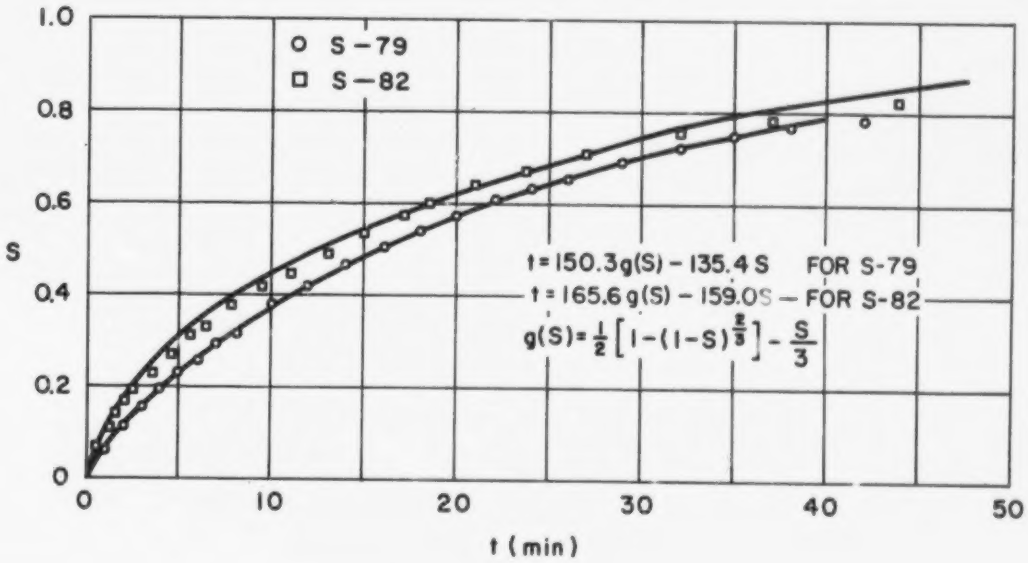

27-3829

Figure 22 SORPTION CURVE FOR S-79 AND S-82

sorbent. For a range of particle sizes the measured effective diffusivities should be constant.

3. General Treatment of Data

The majority of the runs were carried to saturation and the sorption rates at loadings of less than 2 percent of the sorbent weight were inferred from the model fitting the data at higher loadings. The treatment of these data is reported on here. As will be shown in Section IV.D.10, Initial Sorption Rate Measurement, this leads to erroneous estimates of the initial rates although it is fine at loadings above 2 percent.

The raw data from each run were obtained as SO_2 loading, W, or fraction of saturation, S, versus time. The data from runs S-79 and S-82 are plotted in Figure (22). Data points are circled, while the lines drawn are the predicted sorption curves using the model of Section IV.D.1. A three point Lagrangian differentiation formula was used to compute the rate of sorption from these data. The rate curves are plotted as in Figure 23

$$\frac{dW}{dt} \quad vs. \quad W$$

where

W = lb SO_2/lb sorbent

W_o = saturation value of W

t = time (min)

Example rate curves for S-79 and S-82 are given in Figure 23. The factor of 0.8 was used because the sorbate weight gain is due to SO_3 whereas the sorption of SO_2 is the quantity of importance.

From the estimated asymptotic value of W at zero rate of sorption (very long time), the saturation weight gain, W_o, was determined for each run. Then, in accordance with the model presented in Section IV.D.1, plots were made of reciprocal rate versus the quantity $\left[\frac{1-(1-S)^{1/3}}{(1-S)^{1/3}}\right]$ Example plots are given in Figure 24 for runs S-79 and S-82.

A straight line was then fitted to the reciprocal rate plots for each run and the slope and intercept of this line were measured. The slope and intercept were then used for computing the sorption curve, S versus time. The sorption curves were computed according to (46) as given in Section IV.D.2.

The predicted sorption curves for runs S-79 and S-82 are compared with the the data for those runs in Figure 22. According to the proposed model

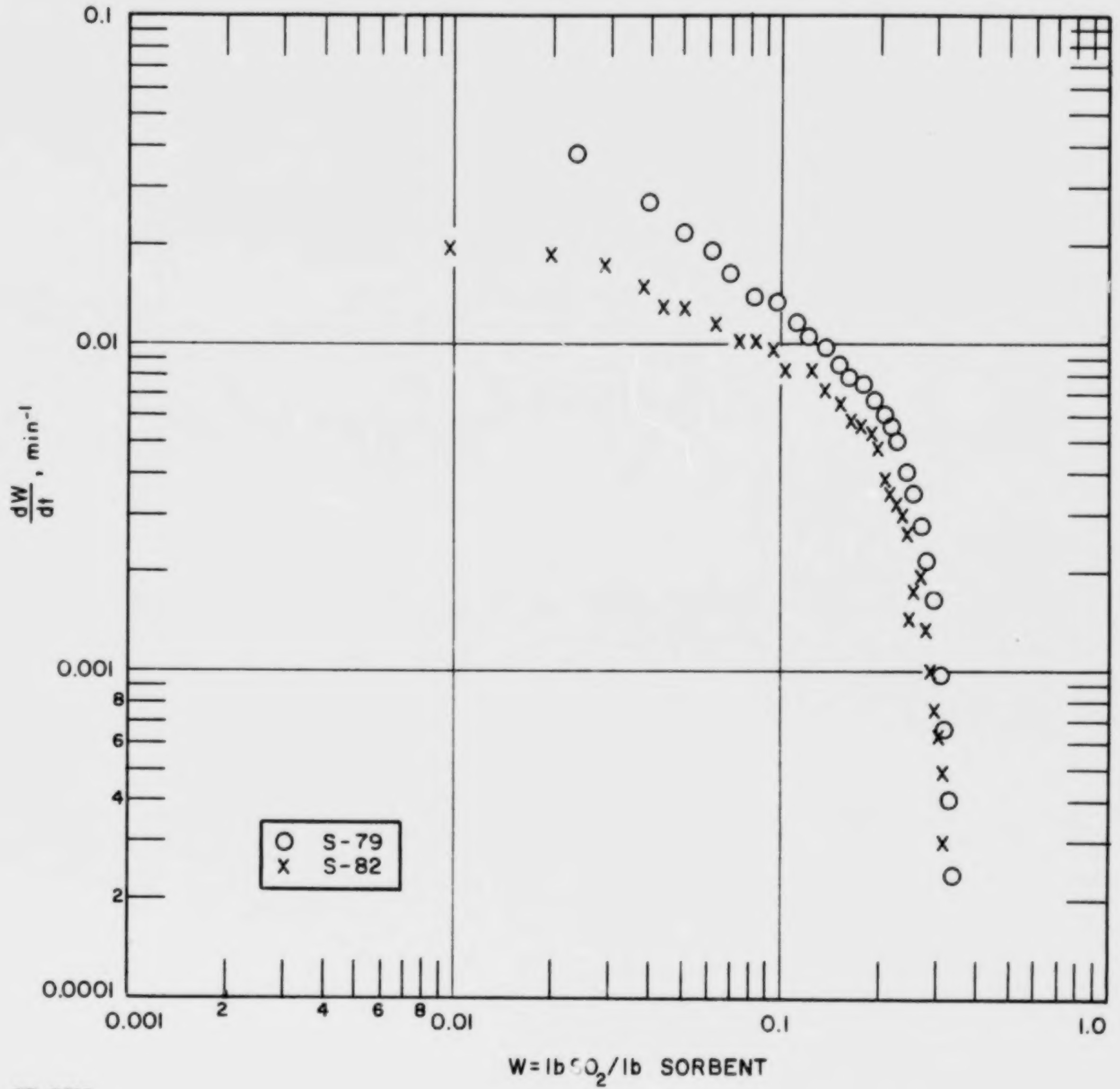

87-8016

Figure 23 SORPTION RATE CURVE FOR S-79 and S-82

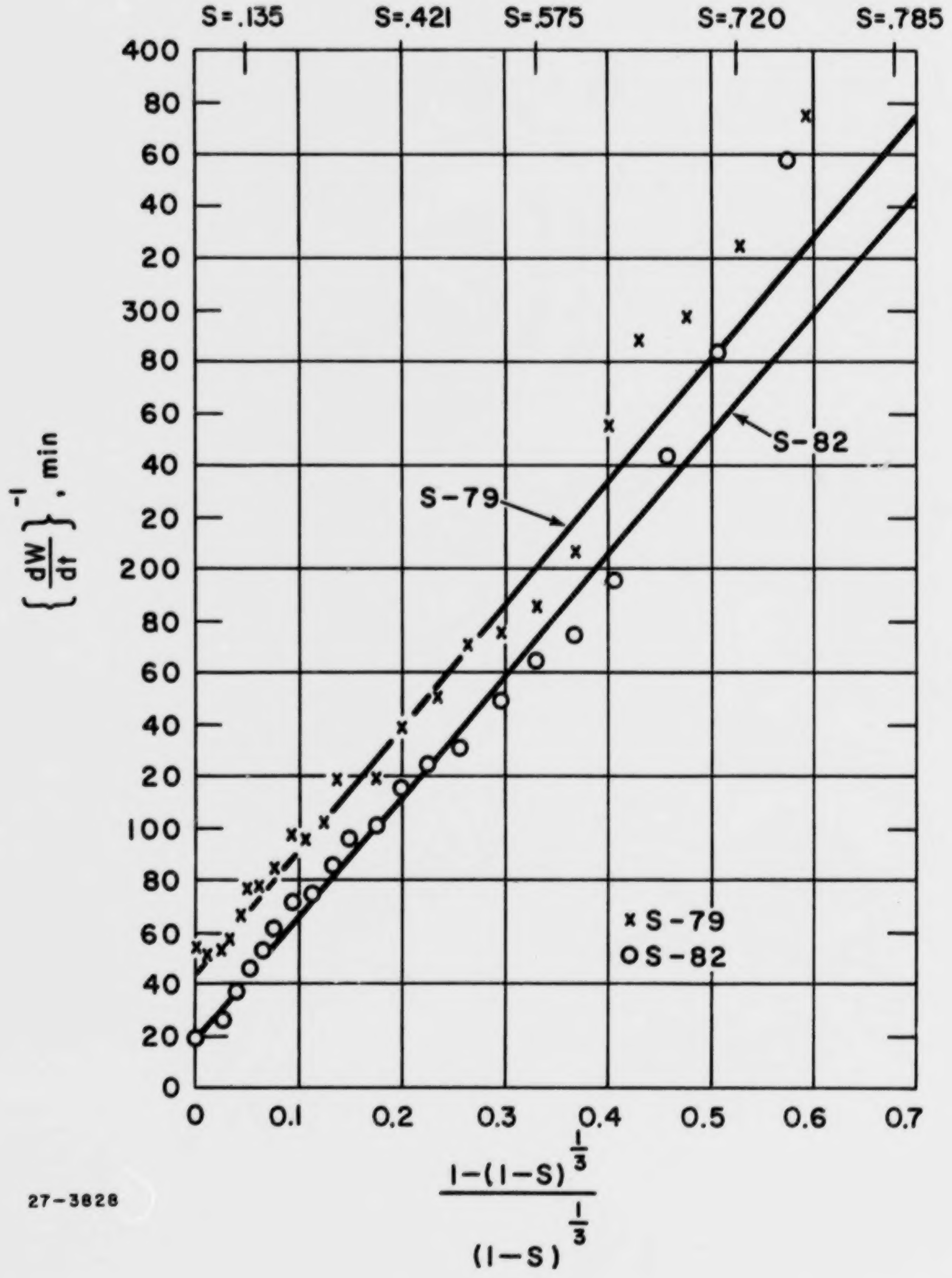

27-3828

Figure 24 RECIPROCAL RATE PLOTS S-79 AND S-82

the slope and intercept can be used to compute a mass transfer coefficient and an effective diffusivity. The mass transfer coefficient is computed according to the formula

$$k_c = \frac{\rho\, d}{384\, C_o} \; W_o \quad (intercept)^{-1} \tag{49}$$

The effective diffusivity is computed as

$$D = \frac{k_c\, d\ (intercept)}{2\ (slope)} \tag{50}$$

An estimated initial rate K was computed as

$$K = \frac{lb\ SO_2}{lb\ sorbent,\ hr,\ mole\ fraction\ SO_2}$$

Note that

$$K = \frac{64\, k_c\, (C_o - C_s)\, A_p}{y_o}$$

where

A_p = ft^2 external surface/lb sorbent.

The relation between K and k_c comes about as k_c is itself a measure of the initial rate according to the model used. Values of k_c, K, D_{eff} and the conditions for the various runs are given in Table V. The values of K were obtained from the experimentally determined rates at loadings of about 2 percent of sorbent weight as $K = \frac{1}{y} \left.\frac{dW}{dt}\right|_{initial}$

A sample calculation of k_c and D is given in Appendix I. As will be seen in Section IV.D.10, the initial rate estimates given here are low.

4. Effect of Moisture and Oxygen in the Flue Gas

A large amount of data was taken early in the program on the mistaken assumption that sorption rates were unaffected by the presence of water vapor in the flue gas. The assumption was based on a series of experiments which were apparently in error. All recent data, and the majority reported on here were taken with a flue gas containing 5-7 percent moisture by volume.

The effect of water vapor was demonstrated by sorptions S-51 through S-55 which were run at 300° C and about 1 percent SO_2. A 216 mg sample of Peter Spence sorbent was used. Run S-51 used dry flue gas and showed a weight gain of 15 mg after 100 minutes. Run S-52 used flue gas with 5.2 percent moisture and gained 96 mg in the same period. In S-53 the dry results of S-51 were replicated at a high oxygen concentration and slightly higher rates were

TABLE V

SUMMARY OF SORPTION DATA

Run No.	Sample	T(^oC)	Gas Velocity (ft/sec)	Vol. Percent SO2 †	Vol. Percent H_2O**	Vol. Percent O2*†	Particle †† Diameter (in.)	Theoretical k_c (ft/hr)	k_c from data (ft/hr)	K from data (hr^{-1})	D from data (cm^2/sec)
S-47	5	300	.5	1.03	0	15.5	.120	505			
S-49	5	300	.5	est 1.0	0	3.6	.120	505			
S-51	6	300	.5	1.03	0	3.6					
S-52	6	300	.64	.83	5.2	16.6					
S-53	6	300	.5	est 1.0	0	21.0					
S-54	6	300	.66	0	7.2	0					
S-55	6	300	.64	.78	5.2	2.85					
S-62	9	300	7.3	.90	3.5	3.27	.102				
S-63	9	300	1.9	.89	7.2	3.145	.102	1050	261		.012
S-64	9	300	1.9	.87	7.2	3.145	.102	1050	161		.024
S-65	9	350	1.9	.95	7.2	3.145	.102		117		.024
S-67	9	200	1.9	.68	7.2	3.145	.102		105		.014
S-68	9	250	1.9	.87	7.2	3.145	.102		103		.014
S-69	9	150	1.9	.91	7.2	3.145	.102		151		.0099
S-70	9	350	1.9	.87	7.2	3.145	.102		179		.012
S-79	12	300	7.6	.81	7.2	3.15	.102	1460	179	139	.019
S-80	12	300	7.6	.96	7.2	3.15	.102	1460	171	118	.013
S-81	13	300	7.6	.85	7.2	3.15	.066	1880	148	332	.0062
S-82	13	300	7.6	.92	7.2	3.15	.066	1880	252	174	.0071
S-83	13	300	7.6	.81	7.2	3.15	.066	1880	145	197	.0085
S-85	14	300	7.6	.96	7.2	3.15	.079	1670	391	312	.012
S-86	14	300	7.6	1.02	7.2	3.15	.079	1670	498	442	.010

*† from pressure change on addition of O_2 to feed cylinder
† by chromatography
†† by sieving
** from humidifier temperature

observed. In S-54 the sorbent was exposed to a mixture containing 7.2 percent H_2O and 92.8 percent N_2 by volume. The weight gain was only 1 mg. The results of S-52 with moist flue gas were replicated in run S-55 at a low oxygen concentration. Sorption curves for each of these runs are given in Figures 25 and 26. Note in Figure 26 that raising the oxygen concentration from 2.8 percent to 16.6 percent had no effect on the sorption in moist flue gas.

Thus, increased concentration of O_2 gave slightly higher sorption rates in the absence of moisture in the gas, but there was no effect of oxygen content with moist gas.

An equal increase in rate over previous dry sorptions was observed with the W. R. Grace material. The effect of water vapor on W. R. Grace sorbent can be seen by comparing runs S-49 (dry, 300° C) with S-79 (7.2 percent moisture, 300° C). The sorption curves are presented in Figure 27 and clearly show the increase in sorption rate in the presence of moisture.

The mechanism by which water vapor accelerates the sorption is not understood. The rate of the surface sorption reaction may be catalyzed by the presence of water. Alternately, capillary condensation of the moisture might allow rapid sorption of SO_2 in the condensed water. A third possibility is that a surface diffusion mechanism might be activated by absorbed water.

The possibility of capillary condensation may be checked with the Kelvin equation which relates vapor pressure lowering to the radius of curvature of a curved surface.*

$$ln \frac{p_o}{p} = \frac{2\gamma}{r\rho} \frac{M}{RT}$$

where

p_o = vapor pressure of water at

p = partial pressure of H_2O in gas phase

γ = surface tension of water at T

ρ = density of condensed liquid

R = gas law constant

M = molecular weight of condensed liquid

T = temperature

r = pore radius

---

*Glasstone, Textbook of Physical Chemistry, van Nostrand, Princeton, N.J. (1946) p. 495.

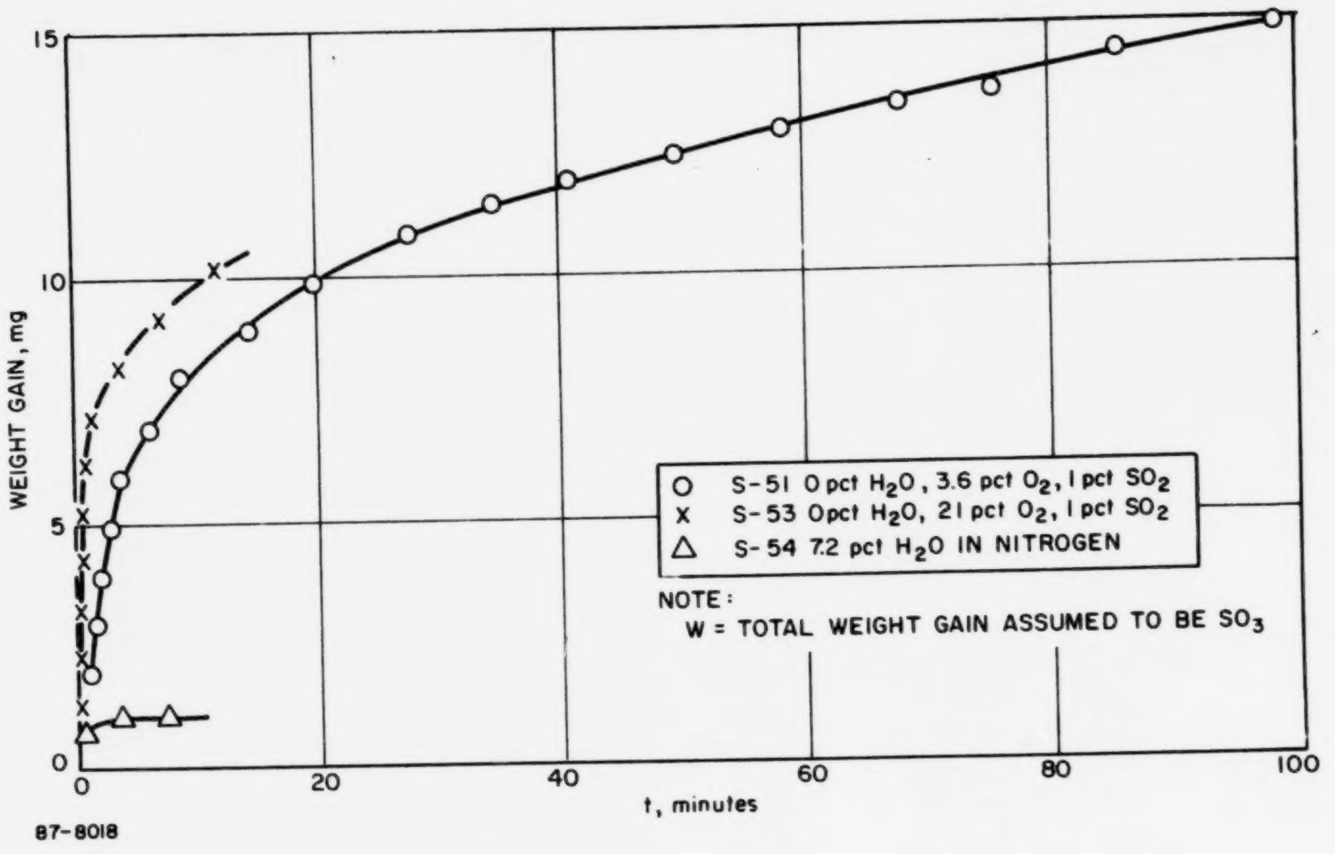

Figure 25 SORPTION DATA FOR SAMPLE NO. 6

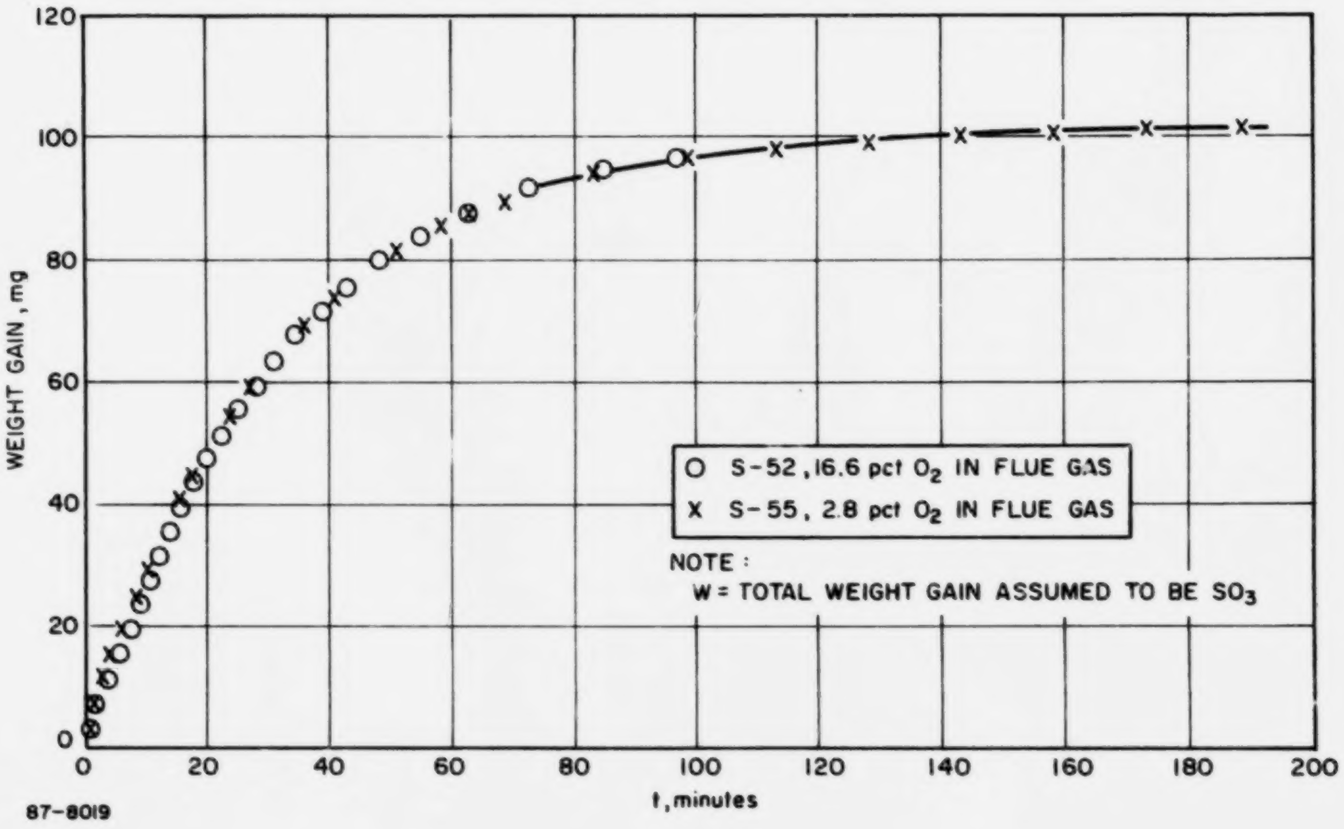

Figure 26 SORPTION DATA FOR SAMPLE NO. 6

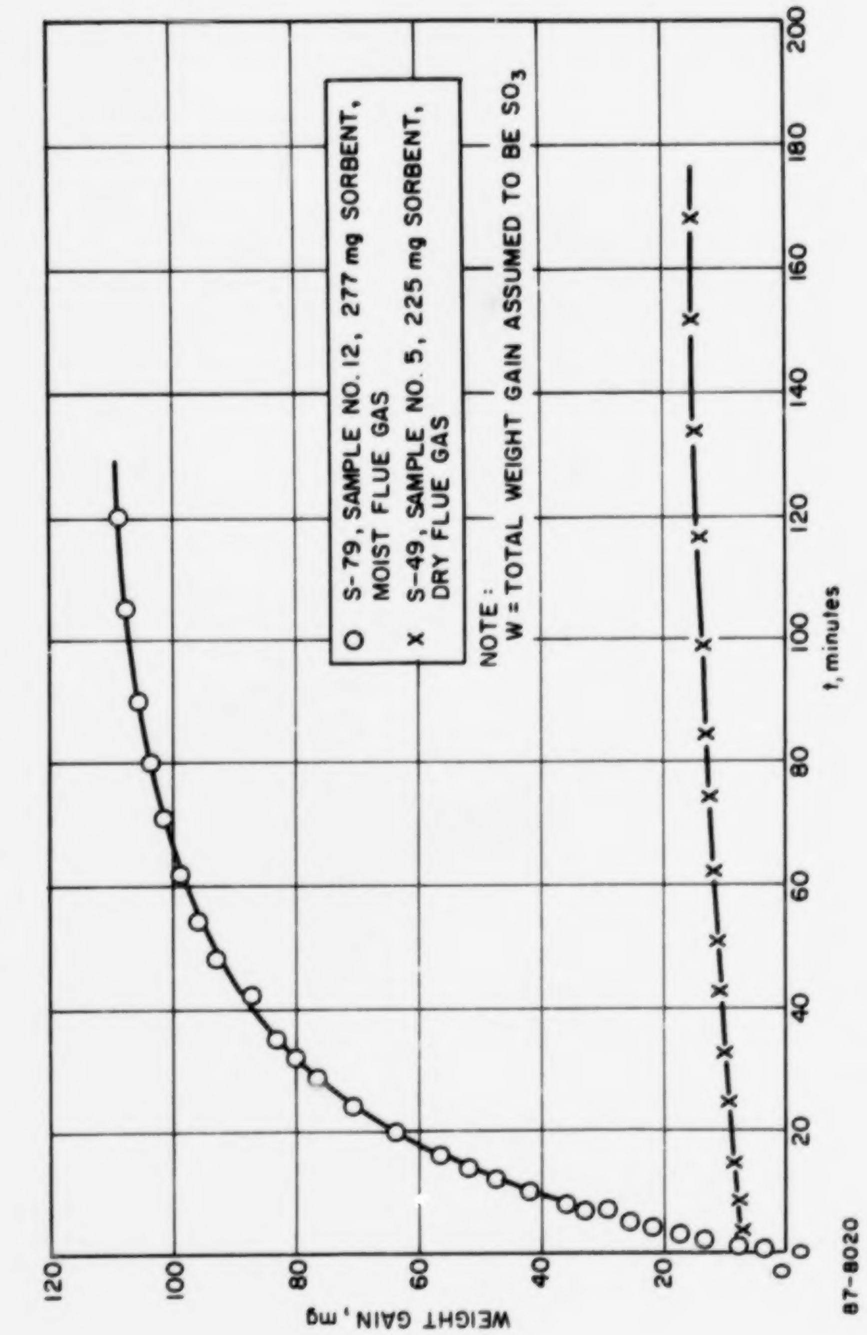

Figure 27 SORPTION DATA FOR WET AND DRY FLUE GAS

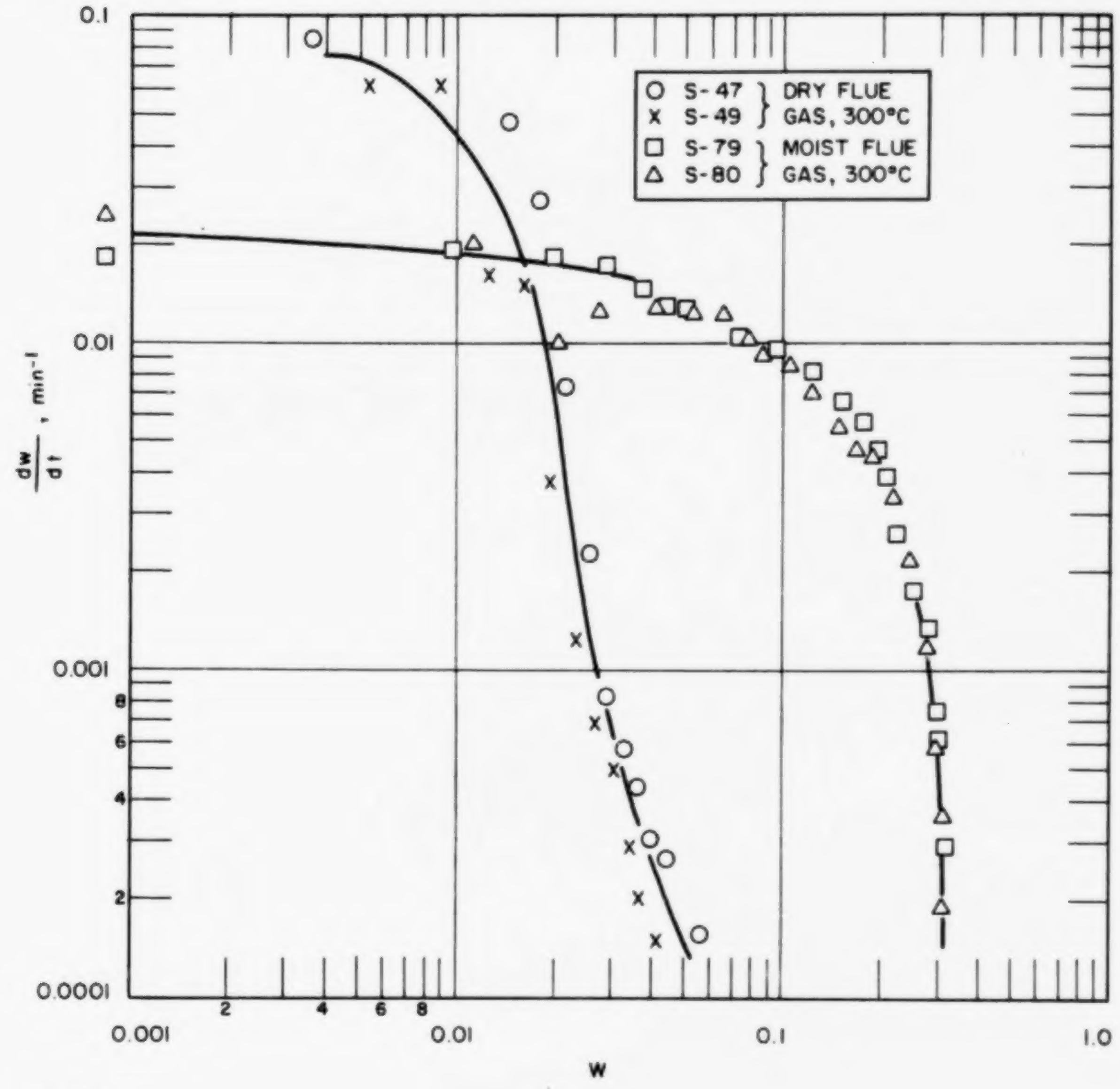

87-8021

Figure 28 SORPTION RATE DATA, W.R. GRACE SORBENT

The maximum pore radius which could support capillary condensation of moisture was computed using typical sorption conditions.

$T(^\circ K)$	p_o (atm)	p (atm)	$\rho \left(\frac{(gm)}{cc}\right)$	$\gamma \left(\frac{(dyne)*}{cm}\right)$	$r(\mathring{A})$
423 (150° C)	4.70	.072	1.0	47	1.2
573 (300° C)	84.8	.072	1.0	20	0.21

The concept of capillary condensation in pores of one molecular diameter is not sensible. As a result capillary condensation is probably not the explanation of the high sorption rate in the presence of moist flue gas.

Alternately, sorbed moisture might provide a path for surface diffusion of SO_2 on the pore walls. If this were an important factor, it could be checked by stopping the sorption periodically by sweeping the sorption chamber with N_2. In the presence of N_2 the surface diffusion would be expected to continue causing a levelling of the sorbate concentration profile. Restoring the sorption should result in a different rate than previous to standing in N_2 due to the redistribution of the sorbate within the particle.

All sorptions from S-78 on have been run on an intermittent basis. Sorption was carried out for a given time, then the sample chamber swept with nitrogen and the sample weighed in static nitrogen. Sorption was then resumed in flowing flue gas. In runs previous to S-78 the sorption and weighing had been continuous. There are no evident differences in the sorption curves or diffusivities obtained in the diffusion controlled region (high loading region) of the sorption. This observation suggests that surface diffusion is not a large contributor to the total diffusion process.

By elimination, the implication is that moisture catalyzes the sorption step at the sorbent surface but this conclusion is by no means based on adequate testing.

The rate of sorption curve, given in Figure 28, indicates that there is a large effect of moisture on the sorption rate at loadings greater than two percent of saturation. However, there was no increase in the initial rate when moisture was added. In fact, the data show a decrease, but this may not be significant in light of the poor resolution of initial rates by these experiments. (See Section IV.D.10).

The moisture levels used, 5.2 percent and 7.2 percent, are similar to those found in actual flue gas. In the region where pore diffusion is controlling, higher moisture content should not affect the sorption rate. The mechanism of the initial rate is not known, nor is the effect of water content on this rate known exactly, although some data relevant to this point are given in Section IV.D.10.

---

*Estimated from values given at temperatures up to 100° C.

5. Fit of Data to Model

Examination of the plots of reciprocal rate versus $\left[\frac{1-(1-S)^{1/3}}{(1-S)^{1/3}}\right]$, i.e. Figure 24, indicates that they are well represented by a straight line up to about 80 percent of saturation. This is in accordance with the proposed model. At higher loadings, the reciprocal rate increases much more rapidly.

In Section IV.F. it is shown that the pore size distribution is trimodal so that this rapid increase in reciprocal rate might be ascribed to saturation of the larger pores resulting in diffusion in the smallest pores being rate limiting.

Typical computed integral or sorption curves are shown in Figure 22 along with the data for each run. The agreement of the data with the predictions of the model for each run is excellent, although there is variability from run to run. For individual runs the model must be concluded to adequately describe the shape of the sorption curves from the first data point at $S = 0.06$ up to loadings of $S = 0.8$.

In order to test for rate limitation by bulk phase mass transfer, a series of sorptions has been run at superficial gas velocities varying from about 0.5 ft/sec to 7.6 ft/sec. The mass transfer coefficients measured in this series (Runs S-63, S-64, S-79, S-80) are given in Table V. Also shown are the coefficients computed from literature correlations for isolated spheres.* The literature values are sufficiently large that it is probable that mass transfer does not seriously limit the rate at $S \geq 0.06$. Runs S-79 and S-80 actually showed a decrease in initial rate relative to S-63 and S-64 as the gas velocity was increased from 1.9 ft/sec to 7.6 ft/sec, further substantiating this conclusion.

This result suggests the possibility that the sorption rate at low loadings (but $S \geq 0.06$) is limited by the actual chemi-sorption process, and that intraparticle diffusion does not become rate limiting until some degree of saturation, hence penetration of the sorbent particle has been achieved. Proof of this would require knowledge of the sorption kinetics in the absence of any diffusion limitation and a model for simultaneous pore diffusion and sorption on the pore walls. The model consists of non-linear partial differential equations and is available in the form of a computer program.** However, considerably more work would be required to measure the kinetics of the reaction rate controlled step in the absence of diffusion limitation.

For purposes of this work it will suffice to accept the model as proposed in the modelling section for loadings greater than 2 percent of sorbent weight ($S \geq 0.06$). Although the model may be unsupportable for low loadings inasmuch as it assumes bulk diffusion control it does provide an accurate empirical description of the sorption process. On this basis, the remainder of the discussion of the sorption process will be couched in terms of this model. In a later section (IV.D.10) the initial sorption rate will be considered in more detail and rates at loadings less than 2 percent shown to be higher than predicted by the model.

---

[*] Sherwood and Pigford, Absorption and Extraction, McGraw-Hill, New York (1952), p. 74.

[**] Regeneration of a Chromia - Alumina Dehydrogenation Catalyst, J. Nestor, Sc.D Thesis, MIT, Dept. of Chem. Eng. 1964.

6. Effect of Particle Diameter

In order to study the effect of sorbent particle diameter on sorption kinetics, various fractions were prepared by screening. Three fractions were selected as follows:

Sample	d_{max}	d_{min}	d_{ave}
#12 (7/8 mesh)	.110 inch	.093 inch	.102 inch
#14 (8/10 mesh)	.093	.078	.086
#13 (10/14 mesh)	.078	.055	.067

All sorptions were run at 300° C using a flue gas with the following analysis:

SO_2	O_2	H_2O	N_2
.6-.9%	3.1%	7.2%	balance

The following runs were considered as providing useful data:

Sample	Runs
No. 12	S-79, S-80
No. 13	S-81, S-82, S-83
No. 14	S-85, S-86

The computed values of D, k_c, and K for these runs are given in Table V. The effective diffusivity is plotted as a function of the particle diameter in Figure 29. The average diffusivities of all runs at each diameter and the range at each diameter are plotted. The diffusivity is seen to increase as the square of the diameter. However, according to the model proposed diffusivity should be constant.

A possible explanation for the discrepancy lies in the pore structure of the sorbent. According to Figures 51 and 52 there are pores at a diameter of about 20 microns. Although contributing little to the surface area and almost no diffusional resistance due to their large size, these pores could partition the sorbent pellet into subsections the size of which could be independent of sorbent particle size. The constant size of these subsections would then control the diffusion rate regardless of the particle size, so long as the particles were larger than the subsections. As the square of the overall particle diameter appears Equations (49) and (50) used for computing the diffusivity this could account for the observed effect.

Reduction of the particle size below that of the subsection size should then result in a constant computed effective diffusivity. Unfortunately the data do not extend to sufficiently small diameters to clarify this point.

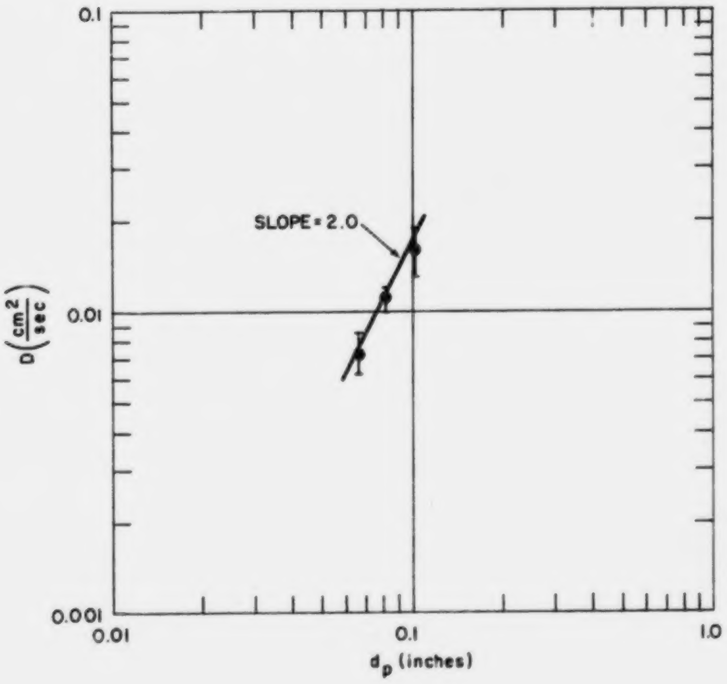

27-3822

Figure 29 EFFECT OF PARTICLE DIAMETER ON DIFFUSIVITY

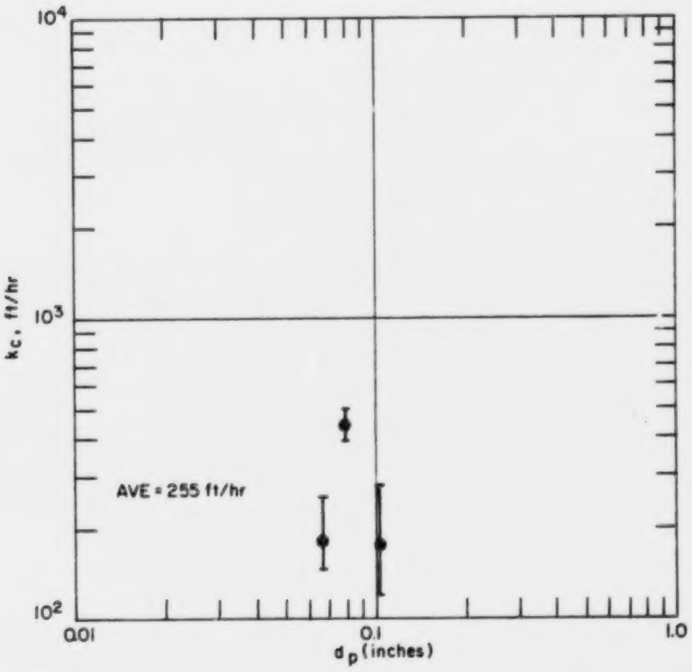

27-3822

Figure 30 EFFECT OF PARTICLE DIAMETER ON K_c

The values of diffusivity computed are on the order of 10 to 20 percent of the diffusivity calculated from theory in Section IV.D.2. on the basis of mean pore diameter. Measured effective diffusivities are normally on the order of 10 percent of those predicted from pore diameter. Thus, the lowest measured diffusivities are in accord with experience.

The computed diffusivities are order of magnitude correct, and the model based on a pore diffusion controlling mechanism fits the shape of the sorption and rate curves quite well. This indicates that in spite of the difficulties with the effect of particle diameter, pore diffusion probably does control the sorption process during its later stages.

The mass transfer coefficient is plotted as a function of particle diameter in Figure 30. The scatter of the data is such that only the constant average value of 255 ft/hr can be assigned.

7. Effect of Temperature

The sorption rate was determined seven times on a single sample of sorbent over the range of 150° C to 350° C. Runs S-62 through S-70 were used, and run conditions and computed parameters are given in Table V.

The effective diffusivity is plotted vs. temperature in Figure 31. When the average diffusivity at each temperature is considered it is seen that the effective diffusivity increases with about the 1.76 power of the absolute temperature. According to Figure 21 the exponent that would be expected on the basis of theory for a pore diameter of $0.09\,\mu$ is about 0.96. The discrepancy may in part be explained by the noticeable scatter of the data, and in part by error in the theoretical estimate of the exponent.

The measured values of the mass transfer coefficient, k_c, are plotted against temperature in Figure 32. The scatter of the data is extreme. If k_c truly represents a mass transfer coefficient, and considerable reason to doubt this has been given elsewhere, then it should increase approximately as the bulk gas diffusivity, that is as $T^{3/2}$. The temperature effect has been arbitrarily taken to be $T^{1.76}$ as this simplifies the rate equations to be given in the next section.

Reference to Figure 32 shows that a $T^{1.76}$ dependence fits the data about as well as any power dependence that could be selected.

8. Effect of Gas Velocity

Runs S-63, S-64, S-79, and S-80 were all made at 300° C with a particle diameter of 0.102 inch. Runs S-63 and S-64 were made at a superficial gas velocity of 1.9 ft/sec and runs S-79 and S-80 at 7.6 ft/sec.

From Table V the average value of k_c is seen to be 211 ft/hr at 1.9 ft/sec and 175 ft/hr at 7.6 ft/sec. The average value of D is 0.018 cm^2/sec at 1.9 ft/sec and 0.016 cm^2/sec at 7.6 ft/sec. Thus, both coefficients have decreased with increasing gas velocity. This decrease is not significant in light of the scatter in the data. What is significant is the fact that no increase was observed in the coefficients indicating that interphase mass transfer was not a rate controlling step. Furthermore, the measured k_c for

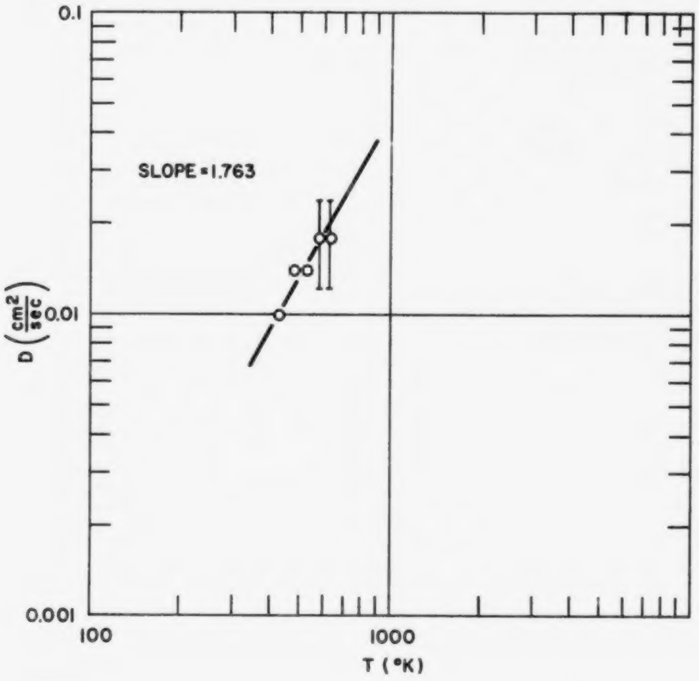

27-3821

Figure 31 EFFECT OF TEMPERATURE ON DIFFUSIVITY

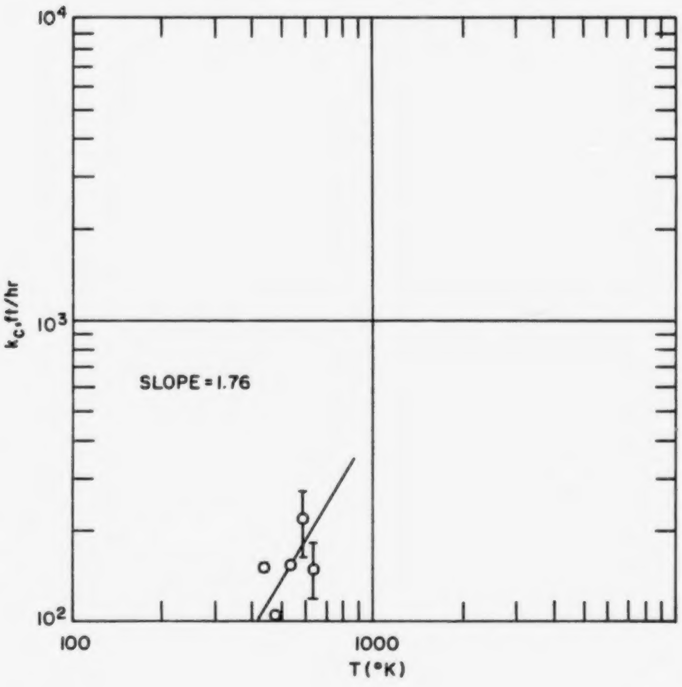

27-3821

Figure 32 EFFECT OF TEMPERATURE ON K_c

Runs S-79 and S-80 averaged 175 ft/hr compared to theoretical mass transfer coefficients of 1460 ft/hr at the same particle diameter and gas velocity.

9. Summary Sorption Model

There are strong indications that the rate at low loadings is not controlled by mass transfer as suggested in the mathematical model that has been developed. Nonetheless, the sorption curves are well described by this model and it yields reasonable values of effective diffusivity. Thus, the model will be used as a basis for a semi-empirical description of the sorption process.

In section IV.D.4. it was shown that oxygen partial pressure did not affect the sorption in the presence of moisture. The rate of sorption will be considered as independent of oxygen partial pressure, and moisture content at humidities typical of actual flue gas. This assumption is valid in the pore diffusion controlling region and as shown in section IV.D.10 the rate is independent of humidity at loadings greater than 2 percent of sorbent weight.

The form of the rate equation is given by (40).

$$\frac{dS}{dt} = \left\{\frac{6\,M\,k_c\,C_o}{\rho\,d\,W_o}\right\} \frac{1}{1 + \frac{k_c\,d}{2D}\left\{\frac{1-(1-S)^{1/3}}{(1-S)^{1/3}}\right\}} \tag{40}$$

The values of k_c and D will be obtained as functions of d and T and substituted in (40).

From Figures 30 and 31,

$$D = (\text{constant})\ d^2 T^{1.76}$$

At d = 0.102 inches, T = 573° K and D = 0.0176 cm^2 from both Figures 29 and 31. Thus,

$$D = 2.37 \times 10^{-5}\ d^2\ T^{1.76}\ \text{cm}^2/\text{sec}$$

$$= 9.18 \times 10^{-5}\ d^2\ T^{1.76}\ \text{ft}^2/\text{hr}.$$

where

d = diameter of particle, inches

T = temperature, °K

From Figures 30 and 32

$$k_c = (\text{constant})\ T^{1.76}$$

At d = 0.102 inches, T = 573° K, Figure 30 gives k_c = 255 ft/hr, and Figure 32 gives k_c = 175 ft/hr. Using the average value, k_c = 215 ft/hr. gives

$k_c = 3.01 \times 10^{-3}\ T^{1.76}$ ft/hr

$\quad = 2.55 \times 10^{-5}\ T^{1.76}$ cm/sec

Substituting in (40)

$$\frac{dS}{dt} = \left\{\frac{0.161\ T^{0.76}\,\pi}{W_o\, d}\right\}\left[\frac{y_o}{1 + \frac{1.37}{d}\left\{\frac{1-(1-S)^{1/3}}{(1-S)^{1/3}}\right\}}\right] hr^{-1} \tag{51}$$

$$= \left\{\frac{0.00268\ T^{0.76}\,\pi}{W_o\, d}\right\}\left[\frac{y_o}{1 + \frac{1.37}{d}\left\{\frac{1-(1-S)^{1/3}}{(1-S)^{1/3}}\right\}}\right] min^{-1} \tag{52}$$

where

d = particle diameter, inches

T = temperature, ^{o}K

π = total pressure, atm

y_o = mole fraction SO_2 in bulk gas stream

W_o = saturation loading, lb SO_2/lb sorbent.

At low loadings, the expansion of this result gives

$$\frac{dS}{dt} = \left\{\frac{0.00268\ T^{0.76}\,\pi}{W_o\, d}\right\}\left[\frac{y_o}{1 + \frac{0.46}{d}\ S}\right] min^{-1} \tag{53}$$

The integrated form is obtained by substituting for k_c and D in (45).

$$t = \frac{765\ W_o}{T^{0.76} y_o \pi}\ [1-(1-S)^{2/3}] + \frac{373\ W_o\, d}{T^{0.76} y_o \pi}\left[1 - \frac{1.37}{d}\right] S\ min \tag{54}$$

For low loadings the expansion gives

$$t = \left[\frac{373\ W_o\, d}{T^{0.76} y_o \pi}\right] S + \left[\frac{85.8\ W_o}{T^{0.76} y_o \pi}\right] S^2\ min \tag{55}$$

The time required for sorption to be twenty percent complete was computed using (55) for low loadings and the conditions for each run considered. The time required to reach fifty percent of saturation was computed from (54) for a series of runs. Temperature varied from 150° C to 350° C, particle diameter from 0.066 inch to 0.102 inch, and four separate samples of sorbent were considered. These times were compared to the experimentally determined times, $t_{0.2}$, $t_{0.5}$. The computed values were low for both $t_{0.2}$ and $t_{0.5}$. The computed times were multiplied by the factor 1.16 giving new computed times t' which were low by 4 percent on the average at 20 percent loading and high by 2 percent at 50 percent loading. The rms error was 29 percent at 20 percent loading and 21 percent at 50 percent loading. A summary of the comparison computations is given in Table VII.

The revised summary equations, incorporating the factor 1.16 are as follows:

at any loading:

$$\frac{dS}{dt} = \left\{ \frac{0.00231\ T^{0.76}\ \pi}{W_o\ d} \right\} \left[\frac{y_o}{1 + \frac{1.37}{d} \left\{ \frac{1-(1-S)^{1/3}}{(1-S)^{1/3}} \right\}} \right] \text{min}^{-1} \qquad (56)$$

$$t = \frac{887\ W_o}{T^{0.76}\ y_o\ \pi} \left[1-(1-S)^{2/3} \right] + \frac{433\ W_o\ d}{T^{0.76}\ y_o\ \pi} \left[1 - \frac{1.37}{d} \right] S \text{ min} \qquad (57)$$

at loadings ≤ 25 percent of saturation

$$\frac{dS}{dt} = \left\{ \frac{0.00231\ T^{0.76}\ \pi}{W_o\ d} \right\} \left[\frac{y_o}{1 + \frac{0.46}{d}\ S} \right] \text{min}^{-1} \qquad (58)$$

$$t = \left[\frac{433\ W_o\ d}{T^{0.76}\ y_o\ \pi} \right] S + \left[\frac{99.5\ W_o}{T^{0.76}\ y_o\ \pi} \right] S^2 \text{ min} \qquad (59)$$

A plot of the Avco data for Runs S-79 and S-82 is shown in Figure 33. Also shown are the curves of (56) at the conditions of the experiments. The figure shows that the model reflects the trend of the data and also illustrates the scatter inherent in the data of which the model is an average representation.

10. Initial Sorption Rate Measurements

Operating data from the Bureau of Mines pilot plant, given in report RI-7021 indicates sorption rates at low loadings that are higher than those given by

TABLE VI

COMPARISON OF SORPTION DATA WITH MODEL

Run No.	$t_{0.20}$ from data (min)	$t_{calc.}$ (Eq. 55) (min)	$t'_{calc.}$ = 1.16 $t_{calc.}$ (min)	$(t' - t_{.2})^2$ (min^2)	$t_{0.50}$ from data (min)	$t'_{calc.}$ (Eq. 54) (min)	$t'_{calc.}$ = 1.16 $t_{calc.}$ (min)	$(t - t_{.5})^2$ (min^2)
S-63	3.6	3.36	3.9	.09	16.0	14.2	16.5	0.25
S-64	3.3	2.79	3.2	.01	11.8	11.8	13.7	3.61
S-65	4.7	2.82	3.3	1.96	14.5	11.9	13.8	0.49
S-67	5.2	5.00	5.8	.36	18.7	17.8	20.7	4.0
S-68	5.2	3.03	3.5	2.89	14.0	10.8	12.5	2.25
S-69	3.7	3.21	3.7	0	15.4	11.5	13.3	4.41
S-70	2.5	1.80	2.1	.16	13.0	6.4	7.4	31.3
S-79	4.1	3.49	4.1	0	15.9	14.9	17.3	1.96
S-80	4.8	2.95	3.4	1.96	17.7	12.6	14.6	9.58
S-81	4.5	2.83	3.3	1.44	16.8	13.3	15.4	1.96
S-82	2.5	2.58	3.0	.25	13.0	12.2	14.2	1.44
S-83	3.6	2.85	3.3	.09	14.8	13.4	15.5	0.49
S-85	2.7	3.88	4.5	3.24	14.2	17.9	20.7	42.2
S-86	2.5	3.58	4.2	2.89	13.7	16.2	18.8	26.0
Average	3.78	3.16 or 13.7 percent low on average	3.66 or 4 percent low on average	rms error = 1.09 or 29 percent	15.0	13.2 or 12.0 percent low on average	15.3 or 2 percent high on average	rms error = 3.2 or 21 percent

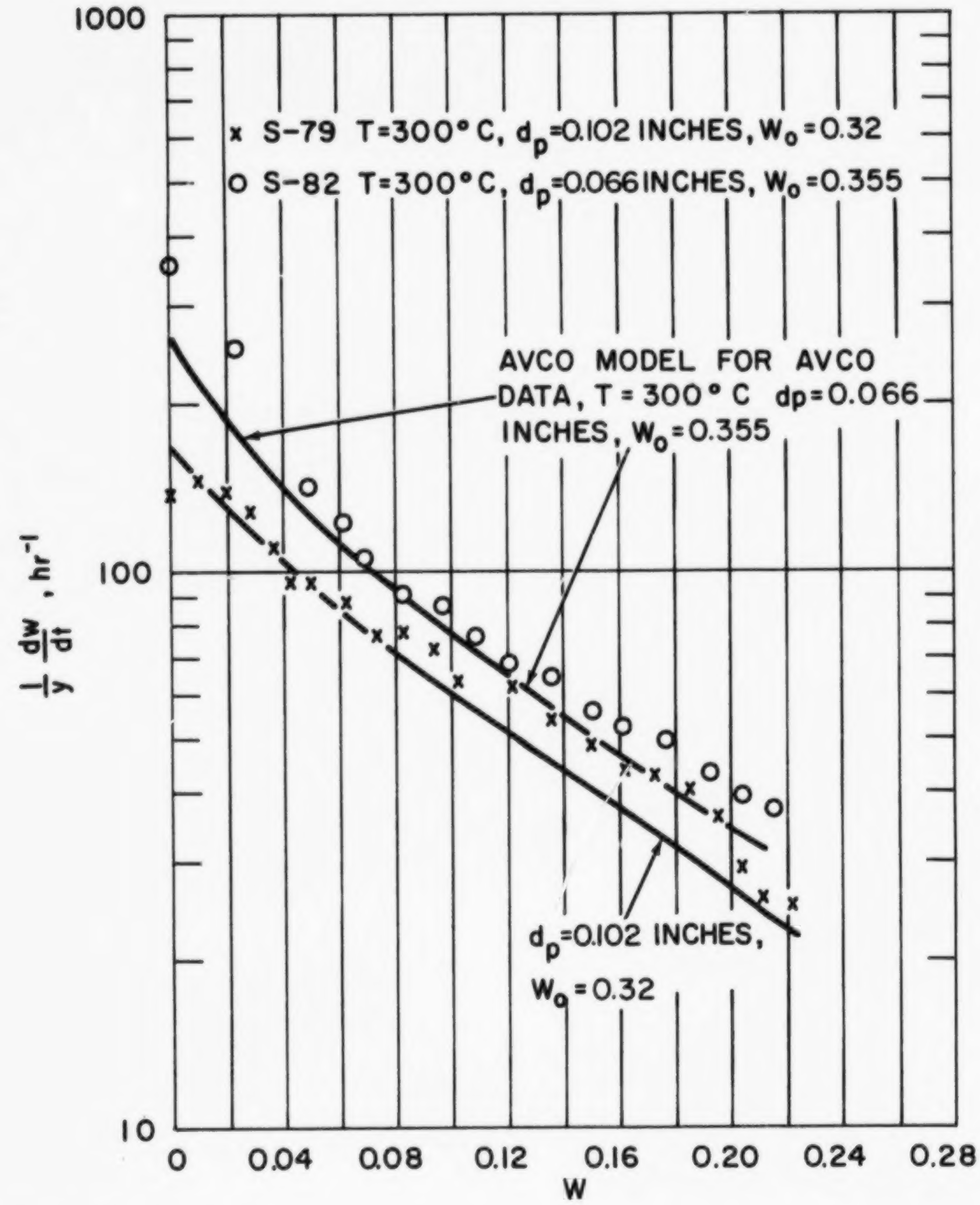

27-3820

Figure 33 COMPARISON OF RATE MODELS WITH DATA

the model in Section IV.D.9 of this report. Because of the discrepancy, more accurate measurements of the initial sorption rate were made. A very dilute simulated flue gas was used to slow the sorption. In addition, the weight gain was measured for very small time increments at the beginning of the sorption step. These measurements were made under conditions summarized in Table VII. The data are given in Appendix II.

In Figure 34 the sorption rate as

$$\frac{0.8}{y_o} \quad \frac{d}{dt} \quad \frac{1}{y} \quad \frac{dW}{dt}, \; hr^{-1}$$

is plotted versus sorbent loading as W. Also plotted on the figure is the Avco model at the conditions of the experiments. Several conclusions can be drawn.

1) Actual initial rates are higher than those predicted by the model by a factor of about 25. They remain somewhat higher up to loadings of 2 percent.

2) The data of the model, obtained at about 1 percent SO_2, and the initial rate data, obtained at about .07 percent SO_2, agree at loadings above 2 percent. This substantiates the assumption of a first order dependence on SO_2 in this region of loading.

3) Initially, the rate increases with the moisture content of the flue gas (see runs ISR-2^1, 4^1, 5^1) but appears to be independent of the moisture level at loadings greater than 2 percent. The independence of moisture content is in accord with the assumption of pore diffusion beginning to control at loadings greater than 2 percent.

The results can be explained by the following postulated sequence of events. Initially when sorption occurs on the outer surface of the particle and there is essentially zero loading there is no pore diffusion limitation and the rate of chemisorption is very fast. Under these conditions the rate is bulk phase mass transfer controlled. As the outer surface becomes saturated the rate of chemisorption decreases until it becomes the rate limiting step. This event appears to occur at loadings of about two percent. Finally, as the saturated region of the sorbent begins to penetrate the particle, pore diffusion becomes the rate limiting step.

Substantiation for this view of matters is obtained from two sources, published correlations on mass transfer rates and Avco data on sorption rates at high loadings. For mass transfer to a spherical particle Bird, Stewart, and Lightfoot give*

$$k_A \; \frac{lb\ moles\ A}{ft^2,\ hr} = \frac{\rho_f D}{M d_p} \; [\, 2.0 + 0.6 \; Re^{\frac{1}{2}} \; Sc^{\frac{1}{3}} \,] \tag{60}$$

---

*Bird, Stewart and Lightfoot, "Transport Phenomena", Wiley, New York, 1960, p. 647.

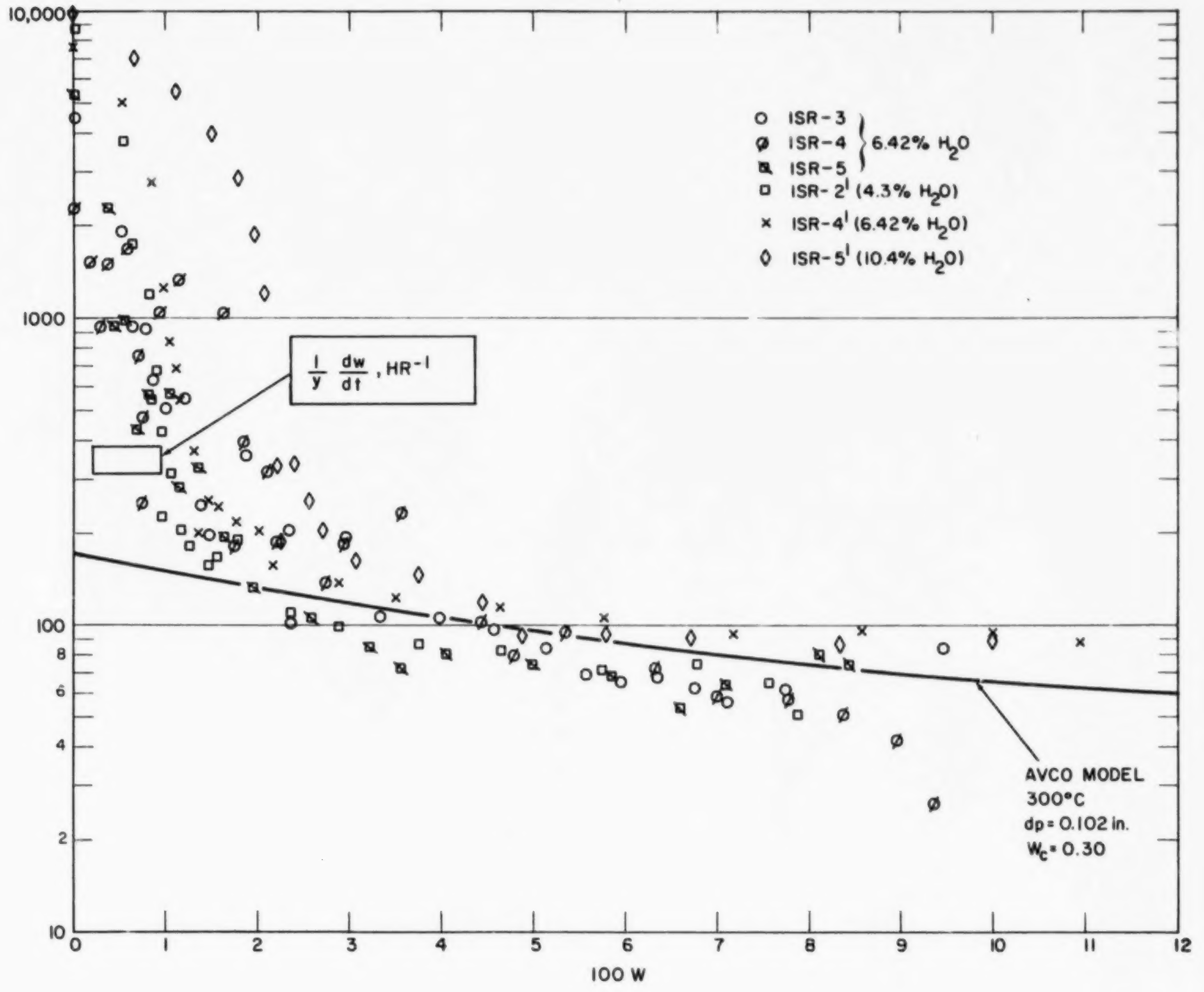

27-3817

Figure 34 INITIAL SORPTION RATE DATA

This number may be converted to an initial sorption rate as follows:

$$K_A \quad \frac{lb\ A}{lb\ sorbent,\ hr,\ mole\ fraction\ A} = k_A\ A_p\ M_A$$

where

M_A = molecular weight of SO_2 = 64

A_p = external surface of sorbent particle, ft^2/lb.

At various gas velocities relative to the particle, and at 300° C and a particle diameter of 0.102 inch (7/8 mesh) the above formula gives the following results.

Velocity, ft/sec	K, hr^{-1}
0	346
1	810
2	990
3	1115
5	1385
10	1810
20	2420

The initial sorption rates measured at a superficial velocity of about 2 ft/sec are higher than those predicted by mass transfer. The difference may be due to the geometry of the TGA unit and reduction of the flow cross section by the presence of the sample. In any case the indication is that since the initial rate is higher than the computed mass transfer rate the initial rate is controlled by bulk phase mass transfer.

Substantiation for the use of the pore diffusion model for higher loadings is given in section IV.D.5.

The range of loadings from two percent to the point where pore diffusion controls requires further study. In particular, to determine if the chemisorption process is rate limiting in this region would require measurements on the rate of this process. This would require measurements on finely powered sorbent to eliminate the possibility of rate limitation by pore diffusion.

TABLE VII

SUMMARY DATA OF INITIAL RATE STUDIES

Run No.	T (^oC)	Gas Velocity (ft/sec)	Vol. Percent SO_2	Vol. Percent H_2O	Vol. Percent O_2	Particle Diameter	Initial Rate From Data, hr^{-1}	Calculated* Initial Rate, hr^{-1}
ISR-3	300	1.9	.0695	6.42	3.12	.102 in.	4460	990
ISR-4	300	1.9	.0695	6.42	3.12	.102 in.	2260	990
ISR-5	300	1.9	.0695	6.42	3.12	.102 in.	5260	990
ISR-2[1]	300	1.9	.0599	4.32	3.19	.102 in.	8632	990
ISR-4[1]	300	1.9	.0585	6.42	3.12	.102 in.	2760	990
ISR-5[1]	300	1.9	.0562	10.4	2.99	.102 in.	9260	990

*Computed as mass transfer rate to single spheres using the volume percent SO_2 in the gas stream as the driving force for mass transfer

11. Comparison of Avco Data with Other Data

Data on the rate of SO_2 sorption on alkalized alumina are available from CERL and Bu Mines as well as Avco. In this section the methods used by the various laboratories will be described briefly. Then the data and rate models from the several sources will be compared. Also, the rates of sorption on W. R. Grace and Peter Spence sorbent will be compared.

a. CERL data

CERL has used two methods to measure the rate of sorption. In the first method particles of alkalized alumina were exposed to pure sulfur dioxide in a sealed chamber. The sorption was monitored by observation of the chamber pressure*. Because of the known large effect of moisture on the SO_2 capacity of alkalized alumina the data from these experiments are not felt to be pertinent to sorption from a flue gas and will not be considered further.

In a second investigation at CERL Billings and Collins used a differential fixed bed of sorbent. The sorbent was exposed to a simulated flue gas and the sulfur oxide uptake was determined by chemical analysis of the sorbent. By varying the time of exposure a sulfur oxide gain vs. time curve was generated. This was repeated at several SO_2 concentrations. The integral data were satisfactorily correlated by an integral form of the Amundson equation

$$\frac{dW}{dt} = Ky(1-S)$$

According to this model the rate of chemisorption is supposed to diminish as $(1-S)$ as sorption sites are occupied. The model presupposes that the rate is controlled by the rate of chemisorption.

The pellets of sorbent studied at CERL were about the same size (cylinders 1/16" x 1/8") as the W. R. Grace sorbent studied at Avco. In section IV.F it is shown that the Peter Spence sorbent has somewhat smaller pores than the Grace sorbent. Further, as shown in Figure 35, the rate of sorption obtained on the Spence material was only slightly less than obtained on the Grace material. Thus, it was felt that pore diffusion was probably rate limiting for the Spence sorbent as well as the Grace sorbent. On this account the Avco model for loadings less than 25 percent of saturation (59) was fitted to the CERL data.

Typical CERL loading vs. time curves are shown in Figure 36. For a rate equation of the form of the Avco model

---

*CERL Laboratory Note RD/L/N 33/63, Billings, Collins, Hearn and Masterson.

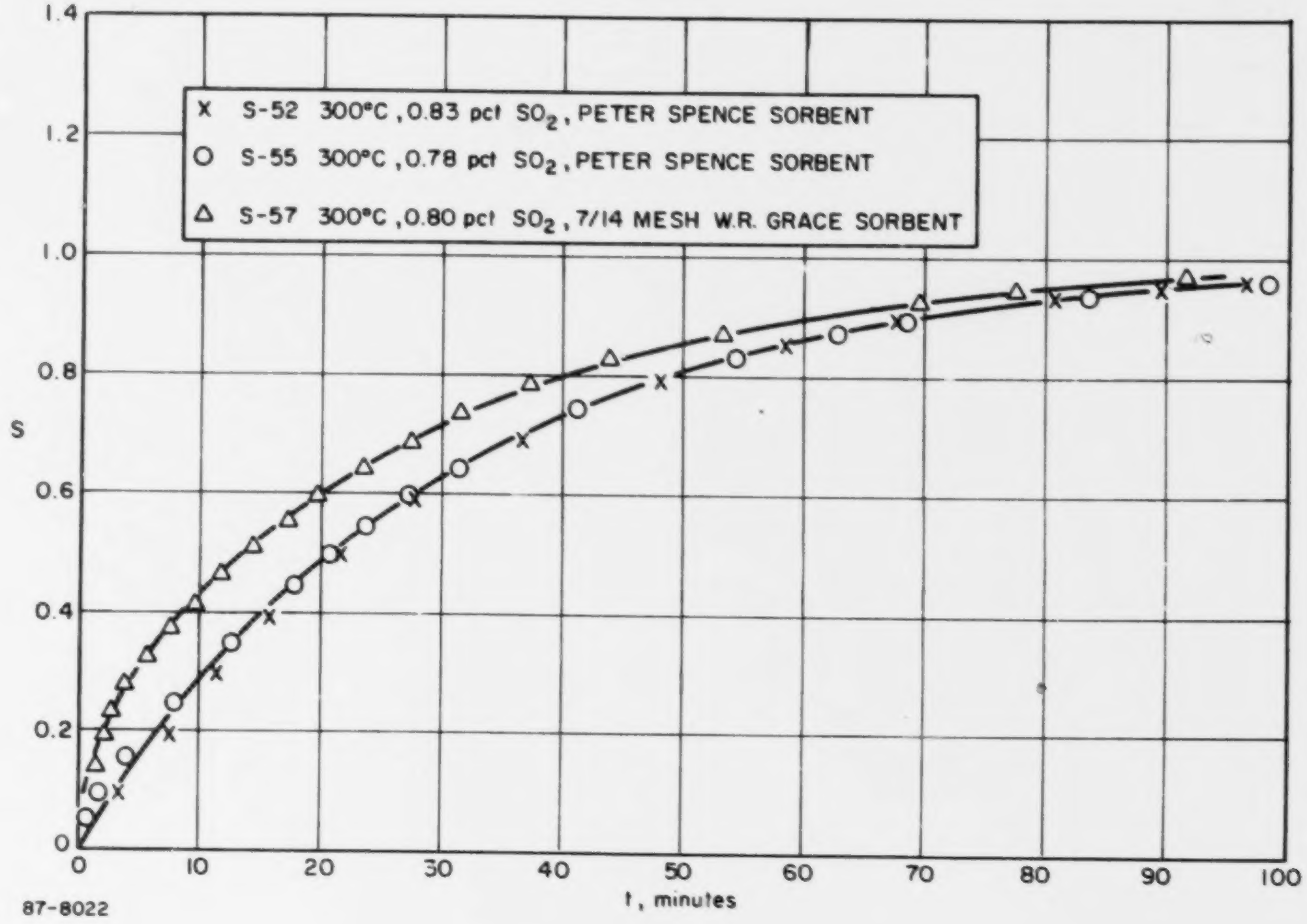

Figure 35 COMPARISON OF PETER SPENCE AND W.R. GRACE SORBENTS

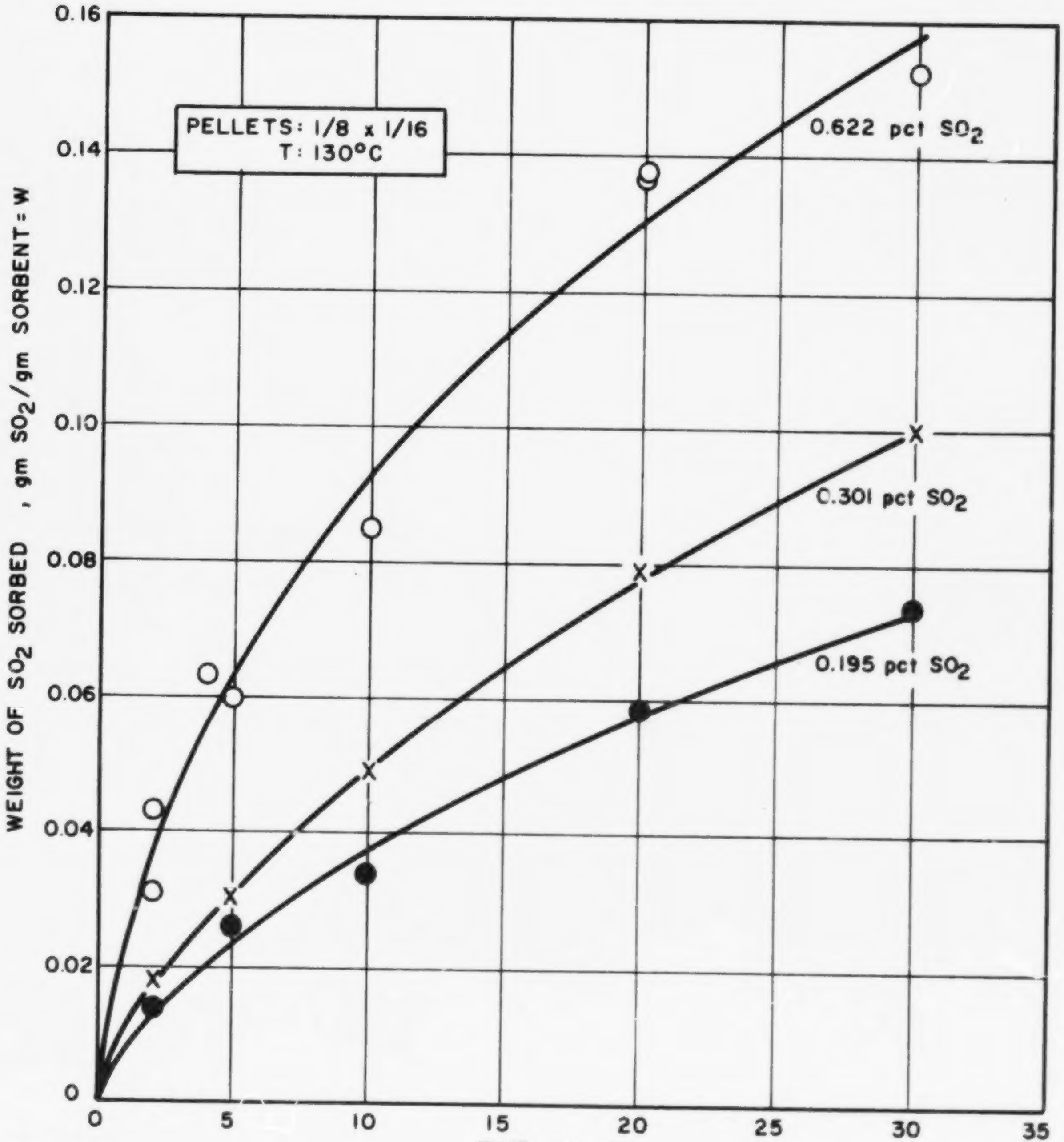

87-8023

Figure 36 SO_2 SORPTION CURVES OF CERL

$$\frac{dW}{dt} = \frac{A\,y}{1 + B\,W} \tag{61}$$

the loading vs. time data should plot as a straight line in s vs. $\sqrt{t}$ coordinates. The curves of Figure 36 are transformed to these coordinates in Figure 37. The fit to straight lines is excellent indicating that the pore diffusion model is appropriate.

The data were then plotted as y/d/dt W vs. W and the constants A and B evaluated from the slope and intercept of the best straight line. The resulting rate equation is

$$\frac{dW}{dt} = \frac{233\,\pi\,y}{1 + 70\,W} \quad hr^{-1} \tag{62}$$

The function 233/1 + 70 W is plotted vs. W in Figure 38. This is the Avco model for the CERL data for sorption on Peter Spence sorbent at 130° C.

Fitting the Amundson equation to the CERL data at 130° C gives the following rate equation:

$$\frac{dW}{dt} = 98.6\,y\,\pi\,(1 - S)\ hr^{-1} \tag{63}$$

where the saturation loading was taken by CERL as 0.24 gm SO_2/gm sorbent. Six concentrations of SO_2 were used ranging from 0.052 v/o to 1.92 v/o. The rate constants varied from 82 hr^{-1} to 118 hr^{-1} as the concentration went from 1.92 to 0.052 v/o. Equation 63 is plotted in Figure 38.

Also plotted in this figure are the rate data for three concentrations of SO_2, obtained by measuring the slope of the CERL sorption curves. The data indicate that the Avco model is the more accurate representation as well as being theoretically more correct.

A third curve plotted on Figure 38, shows the Avco pore diffusion model fitted to the Avco data on W. R. Grace sorbent. This again reflects the somewhat higher sorption rates obtained on W. R. Grace material as previously indicated in VI.D.14. The higher rates on the Grace material at

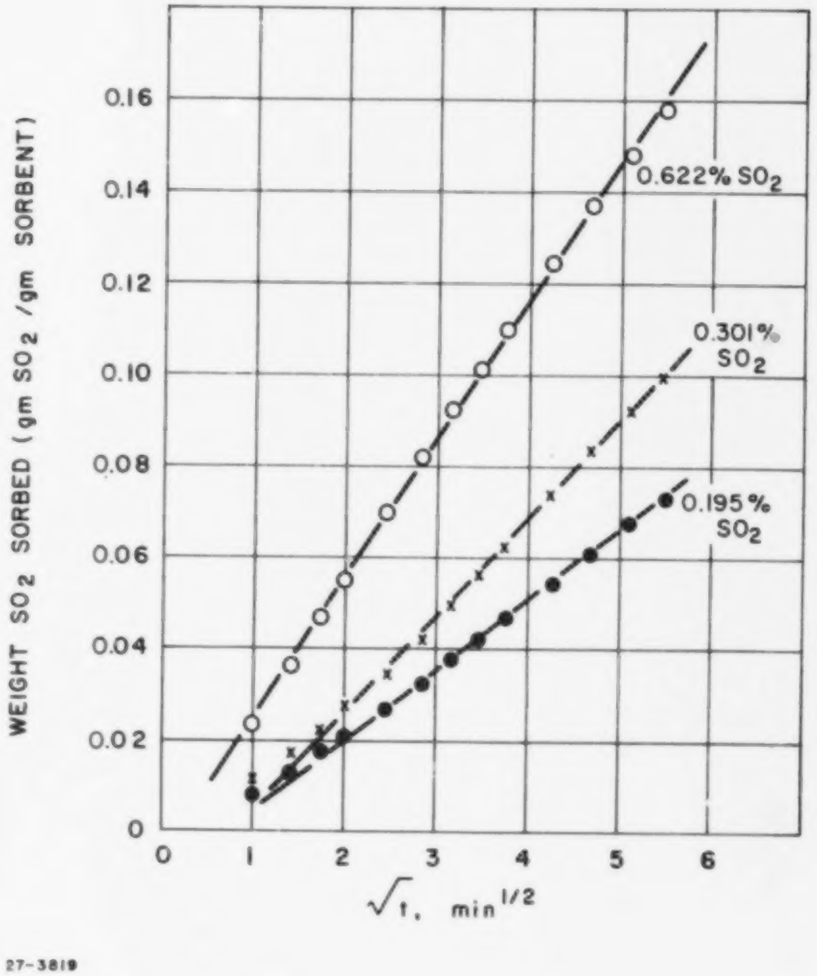

Figure 37 CERL DATA FITTED TO AVCO MODEL

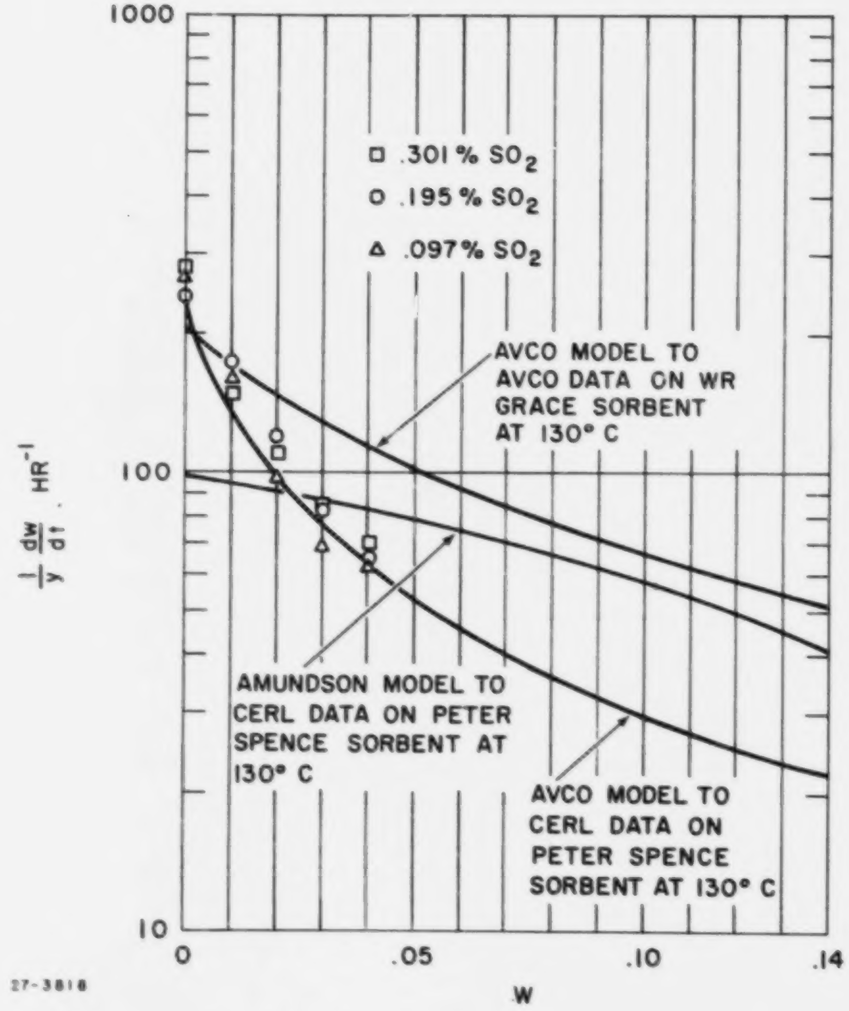

Figure 38 COMPARISON OF AVCO AND AMUNDSON MODELS FOR CERL DATA

high loadings are indicative of the larger pore diameter and higher effective diffusivity in the pores. It should be noted, however, that neither model is derived from data accurate at less than 1 percent loading and the predicted initial rates are low relative to those reported in Section IV.D.10.

b. Bureau of Mines data

Bu Mines, Albany has made direct kinetic measurements using a differential bed contactor and chemical analysis of the sorbent in much the same manner as CERL. In a monthly report communicated by letter on 8/25/67 to Mr. R. P. Hangebrauck at the National Center for Air Pollution Control, the Bureau of Mines presented a tabulation of differential bed data. Sorption rates were computed from this data as $\frac{1}{y}\frac{dW}{dt}$, hr^{-1} . At 300° C and concentrations of 0.315 V/o to 0.07 V/o initial rates from 250 to 290 hr^{-1} were obtained. At 10 percent loadings rates of 35 to 60 hr^{-1} were computed.

The initial rates are considerably lower than the initial rates measured at Avco. This may be due to differences in sorbent properties, particle diameter, resolution of the experiment at low loadings, or mass transfer limitation due to the low gas velocity used (0.5 ft/sec). Also there was evidently some depletion of SO_2 in the gas during the initial part of the sorption. The rates at higher loadings are also lower than those measured at Avco but not to the extent of the initial rates. The differences at the higher loadings must reflect differences in sorbent properties and particle diameter as mass transfer and the resolution of the experiment should not be a problem at the associated lower rates.

E. REGENERATION

Regeneration data for W. R. Grace sorbent have been obtained over a range of loadings of less than 10 percent of saturation to nearly complete saturation. Regeneration temperatures of 550° C to 700° C were used.

The regenerating gas was usually hydrogen. The reaction in hydrogen is assumed to be

$$Na_2SO_4 + Al_2O_3 + 4H_2 \rightarrow 3H_2O + H_2S + 2NaALO_2$$

Also, the effect of reducing the hydrogen partial pressure by dilution with nitrogen was measured. The effects of the presence of moisture, carbon monoxide, and hydrogen sulfide were also measured.

The data obtained were not of the nature required to develop a kinetic model for the regeneration process. As a result, the data are presented as $t_{0.75}$, the time required for the regeneration to be 75 percent complete. This time is called the regeneration time.

There is some loss in weight when heating saturated sorbent in nitrogen prior to regeneration. For obtaining $t_{0.75}$, it is not clear whether we should take

75 percent of the weight gained during sorption or 75 percent of the weight of sorbate remaining after heating to regeneration temperature. We have arbitrarily adopted the former convention. The sorptions S-5B through S-28 were carried out with 15 percent CO_2 in the simulated flue gas while sorptions S-56 through S-72 were carried out in CO_2-free simulated flue gas. There was no appreciable sorption of H_2O in any of the runs. Runs S-56 through S-72 were made with moist flue gas while the earlier sorptions were run dry. Only moist sorptions were considered in discussing thermal weight loss. The thermal weight loss for runs R-56 through R-72 must be sulfur compounds as there was no CO_2 in the sorption gases and the H_2O sorption was negligible.

In the monthly reports issued to date a 90 percent complete regeneration time has been used. A 75 percent regeneration time is used for this report as it can be more accurately determined and still reflects the order of magnitude of time required for complete regeneration. At regeneration times in excess of twice $t_{0.75}$ the regeneration is greater than 90 percent complete. Hence, $\tau = 2\ t_{0.75}$ will be used as an estimate of required regenerator residence time.

Some data were obtained on the Cahn Electrobalance, but the majority were obtained with the torsion balance. The conditions for each run and the value of $t_{0.75}$ are given in Table VIII. Several runs are seen to be omitted. This indicates that either no data were taken during the regeneration half of the cycle for that run, or that there was either an equipment failure or operator error. The weight vs. time curves for typical regenerations are given in Figures 39 through 41. Weight loss vs. time data for all of the runs given in Table VIII are listed in Appendix II.

1. Effect of Hydrogen Partial Pressure

The data from runs R-3, R-5, R-6, R-7, R-8, R-9, R-10, R-13, and R-21 are listed in Table VIII. These data obtained from regeneration of sorbents at low initial loading are presented in Figure 42 as regeneration time vs. volume percent hydrogen. The remainder of the gas is nitrogen. The regeneration time increases uniformly as the hydrogen composition is reduced below 100 percent. There is no noticeable effect of sorbent loading over the small range considered.

2. Extent of Thermal Regeneration

At the completion of each sorption cycle, the apparatus is purged with nitrogen and heated from the sorption temperature to the regeneration temperature. During the heat up in nitrogen a certain amount of weight is lost. This loss is presented in Table VIII as a percentage of the weight gained during the sorption step.

In Figure 43 the data for sorptions made with moist flue gas are presented graphically as thermal weight loss vs. the time required for the sorption step. Runs R-56 through ISR-5[1] inclusive are plotted. Various symbols are used to indicate various regeneration temperatures and the SO_2 content of the flue gas used in sorption.

In spite of the widely scattered data is appears that the degree of thermal regeneration decreases as the sorption time increases. Within the accuracy

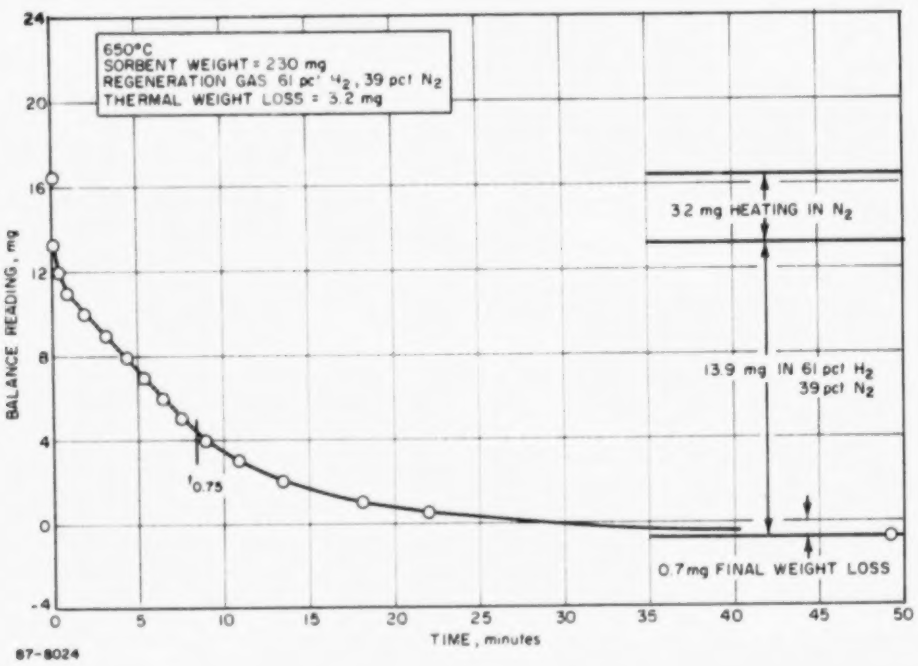

Figure 39 REGENERATION R-13

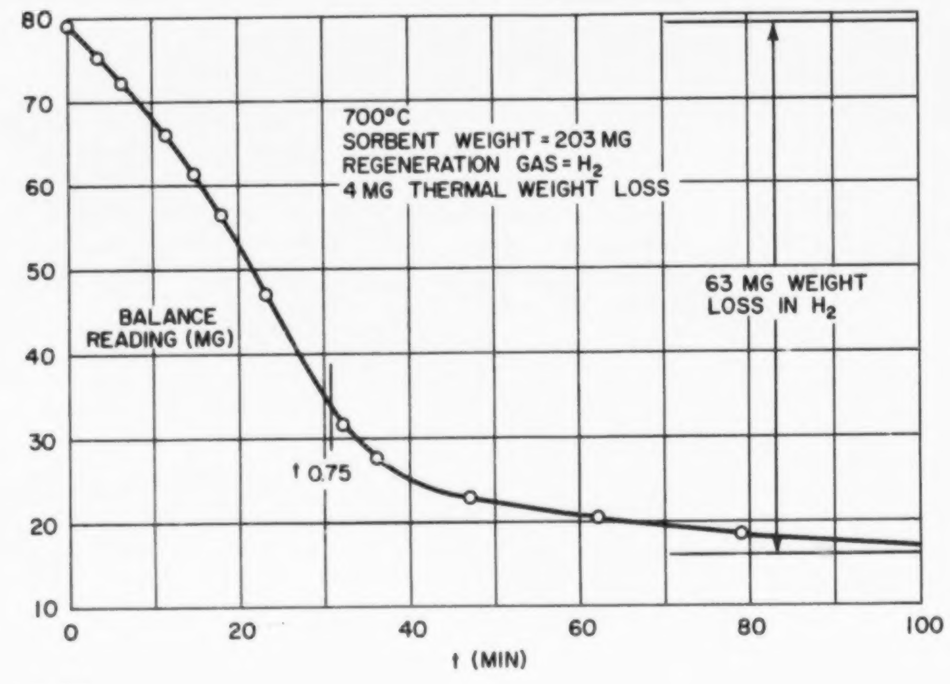

Figure 40 REGENERATION R-58

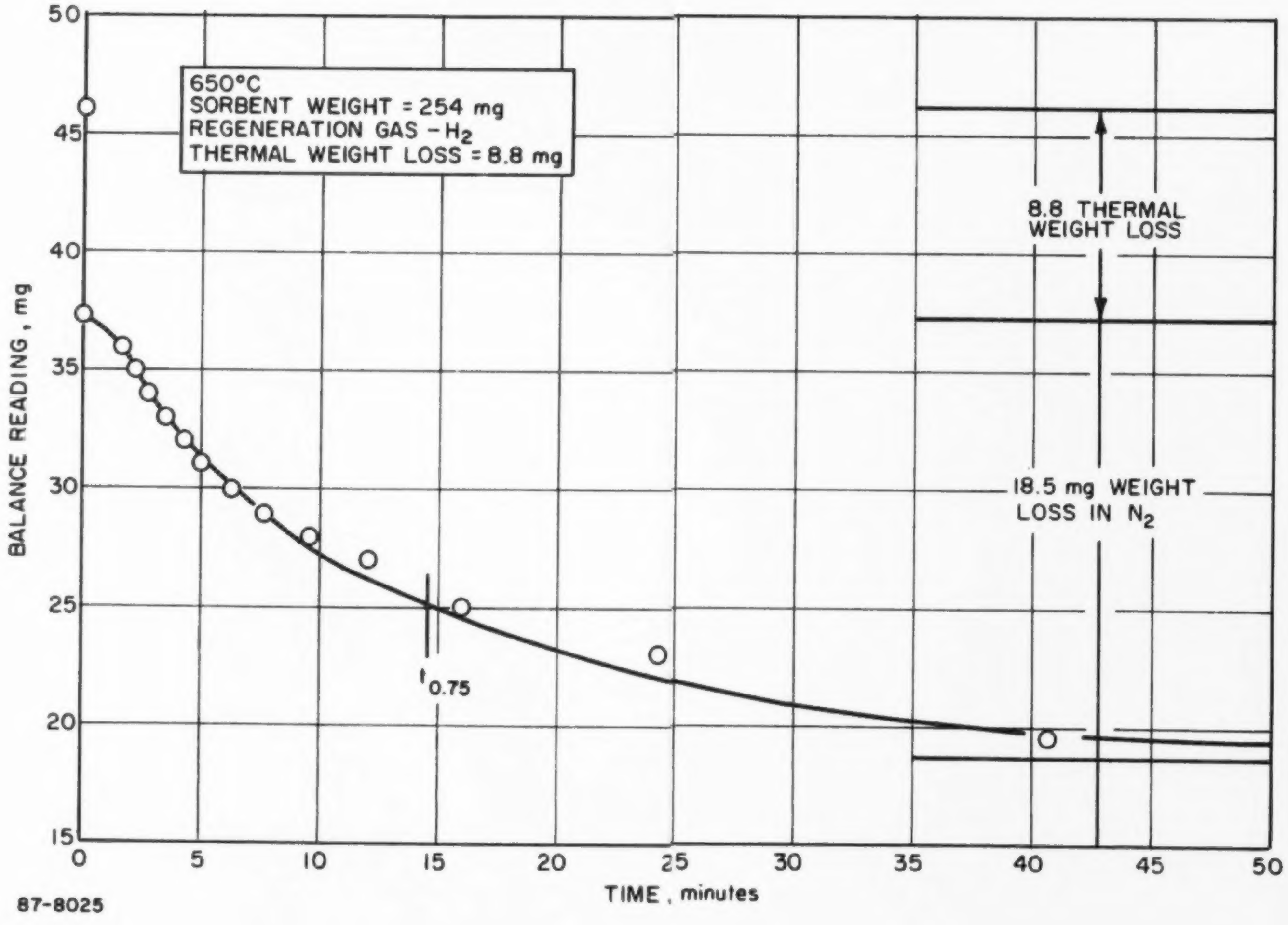

Figure 41 REGENERATION R-72

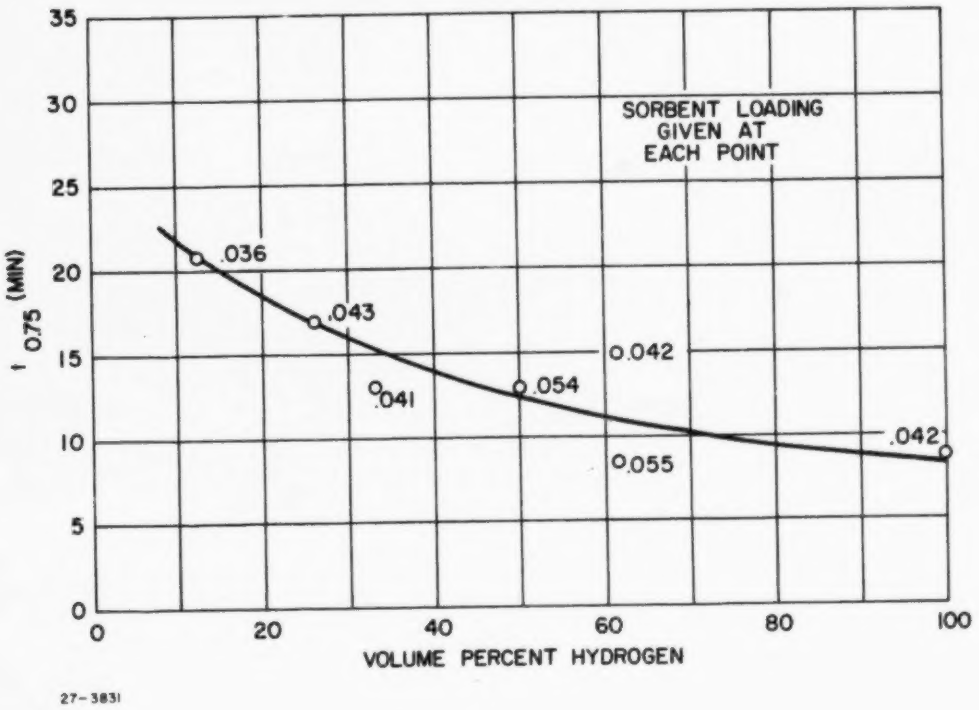

Figure 42 EFFECT OF HYDROGEN CONTENT ON REGENERATION TIME

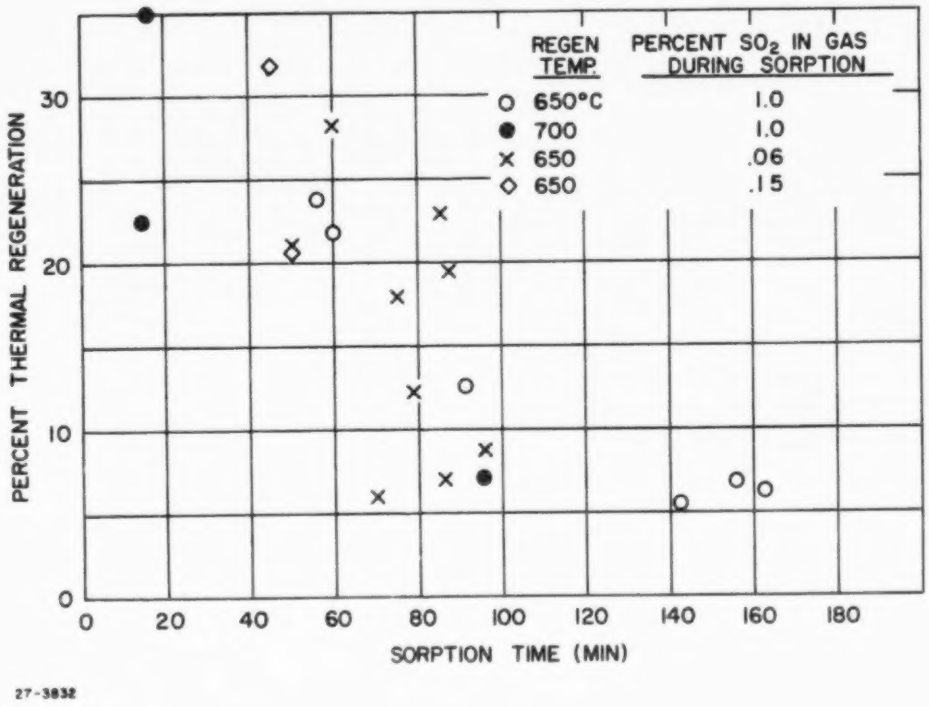

Figure 43 EFFECT OF SORPTION TIME ON THERMAL REGENERATION

of the data there is no effect of the flue gas SO_2 concentration at a given sorption time. This implies independence of the initial SO_2 loading on the sorbent. The longer sorption times may allow a greater portion of the sorbate to diffuse through the solid phase of the sorbent and chemically combine with the sorbent; or, it may allow for oxidation of sorbed sulfite to sulfate and a consequent increase in stability of the sorbate.

Although the data are scattered it must be concluded that the designer of a regenerator would have to account for thermal regeneration in design. At sorption times of under ten minutes, which are typical of the dispersed bed contactor, about thirty percent thermal regeneration is to be expected.

3. Effect of Initial Loading

Runs P5-B, P6-A, R-3, R-5, R-6, R-13, R-17, R-16, R-19, R-20, R-21, R-56, R-57, R-58, R-62, R-63, R-71 and R-72 were made varying initial loadings to test the effect of this parameter on regeneration rate. Regeneration gas was 61 percent H_2 and 39 percent N_2 for Runs R-13 through R-21 and 100 percent H_2 for the remainder. The data of these runs are given in Table VIII and plotted in Figure 44 as regeneration time vs. initial loading. The regeneration times increase rapidly with initial loading and decrease rapidly with increasing temperature.

Two runs R-71, and R-72, in which the sorption was carried out in wet flue gas regenerated at a rate identical with runs made under dry but otherwise identical sorption conditions. Thus, both wet and dry data have been included in the graph.

4. Effect of Carbon Monoxide

In an effort to simulate regeneration by producer gas, mixtures of hydrogen and carbon monoxide have been used. The data of runs R-24, R-27 and R-28 using H_2-CO mixtures have been plotted along with the data of R-3, R-5 and R-6 using pure H_2. Figure 45 shows regeneration time as a function of gas composition. Scatter prohibits determining any trends. However, it is clear that there is no substantial reduction in rate due to the presence of carbon monoxide and that producer gas type regenerating gases should be satisfactory from the point of view of rate.

It has been noticed, however, that in the presence of carbon monoxide the regeneration does not go to completion. That is, after constant weight is reached in the hydrogen-carbon monoxide mixture, exposure to pure hydrogen will result in a further decrease in weight. This effect is shown in Figure 46 where the amount of sorbate not removed in the presence of carbon monoxide is given as a percentage of the total weight loss during regeneration. In pure CO as much as twenty-five percent of the sorbate is unremoved. Regeneration time in the presence of CO is stated as the time required to remove 75 percent of the sorbate that can be removed before reaching equilibrium as opposed to 75 percent of the weight gained during sorption.

In contrast, Bureau of Mines results* indicate complete removal of sorbed sulfur with reformed natural gas and producer gas (mixtures of H_2, CO, CO_2 and N_2). The regeneration gases used by Bu Mines contained CO_2 as well as H_2 and

---

*Bureau of Mines Report of Investigations, RI 7021.

TABLE VIII

REGENERATION DATA FOR SO_2 SORPTION ($T_{sorption} = 300°C$)

Run	T(°C)	Regeneration gas Composition (volume percent)	Initial* Loading (mg/mg)	Regeneration Time (min)	Sorption time (min)	Weight loss upon heating in N_2, percent of gain in sorption
P-5B	650	H_2-100	.028	3.0		-
P-6A	650	H_2-100	.094	17		-
R-3	650	H_2-100	.042	7.7		20.0
R-5	650	H_2-100	.043	7.2		31.0
R-6	650	H_2-100	.042	8.9		23.2
R-7	650	H_2-50, N_2-50	.054	13		4.8
R-8	650	H_2-122, N_2-87.8	.036	20.8		18.7
R-9	650	H_2-26, N_2-74	.043	17		26.6
R-10	650	H_2-33.1, N_2-66.9	.041	13		18.7
R-13	650	H_2-61.2, N_2-38.8	.055	8.5		19.5
R-16	650	H_2-61.2, N_2-38.8	.024	4.0		4.9
R-17	650	H_2-61.2, N_2-38.8	.022	4.9		0
R-19	650	H_2-61.2, N_2-38.8	.061	13		10.4
R-20	650	H_2-61.2, N_2-38.8	.025	5.3		0
R-21	650	H_2-61.2, N_2-38.8	.042	15		5.1
R-23	550	H_2-100	.043	36		4.6
R-24	650	CO-100	.049	5.2		6.9
R-27	650	H_2-75, CO-25	.041	5		14.5
R-28	650	H_2-25.5, CO-74.5	.047	3.2		19.3
R-56	650	H_2-100	.37	95	95	7.0
R-57	700	H_2-100	.33	22	91	12.6
R-58	700	H_2-100	.41	31	162	6.2
R-59	700	H_2-69.7, H_2S-7.2 H_2O-22.8	.367		155	6.8
R-60	700	H_2S + H_2 - H_2S meter broken	.372		142	5.5
R-62	700	H_2-100	.31	8	60	21.8
R-63	700	H_2-100	.285	9	56	23.8
R-71	650	H_2-100	.072	11	14	22.6
R-72	650	H_2-100	.086	14.5	16	34.8
ISR-1	650	H_2-100			45	31.8
ISR-2	650	H_2-100			50	20.6
ISR-3	650	H_2-100			85	22.9
ISR-4	650	H_2-100			37	19.4
ISR-5	650	H_2-100			79	12.2
ISR-6	650	H_2-100			60	28.2
ISR-7	650	H_2-100			70	5.9
ISR-1[1]	650	H_2-100			50	21.0
ISR-2[1]	650	H_2-100			86	6.9
ISR-3[1]	650	H_2-100			75	18.0
ISR-5[1]	650	H_2-100			95.2	8.7

*computed as $\frac{.8 \times \text{(weight gain during sorption)}}{\text{weight of sorbent}}$

Note: CO_2 present in simulated flue gas for P-5B through R-28 absent for R-56 through R-72

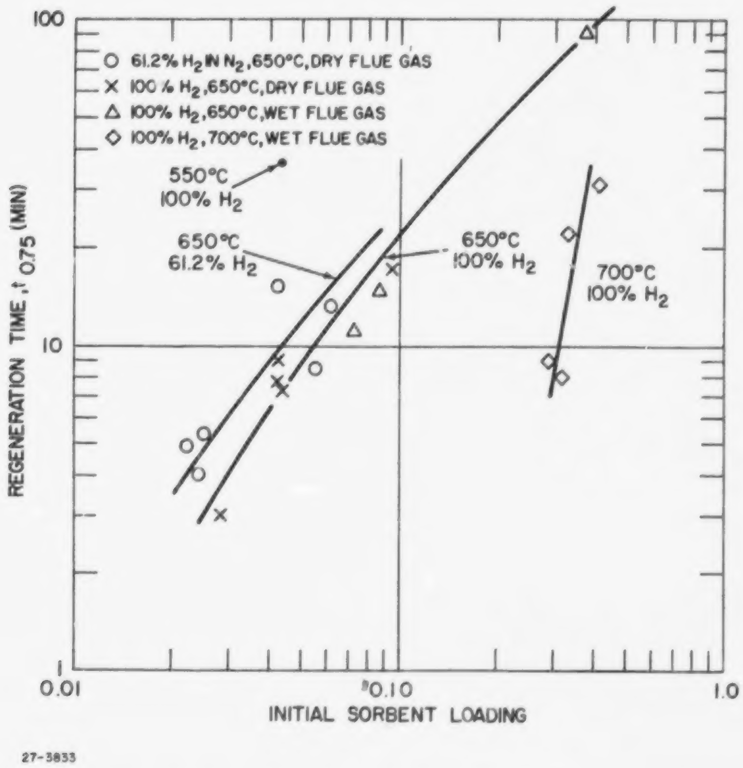

Figure 44 EFFECT OF INITIAL LOADING ON REGENERATION TIME

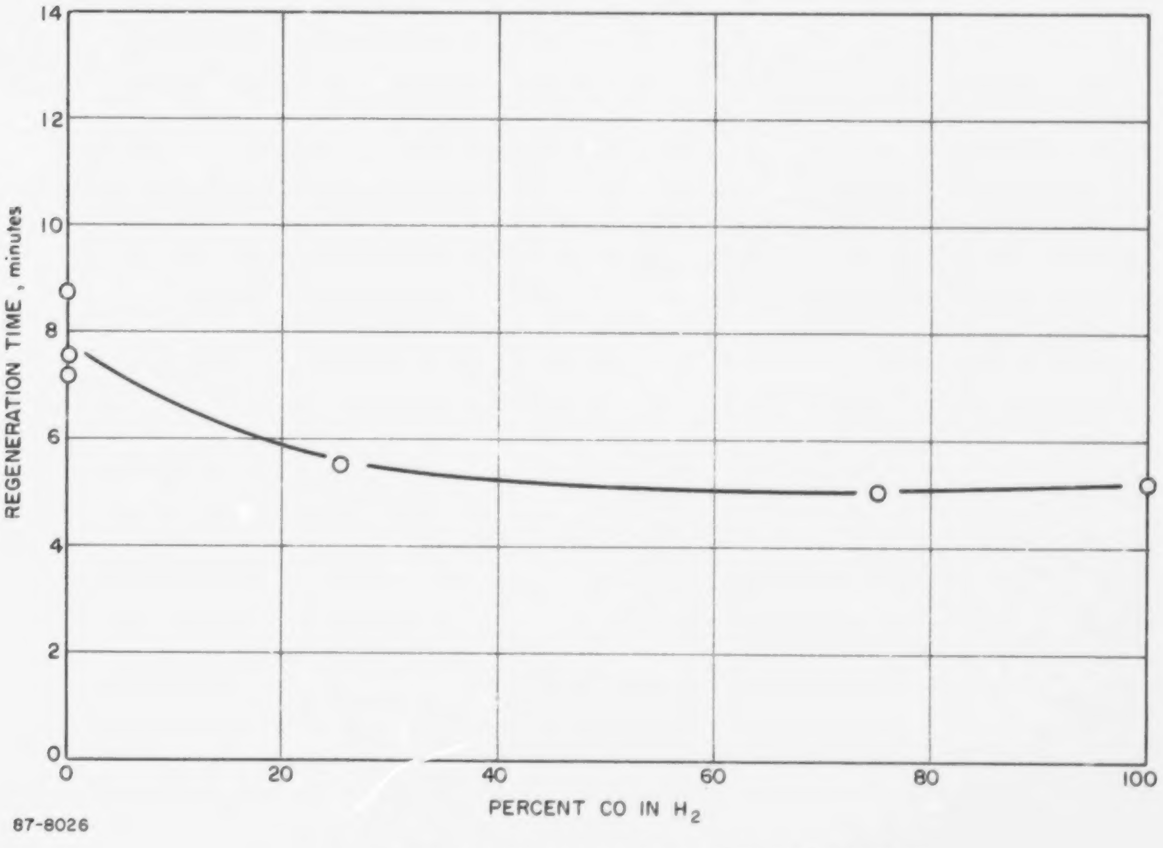

Figure 45 EFFECT OF CO ON REGENERATION TIME

CO and this difference in composition was felt to account for the difference in results. Two regenerations were run at 650° C and with 15.8 percent initial loading. Carbon dioxide was added to the regeneration gas to give a composition of 21.4 v/o CO_2, 31.4 v/o CO, 47.2 v/o H_2. In both runs complete regeneration was obtained. Thus gases of the producer and reformer type seem satisfactory regeneration gases.

5. Effect of Reaction Products

Regenerations were performed in which the regeneration reaction products, H_2S and H_2O, were included in the regeneration gas. In run R-59 the gas was 69.7 percent H_2, the remainder being a stoichiometric mixture (3/1) of water and H_2S. In Run R-60 an estimated five percent H_2S was included with the hydrogen. In both cases the regeneration rate was not significantly lowered by the presence of the reaction products. The time required to reach equilibrium was about 25 minutes which is about what would be expected on the basis of Figure 45. However, the regeneration ceased at about 75 percent of completion and pure hydrogen was required to complete the process. The weight vs. time curves are given in Figure 47.

The effect of reaction products on the completeness of regeneration is not felt to be a serious problem. In a counter current regenerator the solids leaving the regenerator would be in contact with a regenerating gas containing no reaction products, and regeneration could procede to completion.

6. Effect of Temperature

Run R-25 was carried out at 550° C and an initial loading of 0.043 and the regeneration time was 36 minutes. Runs R-3 and R-5, made at 650° C gave regeneration times of 7.2 and 7.7 minutes at the same initial loading. The increase in rate was a factor of 4.8.

Run R-56 was made at 650° C and a loading of 0.37. The regeneration time was 95 minutes. Runs R-57, R-58 were run at 700° C and at similar loadings. The regeneration times were 22 and 31 minutes, or an increase in rate by a factor of 3.6. On the basis of these few runs relative regeneration time as a function of temperature is given in Figure 48 with the time at 650° C arbitrarily selected to be unity. An Arrhenius plot does not give any better approximation to a straight line.

These results can be compared with regeneration times obtained by the Bureau of Mines, Report of Investigations RI 7021, Figure 23, p. 33. The Bu Mines regeneration time at 650° C (1200° F) is 233 minutes and at 700° C (1290° F) is 62 minutes. The ratio is 3.76, in good agreement with the Avco value of 3.6. If the agreement in temperature effect is excellent the agreement in regeneration times is not. The Avco times are less by more than a factor of two in spite of initial loadings higher by more than a factor of two (0.37 lb SO_2/lb sorbent compared to 0.16 lb SO_2/lb sorbent).

In section IV.F.1.a of this report chemical analyses of the W. R. Grace sorbent of 14.8 percent Na (data of Kelly) and 24.9 percent Na (data of Field) are reported. It is not clear that these analyses refer to the same sorbent as used by Bu Mines or Avco or that Avco and Bu Mines used the same sorbent. This may account for the discrepancy in regeneration times.

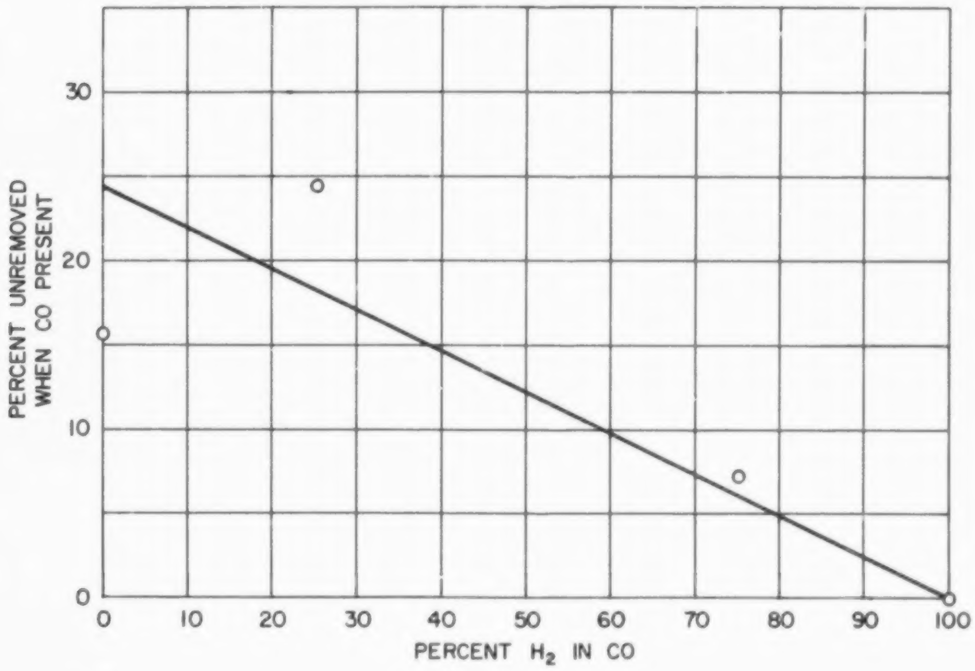

27-3844

Figure 46 UNREMOVED WEIGHT REGENERATING IN CO

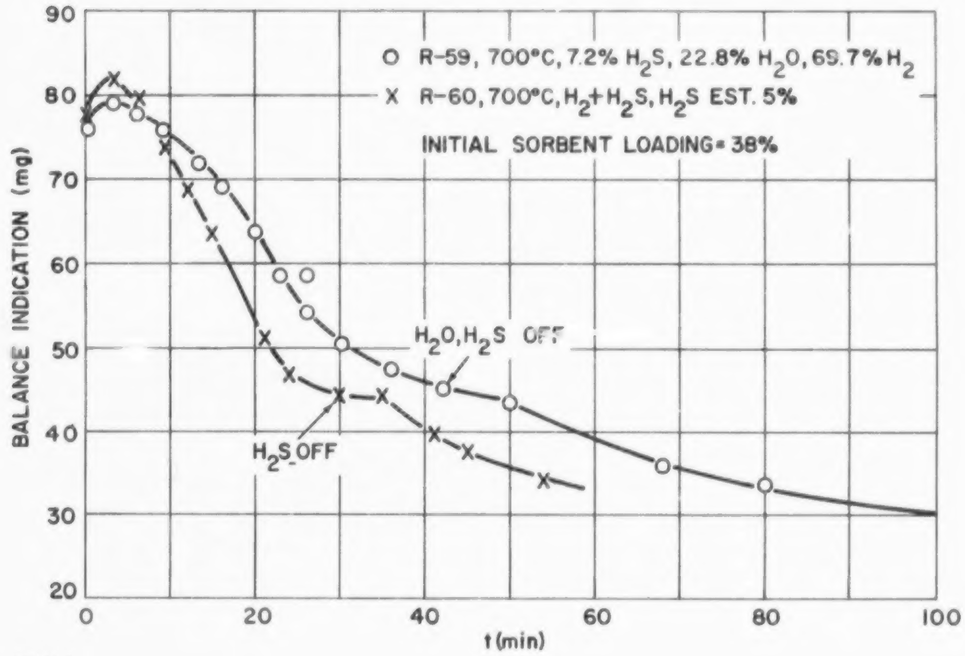

27-3845

Figure 47 REGENERATION IN THE PRESENCE OF REACTION PRODUCTS

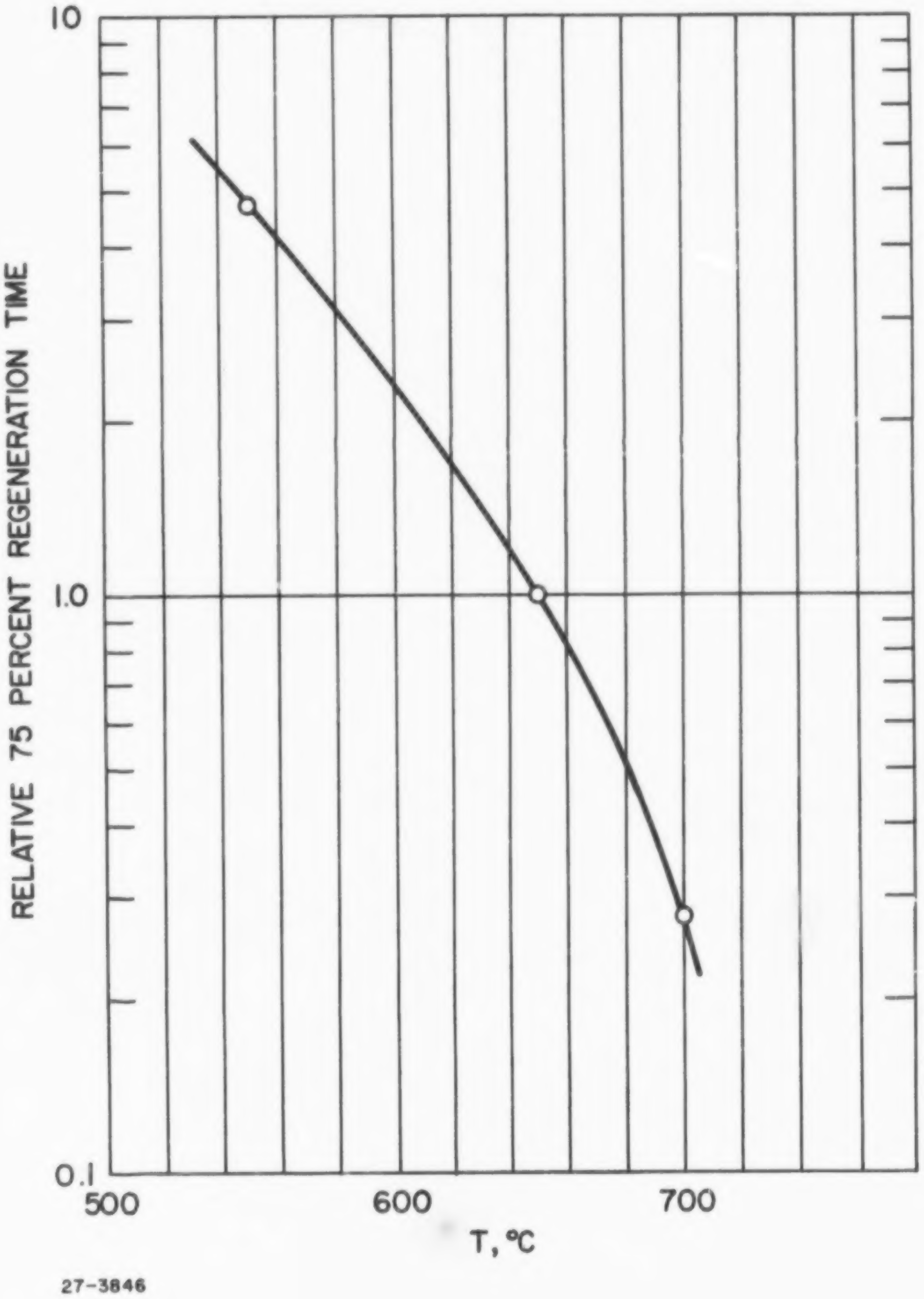

27-3846

Figure 48 RELATIVE REGENERATION TIME AS A FUNCTION OF TEMPERATURE

It is to be noted that the temperature effect from 550° C to 650° C was obtained on sorbents of low initial loading and on which the SO_2 was sorbed from dry flue gas. The temperature effect from 650° C to 700° C was obtained on sorbents with a high loading, loaded in moist flue gas. The effect of the humidity of the flue gas and the initial loading of the sorbent on the temperature dependence should be measured. Also, it should be verified that the same temperature effect applies to the 90 percent regeneration time as to the 75 percent time.

7. Summary of Regeneration Kinetics

The extent of thermal regeneration taking place upon heating from the sorption temperature to the regeneration temperature can be estimated from Figure 43 for sorption temperatures of 300° C and regeneration temperatures of 650-700° C.

From Figure 44 the regeneration time at 650° C in pure hydrogen can be estimated. From Figure 48 the regeneration time at other temperatures may be found.

For example consider sizing a regenerator to operate at 625° C on a sorbent with an initial loading of 0.10 lb SO_2/lb sorbent. From Figure 43 the thermal regeneration would be 30 percent of the initial loading. From Figure 44 the regeneration time at 650° C would be 20 minutes. At 625° C Figure 48 indicates an increase in regeneration time by a factor of 1.5, i.e. to 30 minutes. From Figures 39, 40, and 41 it appears that at a time equal to twice $t_{0.75}$ that the regeneration will be more than 90 percent complete. Using 90 percent regeneration as a design criterion a regenerator residence time of 60 minutes would be called for.

8. Continued Work on Regeneration

Recommendations for continued study of the kinetics of regeneration depend upon the end use of the information to be obtained. For purposes of rough sizing of a regenerator as indicated by example in the previous section a rather direct extension of the work done to date is indicated.

In particular more data should be obtained on both the regeneration time and the extent of thermal regeneration as a function of initial sorbent loading. Much of the data used in this report was obtained by regeneration of sorbent loaded with dry flue gas. The validity of this data should be further verified by using wet flue gas in all future work.

The data on the effect of temperature on regeneration time should be supplemented. Data should be obtained at least at two initial loadings.

It is to be recalled that regeneration was not 100 percent complete in mixtures of H_2 and CO. The addition of CO_2 to the H_2-CO regeneration gas, thus better simulating reformed natural gas or producer gas did effect complete regeneration. Rates of regeneration in actual producer gas and reformer gases should be measured.

A more detailed study of regeneration kinetics would be in order if the mechanism of regeneration were desired. Understanding the reaction mechanism could lead to improvement of the regeneration characteristics of the sorbent and would allow extrapolation of rate data to conditions beyond those studied experimentally.

F. CHEMICAL & PHYSICAL PROPERTIES OF SORBENT

Data on the properties of the sorbent are available from several sources:

1) American Instrument Co., data hereafter referred to as Aminco data

2) Avco Corp., data referred to as Avco data

3) Letter from J. H. Field, Bu Mines, Bruceton, Pa. to R. Hangebrauck, Div. for Air Pollution Control, Cincinnati, Ohio, 11/17/66, data referred to as Field data

4) Letter from H. J. Kelly, Bu Mines, Albany, Ore. to R. Hangebrauck, Div. of Air Pollution Control, Cincinnati, Ohio, 11/23/66, data referred to as Kelly data.

1. Chemical Analysis

Material and Source	Al_2O_3	Na_2O	SO_3	CO_2	H_2O	C
a. W. R. Grace Sorbent						
1) Kelly data, fired 600° C in H_2	56.3	19.9	3.6	1.31	4.26	.4
2) Field data, fired 630-670° C in H_2	57.0*	33.6**	3.0	.16	-	-
3) Avco data, fired 650° C in H_2	-	-	3.66†	-	-	.7††
b. Bureau of Mines, Pilot Plant Sorbent						
1) Kelly data, dried, not fired	57.7	10.8	2.5	5.67	24.0	-
2) Avco data, fired in H_2	53.1	-	-	-	-	-

* Al_2O_3 equivalent to 30.7% Al
**Na_2O equivalent to 24.9% Na
†By Leco Analyzer
†† By F&M 180 Analyzer

2. Physical Properties

a. W. R. Grace sorbent

1) Kelly data -- sorbent H_2 treated for four hours at 600° C

ρ_{pellet} = 1.07 gm/cm^3

S_g = 47.5 m^2/gm

ϵ = 0.61

mean pore diameter = .029μ

A pore size distribution obtained by mercury intrusion is given in Figure 49. The distribution is bimodal with a modes at 0.028μ and another spreading over about 1 to 20 μ

2) Field data -- sorbent H_2 treated for four hours at 600° C

The data reported are identical to those of Kelly. An additional pore size distribution curve is given in Figure 50. This curve is essentially identical to that reported by Kelly when scaled to the same total pore volume. It is presumed that the difference in pore volume is a result of a difference in sample size for the two curves as the porosity was 61 percent for both samples.

b. Aminco data

Samples of several sorbents, subjected to various conditions, were submitted by Avco to American Instrument Co. for pore size distribution and surface area measurement.

1) W. R. Grace sorbent

Sorbent received H_2 treated for ten hours at 630-670° C. -- Fresh sorbent had a mean pore diameter of 0.09 μ. Sorbent that had been cycled seven times had a mean pore diameter of 0.10 μ. The difference is not considered to be significant. Conditions of use were:

Sorption: T = 300° C

Regeneration: T = 650° C

Loading 10 percent of saturation

Flue gas: dry

The mercury intrusion pore size distribution curves for fresh and used sorbent are given in Figures 51 and 52. Inspection of these curves indicates that little or no deterioration of the pore structure occurs with use at the conditions chosen. The distributions are bimodal about 0.09μ and 25μ.

In addition a sample from the same batch was analyzed for pore structure by nitrogen adsorption. Nitrogen adsorption extends the measurements to a diameter of 0.0014μ, considerably below the minimum diameter of 0.012μ obtained with mercury intrusion.

A pore volume of 0.0132 cm^3/gm was measured between 0.012 μ and 0.0014μ. A surface of 12.9 cm^2/gm was measured in the same range, and a mode in the pore size distribution at about 10 Å was observed. Thus, the distribution of pore size is trimodal, the two largest modes detected by mercury intrusion and the smallest mode by nitrogen sorption.

The volume distribution curve obtained from the nitrogen adsorption measurements is given in Figure 53. Note that the measurements extend to a

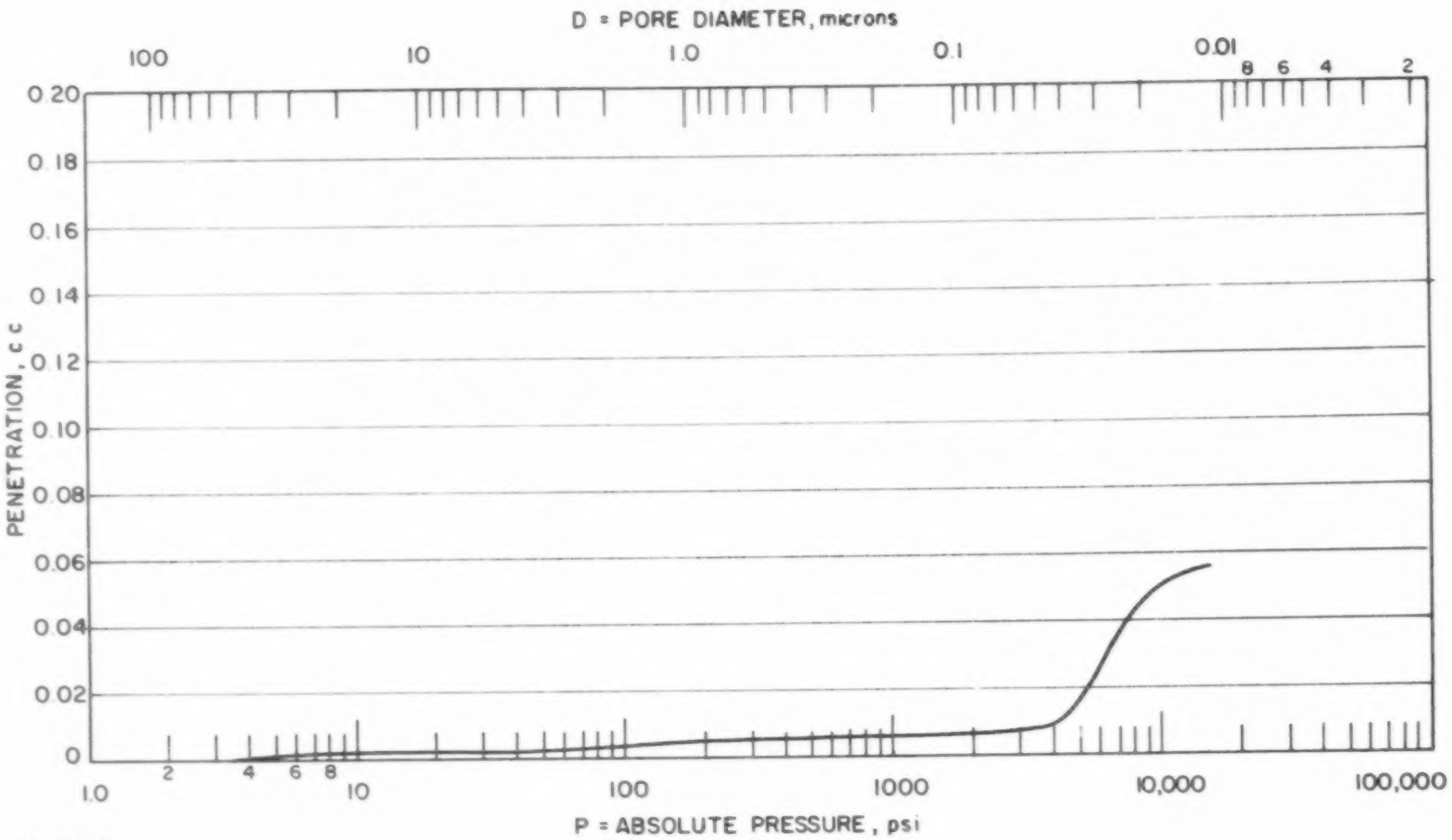

87-8027

Figure 49 PORE SIZE DISTRIBUTION FOR W.R. GRACE SORBENT, KELLY DATA

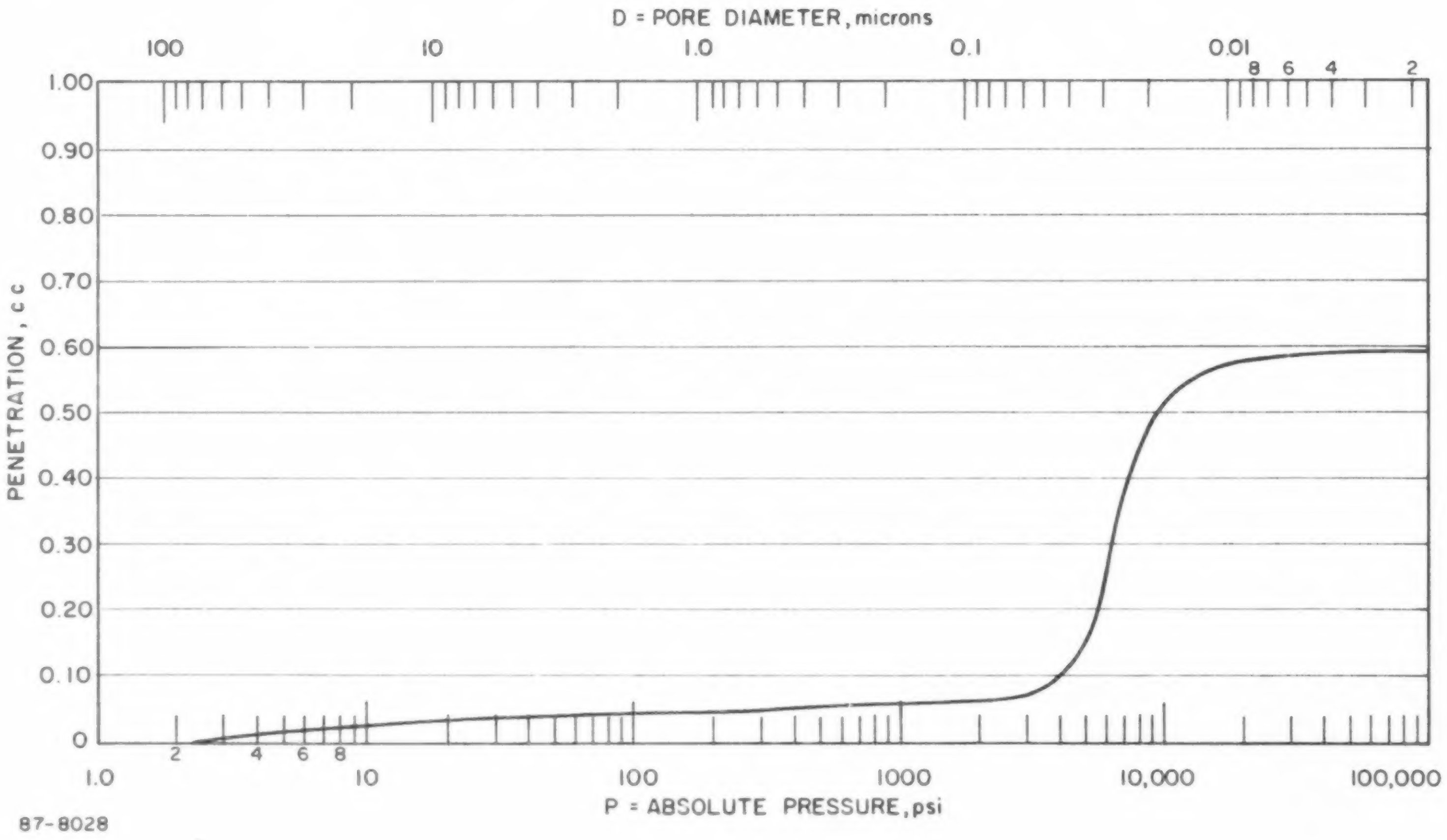

Figure 50 PORE SIZE DISTRIBUTION FOR W.R. GRACE SORBENT, FIELD DATA

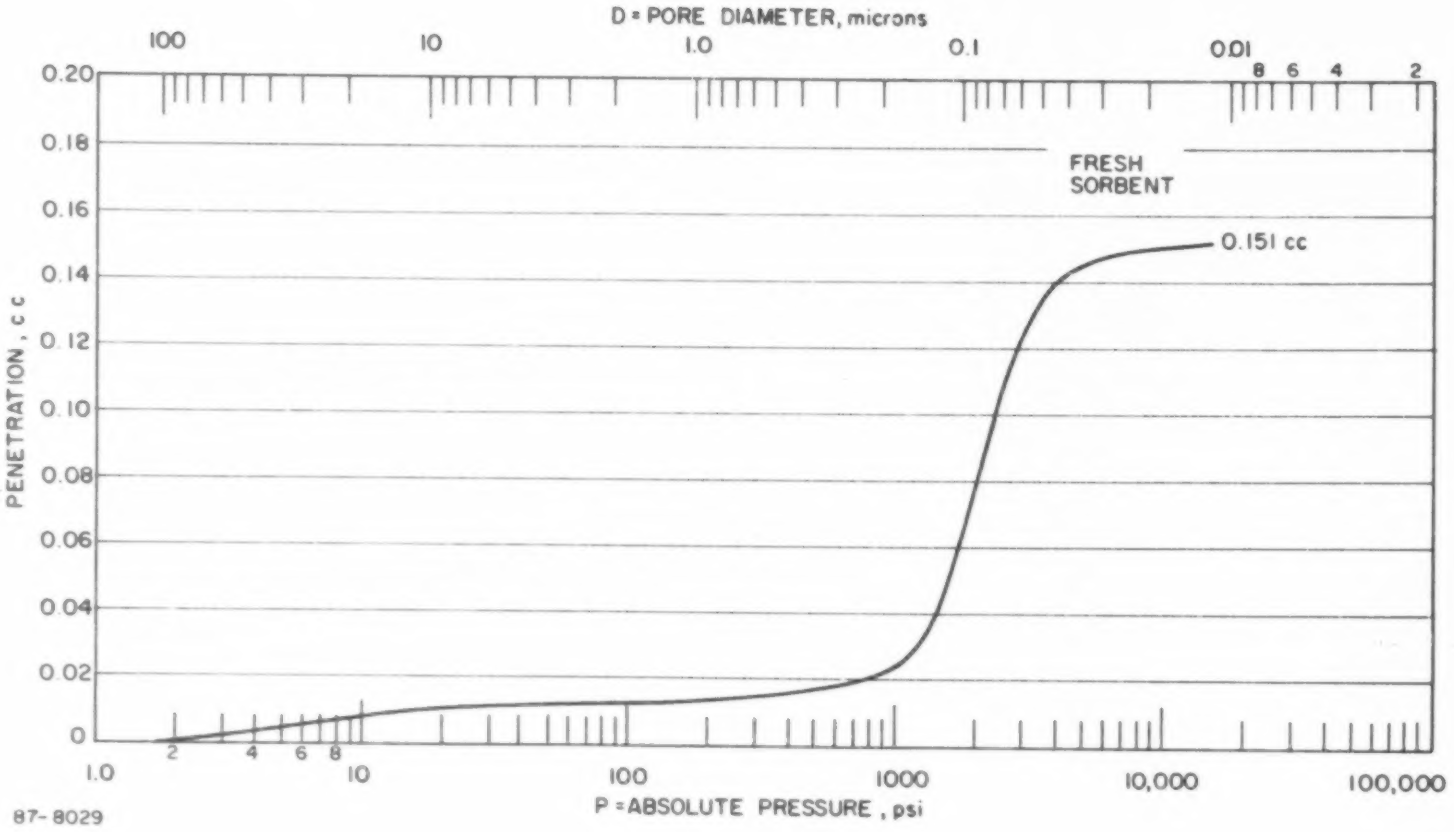

Figure 51 PORE SIZE DISTRIBUTION, FRESH W.R. GRACE SORBENT, AMINCO DATA

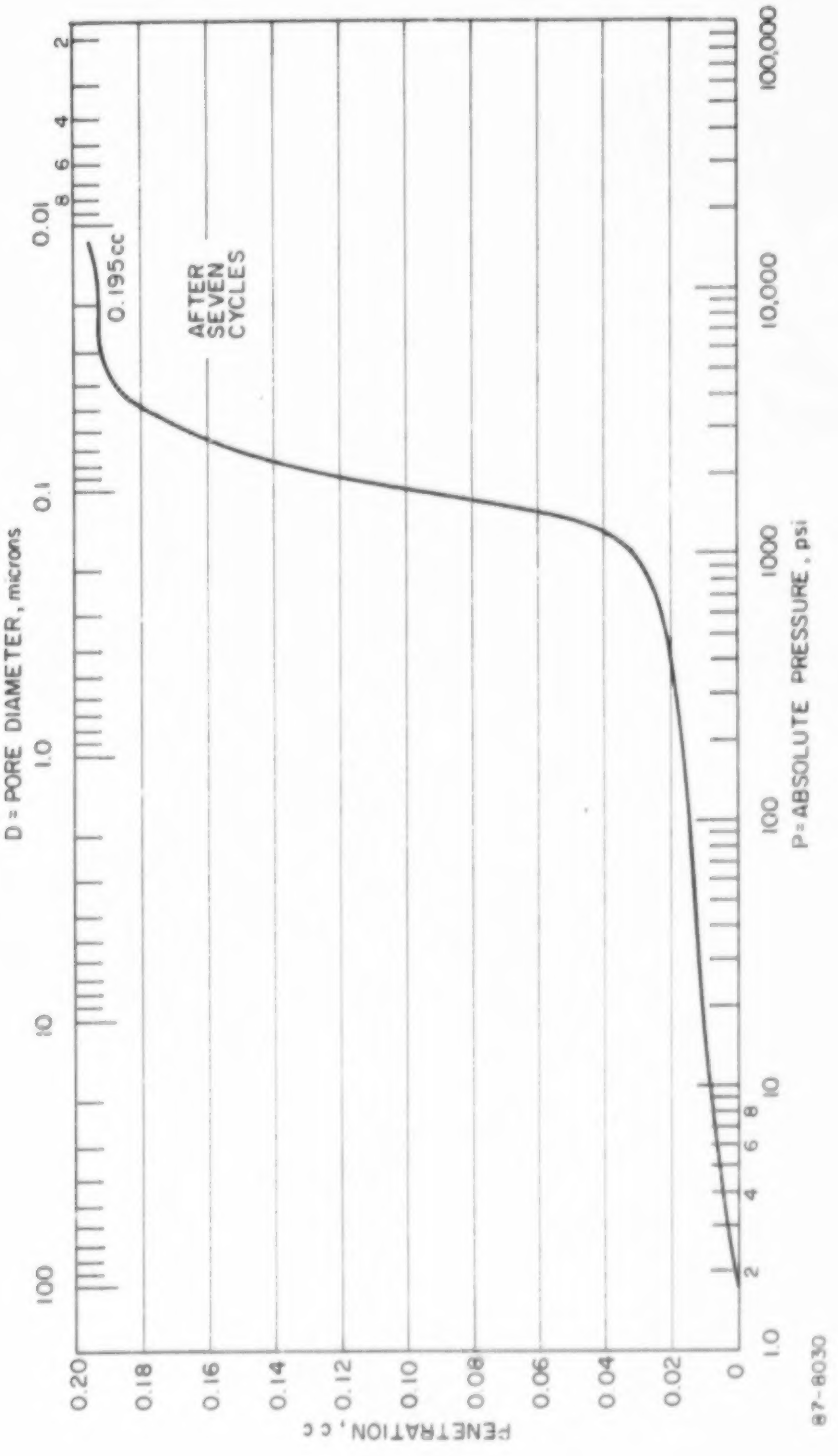

Figure 52 PORE SIZE DISTRIBUTION, USED W.R. GRACE SORBENT, AMINCO DATA

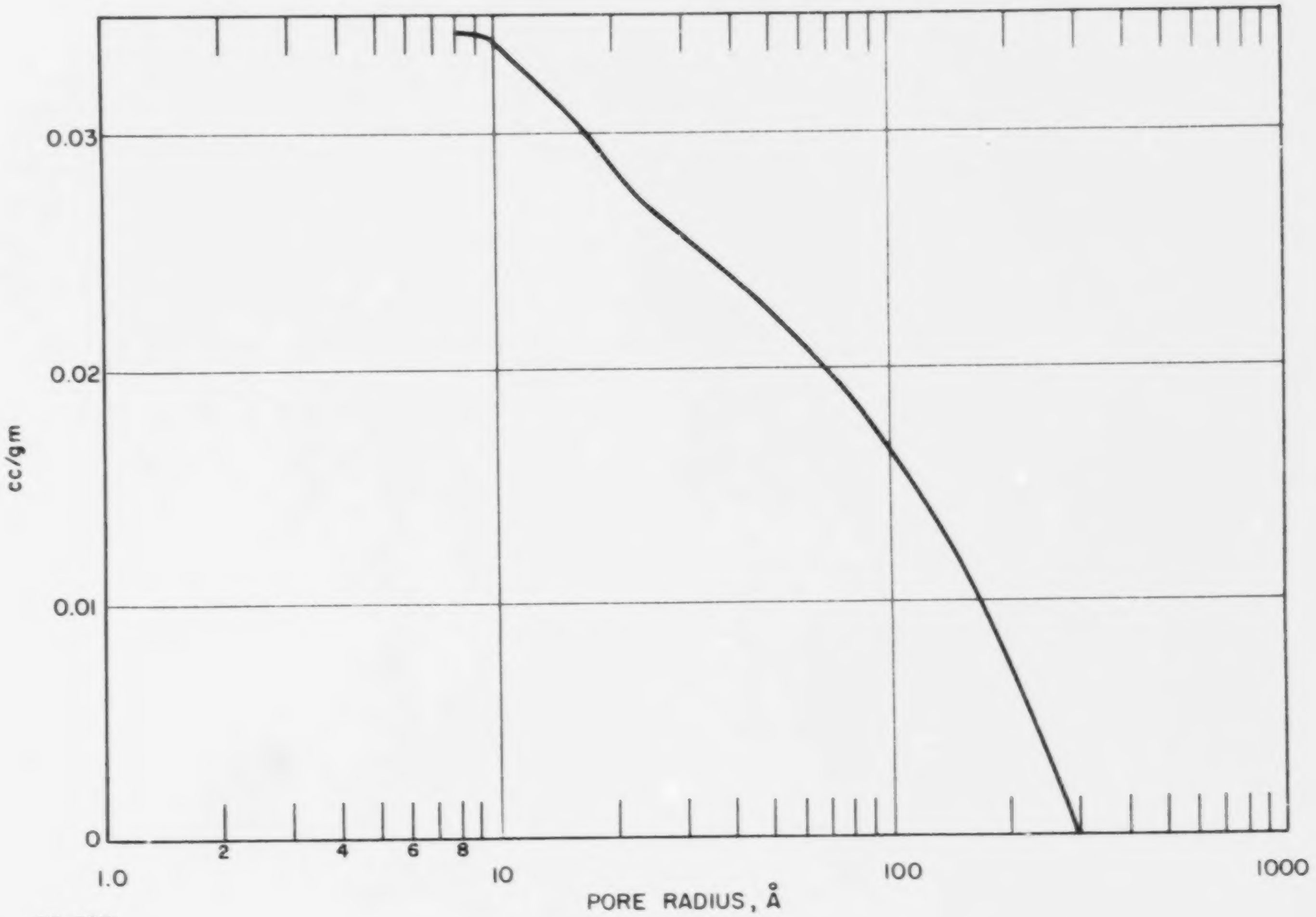

87-8031

Figure 53 PORE SIZE DISTRIBUTION, W.R. GRACE SORBENT, NITROGEN SORPTION METHOD

pore diameter of 0.06 μ, thus overlapping the mercury intrusion measurements. This volume distribution curve is superimposed on the mercury intrusion curve from Figure 51 and the result shown in Figure 54. The nitrogen sorption and mercury intrusion curves do not join smoothly, presumably due to variations in the samples.

By forcing the two curves to coincide at point A a smooth joining can be obtained. When this was done and the data replotted as a pore area distribution the curve shown in Figure 55 is obtained. This curve emphasizes the two small diameter modes of the distribution at 0.07 μ and 0.0035 μ. It also indicates that about one-third of the pore surface is in the smallest mode.

Sorbent H_2 treated by Avco, at 650° C for 10 hours.

$\rho_{pellet} = 0.99 \text{ gm/cm}^3$

$S_g = 33.8 \text{ cm}^2\text{/gm}$

$\epsilon = 0.61$

Mean pore diameter = 0.05 μ

The pore size distribution curve is given in Figure 56. Values of mean pore diameters reported here vary from 0.029 μ (Kelly) to 0.10 μ (Aminco). The variation may be in part due to variations in hydrogen treatment although the following table shows no trend.

	mean pore diameter	S_g
Field - 4 hours at 600° C	0.029μ	$47.5 \frac{m^2}{gm}$
Aminco - 10 hours at 650° C by Bu Mines	0.09μ	
Aminco - 10 hours at 650° C by Avco	0.05μ	$33.8 \frac{m^2}{gm}$

The following data have been selected as representative of the average W. R. Grace sorbent and will be used for computation:

$\rho_{pellet} = 1.05 \text{ gm/cc}$

$S_g = 45 \text{ cm}^2\text{/gm}$

$\epsilon = .61$

Largest mean pore = 0.25μ

Medium mean pore = 0.07μ

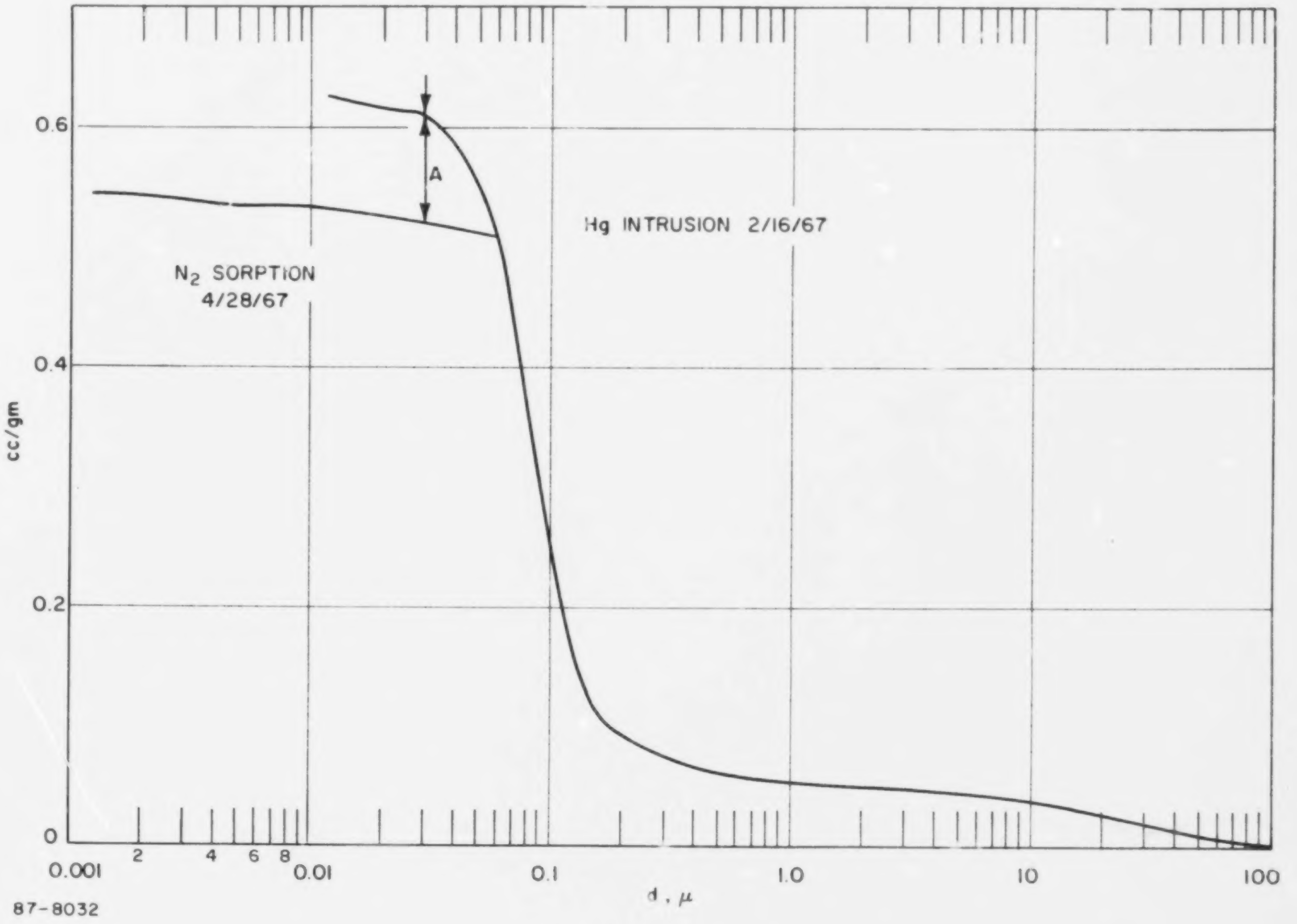

Figure 54 PORE SIZE DISTRIBUTION BY VOLUME, W.R. GRACE SORBENT

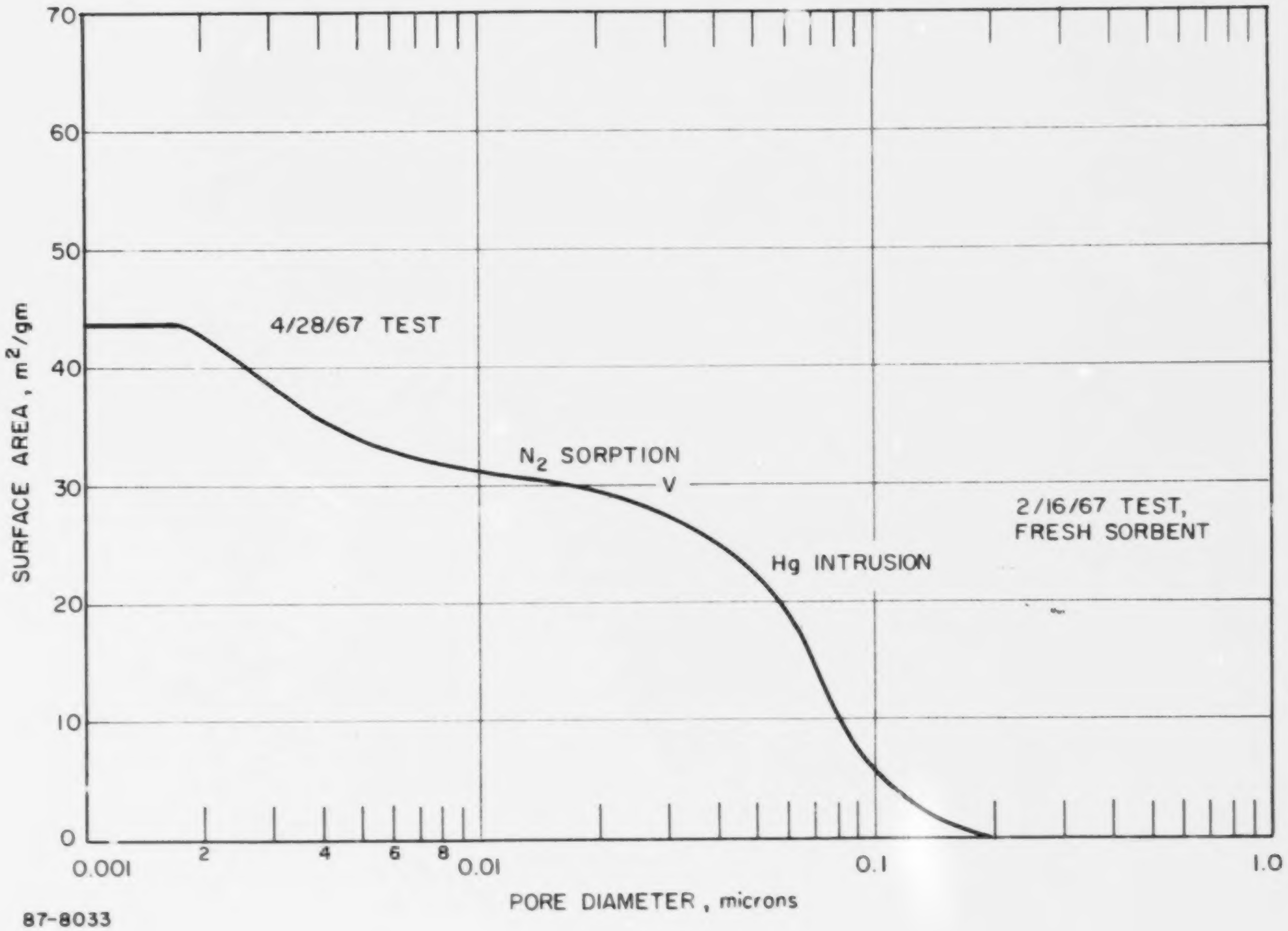

87-8033

Figure 55 PORE SIZE DISTRIBUTION, COMBINED MERCURY INTRUSION AND NITROGEN SORPTION METHOD

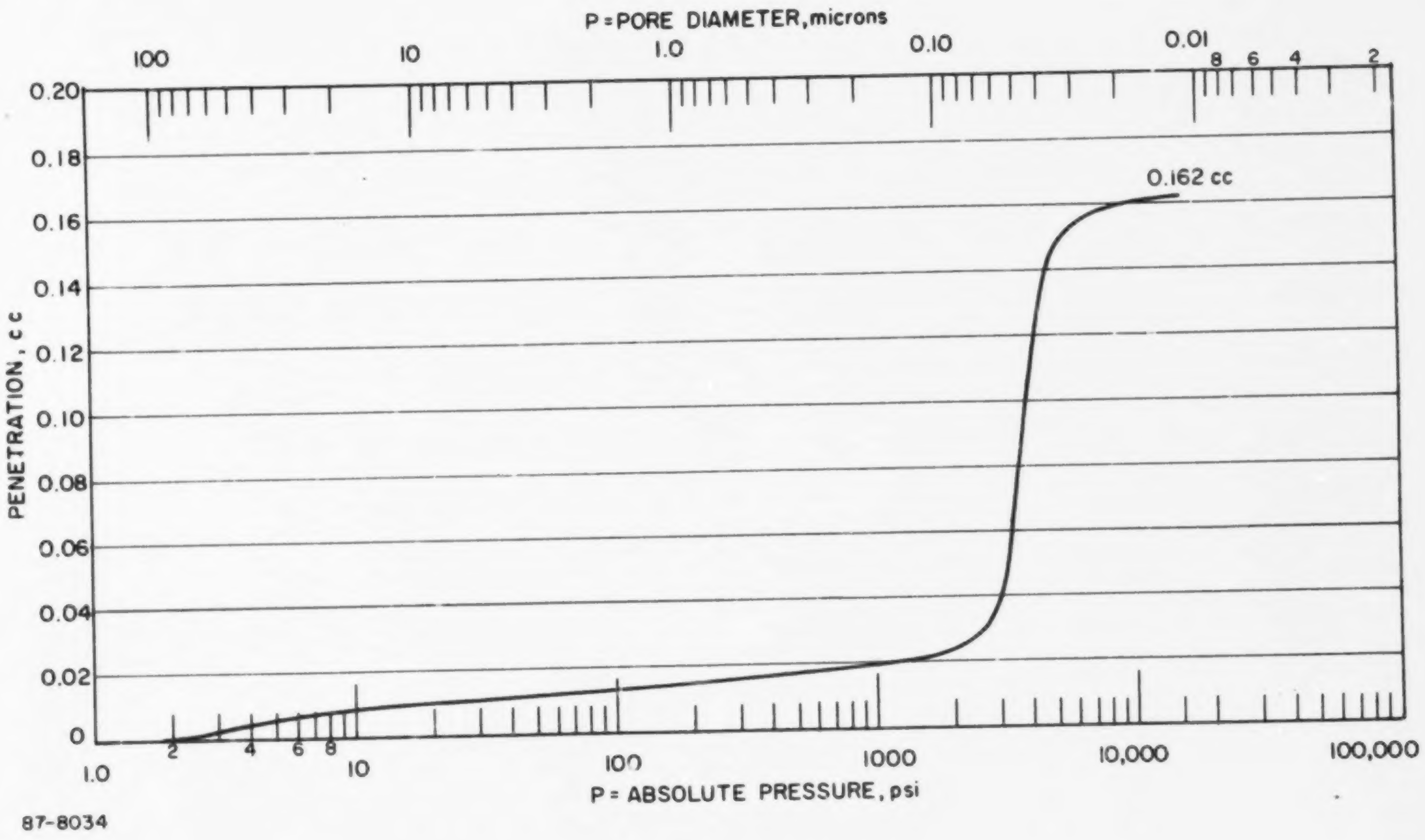

Figure 56 PORE SIZE DISTRIBUTION, W.R. GRACE SORBENT, H_2 TREATED AT AVCO, 650° C FOR TEN HOURS

Smallest mean pore = 0.0035 μ

Area in medium mode = 30 cm^2/gm

Area in smallest mode = 15 cm^2/gm

2) Peter Spence Sorbent -- received H_2 treated

ρ_{pellet} = 1.21 gm/cm^3

S_g = 34.1 cm^2/gm

ϵ = 0.725

mean pore diameter = 0.039 μ

The pore size distribution curve is given in Figure 57.

3) Bu Mines pilot plant sorbent -- received H_2 treated

ρ_{pellet} = 1.71 gm/cc

S_g = 32.1 cm^2/gm

ϵ = 0.718

mean pore diameter = 0.038 μ

The pore size distribution curve is given in Figure 58.

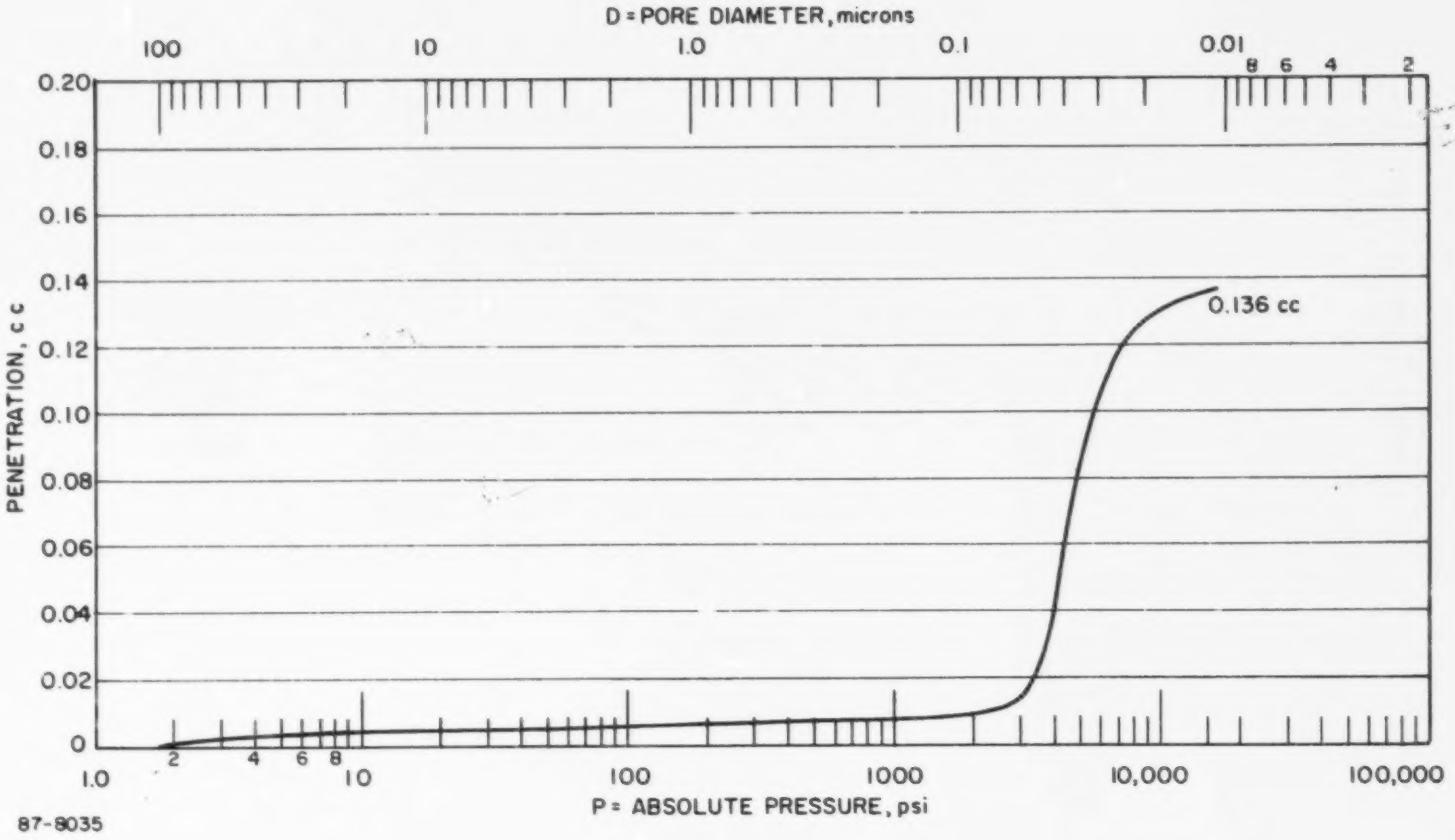

Figure 57 PORE SIZE DISTRIBUTION, PETER SPENCE SORBENT

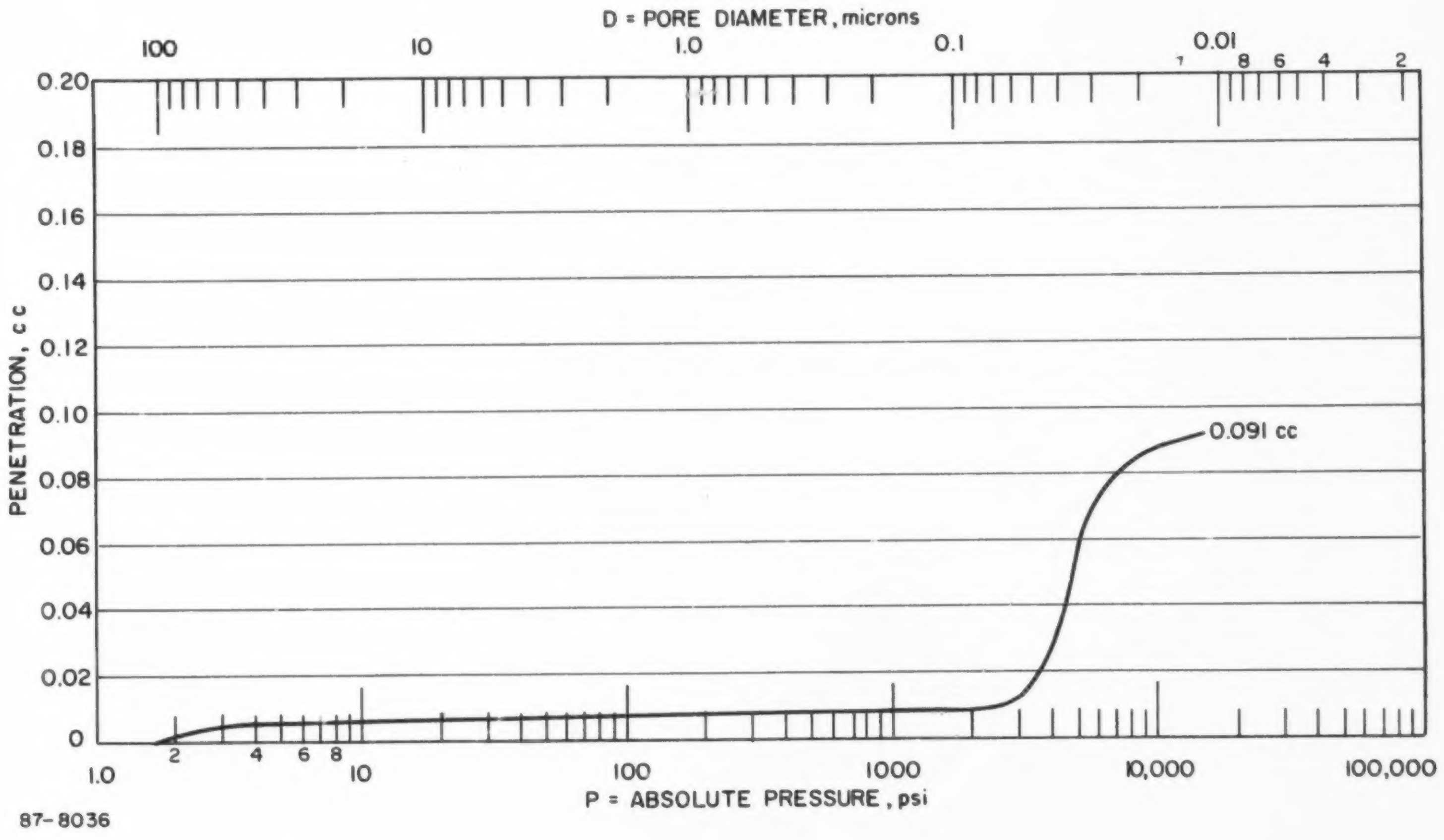

Figure 58 PORE SIZE DISTRIBUTION BU MINES PILOT PLANT SORBENT

APPENDIX I

SAMPLE CALCULATION RUN S-82

The weight gain versus time curve is given in Figure 22 and the rate versus loading curve in Figure 23. From the rate versus loading curve the saturation weight gain is estimated as

$$W_o = 0.355$$

Now the sorbent weight = 270 mg. Thus, the weight gain at saturation (assumed to be SO_3) is (1.25) (0.355) (270) = 120 mg.

Then S is computed in Table A-I, as

$$S = \text{weight gain (assumed to be } SO_3)/120$$

The parameter

$$\frac{1-(1-S)^{1/3}}{(1-S)^{1/3}}$$

is then computed and entered in the table. From the differentiation of the sorption curves as done numerically by machine computation values of $1/R$ were obtained and entered in the table, where

$$R = \frac{dW}{dt} \quad min^{-1} .$$

A plot was then prepared of $1/R$ versus $\dfrac{1-(1-S)^{1/3}}{(1-S)^{1/3}}$

This is shown in Figure 24.

A straight line was drawn through the points representing the first 70-80 percent of the sorption.

The slope and intercept of this line were obtained. The values were multiplied by 0.355 in order that they correspond to the slope and intercept of a plot of $1/(dS/dt)$ versus

$$\frac{1-(1-S)^{1/3}}{(1-S)^{1/3}}$$

The final values were

slope = 165.6 min

intercept = 6.56 min

Predicted values of the sorption curve (S *versus* t) were then computed according to equation

$$t = 165.6 \left[\frac{3}{2} \left(1-(1-S)^{2/3}\right)\right] - (165.5 - 6.56)\,S$$

The computed curve is plotted along with the actual data points in Figure 22. Plots of $\frac{1-(1-S)^{1/3}}{(1-S)^{1/3}}$ versus S and $\frac{3}{2}\ 1-(1-S)^{3}$ versus S were prepared as aids to computation and used to obtain the values in Table A-I.

The mass transfer coefficient was then computed from the intercept according to (49)

$$k_c = \frac{\rho\, d\, W_o}{192\, C_o\, (INTERCEPT)}$$

For S-82

ρ = 65.5 lb/ft^3

d = .00555 ft

C_o = 1.220 x 10^{-5} lb moles/ft^3

W_o = 0.355

Intercept = 6.56/60 hr

$$k_c = \frac{(65.5)\ (0.00555)\ (0.355)\ (60)}{(192)\ (1.22)\ (10^{-5})\ (6.56)} = 504\ \frac{ft}{hr}$$

The effective diffusivity is computed from the following relation, also obtained from (50)

$$D = \frac{dk_c\, (INTERCEPT)}{SLOPE}$$

For S-82 d = 0.17cm

k_c = 4.25 cm/sec

SLOPE/INTERCEPT = 25.5

TABLE A-I

SAMPLE CALCULATIONS FOR RUN S-82

Measured t (min)	S	$\frac{1-(1-S)^{1/3}}{(1-S)^{1/3}}$	1/R (min)	$3/2\,[1-(1-S)^{2/3}]$	Computed t (min)
0	0	0	18.5	0	0
0.5	.065	.027	26.0	.065	.43
1	.108	.039	37.5	.110	1.04
1.5	.140	.052	46.2	.143	1.42
2	.169	.064	52.7	.174	1.94
2.5	.193	.074	61.7	.200	2.43
3.5	.233	.093	71.8		
4.5	.272	.112	75.0	.286	4.11
5.5	.308	.131	85.4		
6.5	.337	.141	96.1	.361	6.20
8.0	.382	.175	101		
9.5	.420	.200	116	.455	8.57
11.0	.455	.224	125		
13.0	.500	.256	131	.554	12.24
15.0	.540	.295	150		
17.0	.575	.330	165	.653	16.71
19.0	.609	.367	175		
21.0	.640	.406	196	.742	21.1
24.0	.677	.458	244		
27.0	.708	.506	285	.840	26.5
32.0	.745	.577	359		
37.0	.785	.671	463	.962	34.5
44.0	.825	.788	600		
56.0	.865	.948	1025	1.108	45.95
68.0	.890	1.085	1524	1.160	

$$D = \frac{(0.17)\ (4.25)}{25.5} = 0.0285\ cm^2/sec$$

The initial rate, K, in hr^{-1} is computed from the initial rate data in min^{-1} by multiplying by 60 and dividing by the mole fraction of SO_2.

$$K = \frac{(0.053)\ (60)}{0.0092} = 345\ hr^{-1}$$

APPENDIX II

TABULATION OF RATE DATA

A. SORPTION DATA

A tabulation of sorbent weight gain versus time is presented on the following pages. The sorbent weight previous to sorption is given as is the weight gained at saturation. The saturation weight gain was estimated by plotting the sorption rate versus sorbent weight gain on log-log coordinates and extrapolating to the weight gain at zero rate. Two such plots are given in Figure 23.

The data of all runs considered in formulating the sorption rate model are given in this tabulation. The conditions obtaining in each run are given in Table V.

S-47
220 mg Sorbent

Time (min.)	Weight gain (mg)
0	0
.04	1
.20	4
.31	5
.72	6
2.02	7
5.68	8
11.4	9
18.3	10
29.0	11
41.7	12
48.5	12.5
56.7	13
68.4	13.5
77.3	14
87.0	14.5
98.1	15
108	15.5
121	16

S-49
220 mg Sorbent

Time (min.)	Weight gain (mg)
0	0
.20	1.5
.25	2.5
.50	3.5
.70	4.5
1.51	5.5
3.89	6.5
8.45	7.5
14.6	8.5
24.3	9.5
32.0	10
42.1	10.5
50.4	11
62.1	11.5
74.5	12
84.0	12.5
98.9	13
117	13.5
135	14
152	14.5
168	15

S-51
215 mg Sorbent

Time (min.)	Weight gain (mg)
0	0
.95	1.9
1.48	2.9
2.10	3.9
2.89	4.9
4.36	5.9
6.16	6.9
8.85	7.9
14.3	8.9
19.9	9.9
27.7	10.9
34.3	11.4
40.6	11.9
49.5	12.4
58.1	12.9
67.9	13.4
75.3	13.9
85.5	14.4
98.1	14.9
111	15.4

S-52
215 mg Sorbent

Time (min.)	Weight gain (mg)	Time (min.)	Weight gain (mg)
0	0	18.9	45.7
.30	1.7	20.0	47.7
.54	2.7	21.2	49.7
.78	3.7	22.4	51.7
.97	4.7	23.7	53.7
1.42	5.7	25.0	55.7
1.84	6.7	26.4	57.7
2.32	7.7	27.9	59.7
2.72	8.7	29.3	61.7
3.08	9.7	30.9	63.7
3.47	10.7	32.6	65.7
3.92	11.7	34.4	67.7
4.63	13.5	36.4	69.7
5.53	15.7	38.5	71.7
6.39	17.7	40.8	73.7
7.28	19.7	43.1	75.7
7.93	21.7	45.1	77.7
8.77	23.7	48.0	79.7
9.56	25.7	50.9	81.7
10.3	27.7	54.2	83.7
11.3	29.7	58.2	85.7
12.0	31.7	62.6	87.7
13.1	33.7	67.6	89.7
13.9	35.7	72.3	91.7
14.9	37.7	80.6	93.7
15.8	39.7	84.2	94.5
16.8	41.7	89.4	95.7
17.7	43.7	96.5	96.7

S-53
215 mg Sorbent

Time (min.)	Weight gain (mg)
0	0
.10	1.2
.15	2.2
.20	3.2
.25	4.2
.42	5.2
.82	6.2
1.32	7.2
3.53	8.2
7.03	9.2
11.8	10.2

S-53
215 mg Sorbent

Time (min.)	Weight gain (mg)
0	0
.54	.7
3.31	1.0
7.21	1.1

S-55
215 mg Sorbent

Time (min.)	Weight gain (mg)
0	0
.26	1.6
.46	3.6
.73	5.6
1.19	7.6
1.68	9.6
2.39	11.6
3.11	13.6
3.86	15.6
4.71	17.6
5.61	19.6
7.82	24.6
10.0	29.6
12.6	34.6
15.4	40.6
17.7	44.6
20.5	49.6
23.7	54.6
27.2	59.6
31.1	64.6
35.8	69.6
41.0	74.6
47.8	79.6
50.8	81.6
54.2	83.6
58.1	85.6
62.6	87.6
68.3	89.6
83.3	93.8
98.3	96.3
113	98.0
128	99.2
143	100
158	101
173	101
188	102

S-62
290 mg Sorbent
161 mg Saturation weight gain

Time (min.)	Weight gain (mg)
0	0
.80	4
1.80	9
3.26	12
4.91	14
7.92	17
8.90	19
10.5	21.5
12.2	24
14.2	28
15.8	31.5
17.4	35
19.2	39
21.7	45
23.4	49
25.3	54
27.6	59
29.6	64
31.9	69
34.0	74
36.1	79
39.7	86.5
41.0	89
43.6	94
46.4	99
49.4	104
52.6	109
56.4	114
60.4	119

S-63
290 mg Sorbent
126 mg Saturation weight gain

Time (min.)	Weight gain (mg)
0	0
.25	2.5
.63	7.5
1.12	12.5
1.82	17.5
4.12	29.5
5.34	32.5
6.81	37.5
8.49	42.5
10.1	47.5
11.9	52.5
13.9	57.5
16.1	62.5
18.0	67.5
20.3	72.5
23.1	77.5
26.3	82.5
30.1	87.5
34.5	92.5
37.7	95.5
41.6	98.5
45.7	101.5
48.6	103.5
51.8	105.5
55.7	107.5

S-64
Sorbent weight = 290 mg
Saturation weight gain = 99.7 mg

Time (min.)	Weight gain (mg)
0	0
.05	2.5
.42	6.5
1.41	11.5
2.57	16.5
3.78	21.5
4.95	26.5
6.17	31.5
7.43	36.5
8.88	41.5
10.5	46.5
12.3	51.5
14.4	56.5
16.7	61.5
19.3	66.5
22.2	71.5
25.3	76.5
30.2	81.5
35.5	86.5
42.6	91.5
49.2	95.5
53.6	97.5
55.8	98.5

S-65
Sorbent weight = 290 mg
Saturation weight gain = 118 mg

Time (min.)	Weight gain (mg)	Time (min.)	Weight gain (mg)
0	0	17.0	66.3
.60	2.3	19.0	71.3
1.38	6.3	21.3	76.3
2.37	11.3	23.9	81.3
3.27	16.3	26.7	86.3
4.35	21.3	30.0	91.3
5.43	26.3	33.8	96.3
6.57	31.3	38.6	101.3
7.65	36.3	41.6	104.3
9.05	41.3	45.4	107.3
10.4	46.3	49.6	110.3
11.9	51.3	52.8	112.3
13.5	56.3	57.1	114.3
15.2	61.3		

S-67
Sorbent weight = 290 mg
Saturation weight gain = 120 mg

Time (min.)	Weight gain (mg)
0	0
.49	2
.79	4
1.09	6
1.42	8
2.12	10
2.90	14
3.74	18
4.64	22
5.57	26
6.62	30
7.79	34
9.18	38
10.5	42
12.0	46
13.7	50
15.7	54
17.6	58
19.5	62
21.6	66
24.1	70
26.5	74
29.1	78
32.0	82
35.3	86
38.8	90
42.4	94
46.4	98
51.7	102
57.1	106
60.4	108
64.3	110
67.9	112

S-68
Sorbent weight = 290 mg
Saturation weight gain = 101.5 mg

Time (min.)	Weight gain (mg)
0	0
.73	2.5
1.16	4.5
1.98	6.5
2.62	8.5
3.12	10.5
3.58	12.5
4.54	16.5
5.36	20.5
6.32	24.5
7.22	28.5
8.22	32.5
9.22	36.5
10.2	40.5
11.4	44.5
13.0	48.5
14.6	52.5
16.2	56.5
17.8	60.5
19.9	64.5
22.1	68.5
24.6	72.5
27.3	76.5
30.0	80.5
33.6	84.5
38.5	88.5
44.7	92.5
55.6	96.5
94.5	99.5
109	99.9

S-69

Sorbent weight - 290 mg
Saturation weight gain = 99.6 mg

Time (min.)	Weight gain (mg)	Time (min.)	Weight gain (mg)
0	0	11.5	42
.30	2	13.3	46
.60	4	15.5	50
.85	6	17.5	54
1.18	8	19.9	58
1.56	10	22.7	62
1.94	12	25.9	66
2.38	14	29.7	70
2.90	16	34.1	74
3.53	18	39.8	78
4.50	22	49.2	82
5.76	26	67.3	86
6.90	30	82.4	88
8.29	34	104	90
9.88	38	126	91.4

S-70

Sorbent weight = 290 mg
Saturation weight gain = 68.9 mg

Time (min.)	Weight gain (mg)	Time (min.)	Weight gain (mg)
0	0	14.2	36
.05	2	17.2	40
.20	6	20.8	44
.63	8	24.7	48
1.23	10	30.7	52
1.79	12	37.8	56
3.24	16	45.9	60
5.47	20	69.6	64
7.20	24	84.4	66
9.16	28	130	67.5
11.6	32		

S-79

Sorbent weight - 277 mg
Saturation weight gain = 111 mg

Time (min.)	Weight gain (mg)
0	0
.5	3.3
1	6.8
1.5	9.8
2	12.8
2.5	15
3	17.3
4	21.5
5	25.4
6	28.6
7	32.6
8	35.3
10	42.0
12	46.8
14	52.0
16	56.0
18	60.1
20	63.9
22	67.6
24	70.6
26	73.0
29	76.6
32	80.0
35	83.0
38	85.5
42	87.3
48	92.4
54	95.5
62	98.7
71	101.2
80	103.4
90	105.6
105	107.3
120	108.4

S-80

Sorbent weight = 277 mg
Saturation weight gain = 111 mg

Time (min.)	Weight gain (mg)
0	0
.50	3.9
1.00	7.0
1.50	7.4
2	9.4
3	14.3
4	18.4
5	22.8
6	27.0
7	29.9
8	33.6
9	36.6
10	39.6
11	42.1
13	46.9
15	51.1
17	54.6
19	57.9
21	61.2
23	64.8
25	67.6
28	71.1
31	75.1
34	78.2
37	81
41	85.3
45	87.1
51	91.4
57	93.8
65	97.2
75	100.5
85	102.7
100	105.5
115	106.5

S-81

Sorbent weight = 270 mg
Saturation weight gain = 121 mg

Time (min.)	Weight gain (mg)
0	0
.5	4.9
1.0	7.5
1.5	9.4
2.0	11.8
3	16.9
4	22.6
5	26.7
6	31.4
7	34.8
8	37.8
9	43.8
10	47.7
12	51.9
14	55.5
17	61.1
20	65.2
23	69.4
26	73.2
29	77.4
32	81.2
35	84.2
39	88.9
43	92.2
48	95.6
53	98.5
61	102.4
69	105.7
79	108.1
94	111.2
109	114.5
124	116.5

S-82

Sorbent weight = 270 mg
Saturation weight gain = 120 mg

Time (min.)	Weight gain (mg)
0	0
.5	7.8
1.0	13.0
1.5	16.8
2.0	20.3
2.5	23.2
3.5	28.0
4.5	32.6
5.5	37.0
6.5	40.5
8.0	45.8
9.5	50.5
11.0	54.5
13.0	60.0
15.0	64.8
17.0	69.0
19.0	73.0
21.0	76.7
24.0	81.3
27.0	85.0
32.0	90.5
37.0	94.4
44.0	99.0
56.0	103.8
68.0	106.9
88.0	110.1
112	112.7

S-83

Sorbent weight = 238 mg
Saturation weight gain = 102.7 mg

Time (min.)	Weight gain (mg)
0	0
.5	4.2
1.0	8.6
1.5	11.4
2.0	13.8
3.0	18.1
4.0	21.7
5.5	26.8
7.0	31.6
8.5	36.1
10.5	41.6
12.5	46.4
14.5	51.0
17.0	56.2
20.0	61.5
23	65.7
27	69.6
32	74.4
38	80.8
44	85.0
52	88.6
62	92.0
77	95.3
92	97.8
107	99.8

S-85

Sorbent weight = 225 mg
Saturation weight gain = 140.7 mg

Time (min.)	Weight gain (mg)
0	0
.5	7.5
1.0	15.0
1.5	18.9
2.0	23.8
3	30.2
4	35.5
5	40.7
6	44.4
7	48.5
8	52.4
9	55.7
10	59.2
11	62.0
13	67.6
15	72.9
17	77.3
19.5	82.5
22	87.1
25	92.5
28	96.5
32	101.5
37	106.3
43	109.6
53	116.6
63	120.8
73	124.1
88	128.5
98	131.8
123	133.0

S-86

Sorbent weight = 225 mg
Saturation weight gain = 137.8 mg

Time (min.)	Weight gain (mg)
0	0
.5	11.9
1.0	17.9
1.5	21.4
2.0	24.8
3	30.7
4	36.4
5	41.1
6	45.1
7	48.8
8	52.7
9	55.9
11	61.8
13	67.3
15	71.9
19	81.2
21	84.8
24	89.3
27	93.7
30	97.1
34	102.1
38	105.6
43	109.8
49	113.7
56	117.5
66	120.0
76	124.3
86	127.5
116	133.6
131	134.9

ISR-3

Weight of sorbent = 217 mg

Time	Weight gain (mg)
0 sec	0
8.3	1.4
15.0	1.7
22.5	2.1
30.0	2.4
45.0	2.7
1 min	3.2
1.5	3.8
2	4.0
3	5.1
4	6.3
5	6.4
7	8.0
10	9.0
15	10.8
20	12.4
25	13.9
30	15.1
35	16.1
40	17.2
45	18.3
50	19.2
60	21.0
80	25.7
85	26.6

ISR-4

Weight of sorbent = 217 mg

Time	Weight gain (mg)
0 sec	0
5	.5
10	.8
15	1.0
20	1.6
25	1.9
30	2.0
40	2.0
50	2.5
60	3.1
1.25 min	4.4
1.50	4.7
1.75	4.7
2.0	5.0
2.5	5.7
3.0	6.0
5.25	7.4
8	8.0
10	9.7
15	12.0
20	12.9
25	14.5
35	17.2
45	19.0
55	21.0
65	22.7
75	24.3
85	25.4

ISR-5

Weight of sorbent = 217 mg

Time	Weight gain (mg)
0 sec	0
5	1
10	1.2
15	1.5
30	1.9
45	2.2
1 min	2.8
1.5	3.1
2	3.7
3	4.4
5	5.3
10	7.0
15	8.7
20	9.7
25	11.0
35	13.5
45	15.8
55	17.9
65	19.2
75	22.0
79	23.0

ISR-2[1]

Weight of sorbent = 356 mg

Time	Weight gain (mg)
0 sec	0
5	2.3
10	2.8
15	3.6
20	3.7
25	4.0
30	4.2
45	4.3
1 min	4.7
1.5	5.2
2	5.6
3	6.4
4	7.0
5	7.9
10	10.5
15	12.8
25	16.6
35	20.6
50	25.4
65	30.2
75	33.7
80	35.0

ISR-4[1]

Weight of sorbent = 356 mg

Time	Weight gain (mg)
0 sec	0
5	2.3
10	3.7
15	4.3
20	4.6
25	4.9
30	5.1
45	5.7
1 min	5.9
1.5	6.4
2	7.0
3	7.8
4	8.9
5	9.6
10	12.8
15	15.6
25	20.6
35	25.7
50	32.0
65	38.2
80	44.7
90	48.7

ISR-5[1]

Weight of sorbent = 356 mg

Time	Weight gain (mg)
0 sec	0
5	2.9
10	4.9
15	6.7
20	7.9
25	8.7
30	9.2
45	9.8
1 min	9.9
1.5	10.7
2	11.3
3	12.1
4	13.0
5	13.7
10	16.7
15	19.8
20	21.7
30	25.8
40	29.8
60	37.1
80	44.6

B. Regeneration Data

A tabulation of the regeneration data for all regeneration runs considered in this report is given in the following pages. The sorbent weight previous to sorption is given. The thermal weight loss incurred upon heating the sorbent from the sorption temperature to the regeneration temperature in a nitrogen atmosphere is also given.

The conditions obtaining during the regenerations are given in Table VIII.

P-5B

Weight of sorbent = 69.0 mg

Time (min.)	Balance Reading (mg)
0	2.48
.5	2.10
1.0	1.72
1.5	1.36
2.0	1.05
2.5	0.73
3.0	0.45
3.5	0.33
4.0	0.23
4.5	0.16
5.0	0.14
7.0	0.08
10.0	0.05

P-6A

Weight of sorbent = 70.3 mg

Time (min.)	Balance Reading (mg)
0	7.15
2	6.50
4	5.75
6	4.95
8	4.35
10	3.75
12	3.20
14	2.70
16	2.25
18	1.85
20	1.50
30	0.50
50	0

R-3

Weight of sorbent = 238 mg
Thermal weight loss = 2.5 mg

Time (min.)	Balance Reading (mg)
0	37.3
.98	36
2.01	35
3.10	34
3.98	33
4.83	32
5.84	31
6.49	30
7.53	29
9.09	28
11.6	27
17.0	26
44.0	25.3

R-5

Weight of sorbent = 238 mg
Thermal weight loss = 4.0 mg

Time (min.)	Balance Reading (mg)
0	32.4
1.2	31
2.47	30
3.37	29
4.57	28
5.55	27
6.45	26
7.75	25
9.50	24
12.5	23
21.3	22
37.0	21.4
130	20.7
160	20.4

R-6

Weight of sorbent = 238 mg
Thermal weight loss = 2.6 mg

Time (min.)	Balance Reading (mg)
0	32.5
.58	31
1.52	30
2.47	29
3.48	28
4.43	27
5.33	26
6.73	25
7.63	24
9.68	23
13.3	22

R-6 cont'd

20.2	21.5
51.2	20.5
198	19.8

R-7

Weight of sorbent = 238 mg
Thermal weight loss = 0.4 mg

Time (min.)	Balance Reading (mg)
0	34.6
.53	33
1.18	32
2.18	31
3.06	30
4.06	29
5.05	28
6.19	27
6.99	26
8.33	25
10.33	24
11.73	23
14.26	22
19.18	21
26.13	20
52.53	19.2

R-8

Weight of sorbent = 238 mg
Thermal weight loss = 2.1 mg

Time (min.)	Balance Reading (mg)
0	31.2
1.68	30
4.18	29
7.15	28
9.90	27
12.2	26
14.2	25
17.3	24
21.0	23
28.7	22
39.7	21.3
63.7	20.5
99.7	20.2

R-9

Weight of sorbent = 238 mg
Thermal weight loss = 1.7 mg

Time (min.)	Balance Reading (mg)
0	32.7
.84	32
2.04	31
3.53	30
5.18	29
6.31	28
7.42	27
9.26	26
11.3	25
15.2	24
21.4	22.5
38.4	20.6
102.4	19.9

R-10

Weight of sorbent = 238 mg
Thermal weight loss = 2.3 mg

Time (min.)	Balance Reading (mg)
0	30.5
1.12	30
2.46	29
5.09	28
7.06	27
8.91	26
10.8	25
12.6	24
15.3	23
19.7	22
26.9	21.3
33.9	20.5
48.9	20.2
59.9	19.9

R-13

Weight of sorbent = 238 mg
Thermal weight loss = 3.2 mg

Time (min.)	Balance Reading (mg)
0	34.7
.07	34.5
.41	33.5
.92	32.5
1.79	31.5
3.07	30.5
4.39	29.5
5.36	28.5
6.43	27.5
7.48	26.5
8.94	25.5
10.8	24.5
13.5	23.5
18.1	22.5
22.1	22.0
49.1	20.8

R-16

Weight of sorbent = 238 mg
Thermal weight loss = 0.3 mg

Time (min.)	Balance Reading (mg)
0	28.1
.09	28.4
.26	27.4
.76	26.4
1.33	25.4
1.78	24.4
2.83	23.4
5.00	22.4
7.85	22.0
29.5	20.9

R-19

Weight of sorbent = 238 mg
Thermal weight loss = 1.9 mg

Time (min.)	Balance Reading (mg)
0	36.3
.11	36
.76	35
1.42	34
2.56	33
3.96	32
5.16	31
6.37	30
7.35	29
8.68	28
10.3	27
12.2	26
14.4	25
18.0	24
24.5	23
37.5	21.9
50.0	21.5
70.5	21.0

R-21

Weight of sorbent = 238 mg
Thermal weight loss = 0.7 mg

Time (min.)	Balance Reading (mg)
0	32.7
.06	32.5
.81	31.5
1.34	30.5
2.26	29.5
3.71	28.5
5.42	27.5
7.42	26.5
8.66	25.5
11.3	24.5
15.7	23.5
23.8	22.4
56.9	20.4

R-17

Weight of sorbent = 238 mg
Thermal weight loss = 0 mg

Time (min.)	Balance Reading (mg)
0	27.5
.10	27.5
.63	26.5
1.18	25.5
1.78	24.5
2.97	23.5
4.92	22.5
8.17	21.9
21.4	21.0

R-20

Weight of sorbent = 238 mg
Thermal weight loss = 0 mg

Time (min.)	Balance Reading (mg)
0	28.3
.40	28.0
.88	27
1.34	26
1.95	25
2.91	24
4.75	23
8.53	22.4
14.1	21.7
25.9	21.2
42.5	20.8

R-23

Weight of sorbent = 238 mg
Thermal weight loss = 0.6 mg

Time (min.)	Balance Reading (mg)
0	33.5
1.51	32.5
3.71	31.5
5.02	30.5
9.91	29.5
21.5	28.5
34.8	27.5
48.2	26.5
63.7	25.5
80.3	24.5
91.2	24.0

R-24

Weight of sorbent = 238 mg
Thermal weight loss = 1.0 mg

Time (min.)	Balance Reading (mg)	Time (min.)	Balance Reading (mg)
0	32.6	5.78	25
.63	31	8.20	24
1.38	30	16.7	23
1.88	29	30.9	22.5
2.41	28	71.4	22.8
2.96	27	116.4	20.6
4.30	26		

An additional 2.2 mg was lost when CO shut off and pure H_2 turned on.

R-27

Weight of sorbent = 238 mg
Thermal weight loss = 1.8 mg

Time (min.)	Balance Reading (mg)	Time (min.)	Balance Reading (mg)
0	34	6.02	27
.86	30	8.86	26
2.16	29	24.9	25
4.11	28		

An additional 0.5 mg was lost in pure H_2

R-28

Weight of sorbent = 238 mg
Thermal weight loss = 2.7 mg

Time (min.)	Balance Reading (mg)	Time (min.)	Balance Reading (mg)
0	36.8	3.12	31
.37	35	4.88	29
.67	33	11.18	28.8
1.59	32		

An additional weight loss of 2.7 mg occured over a period of two hours in pure H_2.

R-56

Weight of sorbent = 202 mg
Thermal weight loss = 7.2 mg

Time (min.)	Balance Reading (mg)	Time (min.)	Balance Reading (mg)
0	109	113	34.5
10	103	124	30
22	99	134	28
39	91	159	23.5
71	66	177	22.0
93	46.5	215	20.8
104	39.2		

R-57

Weight of sorbent = 202 mg
Thermal weight loss = 10.6 mg

Time (min.)	Balance Reading (mg)
0	96.2
6	88
12	79
15	69
18	58
21	47.7
24	40.5
30	34.5
43	30.2
60	28
78	24.8
95	23.5
142	21.5

R-58

Weight of sorbent = 126 mg
Thermal weight loss = 4.0 mg

Time (min.)	Balance Reading (mg)
0	79
3	75
6	72
12	66
15	61.5
18	56.3
23	47
32	31.5
36	27.6
47	23
62	20.3
79	18.3
108	16.6

R-59

Weight of sorbent - 126 mg
Thermal weight loss = 3.9 mg

Time (min.)	Balance Reading (mg)
0	76
3	79.2
6	78
9	76
13	72
16	69.2
20	63.7
23	58.7
26	54
30	50.5
36	47.2
42	45
50	43.5
68	36
80	34
101	29.7
132	24
156	21

H_2O and H_2S shut of at 50 minutes. Pure H_2 used from 50 minutes to 156 minutes.

R-60

Weight of sorbent = 126 mg

Time (min.)	Balance Reading (mg)
0	77.5
3.5	82
6	79
9	74.5
12	68.7
15	63.8
21	50.5
24	47
30	44
35	44
41	39.5
45	37.7
54	34

H_2S shut off at 35 minutes. Pure H_2 used from 35 minutes to 54 minutes

R-71

Weight of sorbent = 290 mg
Thermal weight loss = 24.0 mg

Time (min.)	Balance Reading (mg)
0	124
3	109.5
6	80
9	55
12	49
15	47.3
24	44
30.5	41.5
51	36
74	32.2
87	31.5

R-63

Weight of sorbent = 290 mg
Thermal weight loss = 25.5 mg

Time (min.)	Balance Reading (mg)
0	116
3	103.5
6	61
9	55.5
11	51
21	45
27	43.5
57	35.5
83	33.0
132	30.5

R-71

Weight of sorbent = 254 mg
Thermal weight loss = 5.2 mg

Time (min.)	Balance Reading (mg)
0	37.3
1.3	36
2.3	35
3.5	34
4.7	33
5.6	32
6.4	31
7.4	30
8.1	29
9.0	28
9.9	27
11.3	26
13.2	25
15.8	24
18.7	23
22.3	22
29.4	20
38.1	19

R-72

Weight of sorbent = 254 mg
Thermal weight loss = 9.5 mg

Time (min.)	Balance Reading (mg)
0	37.3
1.6	36
2.0	35
2.8	34
3.4	33
4.1	32
5.0	31
6.2	30
7.6	29
9.5	28
11.9	27
16.0	25
24.1	23
40.6	19.5
52.6	18.8

DISTRIBUTION

Addressee	No. of Copies
Mr. R. Hangebrauck Laboratory of Engineering and Physical Science National Center for Air Pollution Control Cincinnati, Ohio 45226	25
Reports Distribution	15
Research Library -- Lowell	3
Research Library -- Wilmington	1